学位論文

Dark Matter in the Minimal $\mathbf{U(1)_X}$ Extended Standard Model

(最小 $\mathrm{U(1)_X}$ 拡張標準模型におけるダークマターの研究)

March, 2018

Graduate School of Science and Engineering
Yamagata University

Satomi Okada

Doctoral thesis

Dark Matter in the Minimal $\mathbf{U(1)_X}$ Extended Standard Model

March, 2018

Graduate School of Science and Engineering
Yamagata University

Satomi Okada

Abstract

The Standard Model (SM) of particle physics is the best theory to describe elementary particles and fundamental interactions among them (strong, weak, and electromagnetic interactions), and agrees with a number of experimental results in a high accuracy. Despite of its success, there are some observational problems that the SM cannot account for. There are two missing pieces in the SM. One is the neutrino masses and neutrino flavor mixings, which are observed through the neutrino oscillation phenomena. The other is a dark matter candidate. Current cosmological observations have established the existence of dark matter in the universe. However no suitable dark matter candidate is not included in the SM particle content. We need to extend the SM to supplement these missing pieces into the SM.

In this thesis, we first consider a dark matter scenario in the minimal gauged $B-L$ extension of the SM, where the global $B-L$ (baryon number minus lepton number) symmetry in the SM is gauged, and three generations of right-handed neutrinos and a $B-L$ Higgs field are introduced. Associated with the $B-L$ gauge symmetry breaking by a vacuum expectation value of the $B-L$ Higgs field, the seesaw mechanism for generating the neutrino mass is automatically implemented after the electroweak symmetry breaking in the SM. In this model context, we introduce a Z_2 symmetry and assign an odd parity for one right-handed neutrino while even parities for the other fields. The dark matter candidate is identified as the right-handed Majorana neutrino with Z_2-odd. The so-called minimal seesaw is implemented in this model with only two Z_2-even right-handed neutrinos. When the dark matter particle communicates with the SM particles mainly through the $B-L$ gauge boson (Z'_{B-L} boson), its relic density is determined by only three free parameters, the $B-L$ gauge coupling (α_{B-L}), the Z'_{B-L} boson mass ($m_{Z'}$) and the dark matter mass (m_{DM}). With the cosmological upper bound on the dark matter relic density, we find a lower bound on α_{B-L} as a function of $m_{Z'}$. On the other hand,

we interpret the recent LHC Run-2 results on search for Z' boson resonance to an upper bound on α_{B-L} as a function of $m_{Z'}$. Combining the two results we identify an allowed parameter region for this " Z'_{B-L} portal " dark matter scenario, which turns out to be a narrow window with the lower mass bound of $m_{Z'} \geq 3.6$ TeV.

Next, we generalize the minimal $B-L$ model to the minimal $U(1)_X$ model. Introducing the Z_2 symmetry, the Z_2-odd right-handed neutrino serves as a dark matter in the universe. The " Z' portal " right-handed dark matter scenario is controlled by only four free parameters: the $U(1)_X$ gauge coupling (α_X), the Z' boson mass ($m_{Z'}$), the dark matter mass (m_{DM}), and the $U(1)_X$ charge of the SM Higgs doublet (x_H). We consider various phenomenological constraints to identify a phenomenologically viable parameter space. The most important constraints are the observed dark matter relic density and the LHC Run-2 results on the search for a narrow resonance with the dilepton final state. We find that these are complementary with each other and narrow the allowed parameter region, leading to the lower mass bound of $m_{Z'} \geq 2.7$ TeV. Future LHC experiments will fully cover the current allowed region, and the Z' boson of the minimal $U(1)_X$ extended SM might be discovered in the near future.

Acknowledgements

First, I would like to greatly appreciate my supervisor, Professor Ryusuke Endo, for valuable discussions and helpful comments. I also appreciate Professor Masato Arai for helpful comments and encouragements. I would like to thank Professor Minoru Eto for useful comments and feedback. I also thank Professor Takashi Sano for helpful comments. I would like to sincerely appreciate Professor Shinsuke Kawai at Sungkyunkwan University for constructive advices and considerable encouragements. I would like to express my gratitude to Professor Nobuhito Maru at Osaka City University, Takashi Miyaji, and Digesh Rant at the University of Alabama for research collaborations. I would like to thank Daisuke Takahashi, Dr. Satsuki Oda at Okinawa Institute of Science and Technology Graduate University, Dr. Arindam Das at Korea Institute for Advanced Study, and Desmond Villalba at the University of Alabama for valuable discussions and useful comments. I would like to thank all members of the particle theory group at Yamagata University for useful comments. I am very grateful to FUSUMA Alumni Association at Yamagata University for travel supports for my visit to the University of Alabama. I would also like to thank the Department of Physics and Astronomy at the University of Alabama for hospitality during my visit for collaborations.

Finally, I would like to deepest appreciate my husband and collaborator, Professor Nobuchika Okada at the University of Alabama, for extensive discussions, tremendous supports, and continuous encouragements. Without him, this thesis would not have been possible. I am also deeply grateful to Andy Okada for constant encouragements.

Notation

- Natural units:

$$\hbar = c = k_B = 1,$$

  where c is the speed of light, $\hbar = h/(2\pi)$ (h is the Planck constant) is the reduced Planck constant, and k_B is the Boltzmann constant.

- Pauli matrices:

$$\sigma^1 = \begin{pmatrix} 0 & 1 \\ 1 & 0 \end{pmatrix}, \ \sigma^2 = \begin{pmatrix} 0 & -i \\ i & 0 \end{pmatrix}, \ \sigma^3 = \begin{pmatrix} 1 & 0 \\ 0 & -1 \end{pmatrix}.$$

- γ matrices (chiral representation):

$$\gamma^0 = \begin{pmatrix} \mathbf{0} & \mathbf{1} \\ \mathbf{1} & \mathbf{0} \end{pmatrix}, \ \gamma^i = \begin{pmatrix} \mathbf{0} & \sigma^i \\ -\sigma^i & \mathbf{0} \end{pmatrix},$$

  where $\mathbf{0}$ is the 2×2 zero matrix, $\mathbf{1}$ is the 2×2 unit matrix, and $i = 1, 2, 3$.

- Chirality:

$$\psi_L = P_L \psi = \frac{1 - \gamma_5}{2} \psi,$$
$$\psi_R = P_R \psi = \frac{1 + \gamma_5}{2} \psi,$$

  where

$$\gamma_5 = i\gamma^0\gamma^1\gamma^2\gamma^3 = \begin{pmatrix} -\mathbf{1} & \mathbf{0} \\ \mathbf{0} & \mathbf{1} \end{pmatrix}.$$

- Dirac adjoint:

$$\overline{\psi} = \psi^\dagger \gamma^0.$$

- Charge conjugation:

$$\psi^C = C\psi^*,$$

where

$$C = i\gamma^2\gamma^0 = \begin{pmatrix} i\sigma^2 & \mathbf{0} \\ \mathbf{0} & -i\sigma^2 \end{pmatrix}.$$

Contents

Chapter 1

Introduction

In 2012, the Higgs boson, which is the last piece of the Standard Model (SM), was discovered by the A Toroidal LHC ApparatuS (ATLAS) and Compact Muon Solenoid (CMS) experiments at the Large Hadron Collider (LHC) [1, 2]. The SM is the best theory to describe elementary particles and fundamental interactions among them (strong, weak, and electromagnetic interactions), and agrees with a number of experimental results in a high accuracy. For example, W and Z gauge bosons in the SM had been discovered by the Underground Area 1 (UA1) and the UA2 experiments at the Super Proton Synchrotron Proton-Antiproton Collider in 1983 [3, 4], whose properties such as masses and couplings with quarks and leptons were measured at the Large electron-positron collider (LEP) with a very high degree of precision [5, 6]. Properties of the Higgs boson have also been measured to be consistent with the SM predictions at the LHC [7].

Despite of its success, there are some observational problems that the SM cannot account for. One of major missing pieces in the SM is the neutrino mass matrix. Right-handed neutrinos are not included in the SM particle content in contrast to the other fermions, so that neutrinos do not have their masses. However neutrino oscillation phenomena among three neutrino flavors have been confirmed by the Super-Kamiokande experiments in 1998 [8] and the Sudbury Neutrino Observatory (SNO) in 2001 [9]. Neutrino oscillation phenomena require neutrino masses and flavor mixings, and therefore we need a framework beyond the SM. The seesaw mechanism [10, 11, 12, 13, 14] is probably the most natural way to incorporate the tiny neutrino masses and their flavor mixing, where right-handed neutrinos with Majorana masses are introduced.

Another major missing piece in the SM is the candidate of the dark matter particle.

Based on the recent results of the precision measurements of the cosmic microwave back ground (CMB) anisotropy by the Wilkinson Microwave Anisotropy Probe (WMAP) [15] and the Planck satellite [16, 17], the energy budget of the present universe is determined to be composed of 73% dark energy, 23% cold dark matter and only 4% from baryonic matter. It is a prime open question in particle physics and cosmology to identify the properties of the dark matter particle, although the SM has no suitable candidate for it. Therefore, we need to extend the SM to incorporate the cold dark matter particle. One of the most promising candidates for the dark matter in the present universe is the weakly interacting massive particle (WIMP) [18]. The WIMP was in thermal equilibrium in the early universe and its relic density is determined by the interactions with the SM particles. Note that the calculation of the relic density is independent of the history of the Universe before the dark matter has gotten in thermal equilibrium.

The minimal $B-L$ extended SM [19, 20, 21, 22, 23] is a very simple extension of the SM to naturally incorporate the seesaw mechanism. In this model, the accidental global $B-L$ (baryon number minus lepton number) symmetry in the SM is gauged, and an introduction of three generations of right-handed neutrinos is required to keep the model from the gauge and gravitational anomalies. Associated with the $B-L$ gauge symmetry breaking, the right-handed neutrinos acquire Majorana masses, and the SM neutrino Majorana masses are generated through the seesaw mechanism after the electroweak symmetry breaking. The mass spectrum of new particles introduced in the minimal $B-L$ model, the $B-L$ gauge boson (Z'_{B-L} boson), the right-handed Majorana neutrinos and the $B-L$ Higgs boson, is controlled by the $B-L$ symmetry breaking scale. The $B-L$ model can be tested at the LHC, if the breaking scale lies around the TeV scale.

Although the minimal $B-L$ model incorporates the neutrino masses and mixings, a candidate for the cold dark matter is still missing in the model. A simple and concise way to introduce a dark matter candidate in the context of the minimal $B-L$ model has been proposed in [24], where only a Z_2 symmetry is introduced without any extensions of the particle content of the model. An odd parity is assigned to one right-handed neutrino, while the other particles have even parties. Because of the Z_2 symmetry conservation, the Z_2-odd right-handed neutrino cannot decay into other particles and hence plays a role of dark matter. The neutrino oscillation data can be reproduced by the so-called minimal seesaw [25, 26], where only two generations of the right-handed neutrinos are

involved, predicting one massless neutrino. Dark matter phenomenology in this model context has been investigated in [24, 27, 28]. The right-handed neutrino dark matter can annihilate into the SM particles through its interactions with (i) the Z'_{B-L} boson and (ii) two Higgs bosons which are realized as linear combinations of the SM Higgs and the $B-L$ Higgs bosons. The case (i) and (ii) are called " Z' portal " and " Higgs portal " dark matter scenarios, respectively. The Higgs portal dark matter scenario has been extensively studied in [24, 27, 28].

Recently, the Z' portal dark matter has atracted a lot of attention [29, 30, 31, 32, 33, 34, 35, 36, 37, 38, 39, 40, 41], where a dark matter particle is introduced along with an extra gauge extension of the SM, and the dark matter particle communicates with the SM particles through an electric charge neutral gauge boson (Z' boson), associated with an extra gauge group. The Z' boson as a mediator allows us to investigate a variety of dark matter physics, such as the dark matter relic density and the direct and indirect dark matter search. Interestingly, the search for Z' boson resonance at the LHC provides information that is complementary to dark matter physics.

The minimal $B-L$ model with the right-handed neutrino dark matter discussed above is a very simple example of the Z' portal dark matter model. In this thesis, we first investigate the Z' portal dark matter in the minimal $B-L$ model. Because of the simplicity of the model, dark matter physics is controlled by only three free parameters, the $B-L$ gauge coupling (α_{B-L}), the Z'_{B-L} boson mass ($m_{Z'}$) and the dark matter mass ($m_{\rm DM}$). We will identify allowed parameter regions of the model by considering the cosmological bound on the dark matter relic density and the recent results by the LHC Run-2 on search for Z' boson resonance with dilepton final states [42, 43].

Next, we generalize the minimal $B-L$ model to the so-called nonexotic $U(1)_X$ extension of the SM [44]. The $U(1)_X$ model is the most general extension of the SM with an extra anomaly-free $U(1)$ gauge symmetry. A new parameter x_H, which is the $U(1)_X$ charge of the SM Higgs doublet, is introduced. The minimal $B-L$ model corresponds to the limit of $x_H = 0$. The particle content of the model is the same as the one in the minimal $B-L$ model except for the generalization of the $U(1)_X$ charge assignment for particles. Hence, we can easily extend the minimal $B-L$ model with right-handed neutrino dark matter to the $U(1)_X$ case. In this context, we perform detailed analyses to identify a phenomenologically viable parameter region through the complementarity

between dark matter physics and the LHC Run-2 results. Because of the $U(1)_X$ generalization, the Z' boson couplings with the SM particles are modified for $x_H \neq 0$ and the allowed parameter region is found to be quite different from the one obtained in the $B-L$ model ($x_H = 0$).

This thesis is organized as follows. In Chapter 2, we briefly review particle cosmology, in particular, we focus on WIMP dark matter physics. We begin with the Big Bang cosmology, which is the standard cosmological theory of the expanding universe. Based on the evolution of the Big Bang cosmology, we discuss the thermal history of the early universe, and how the WIMP dark matter decouples from the thermal plasma. We present the procedure to calculate the relic density of the WIMP dark matter. In Chapter 3, we give a review on the basic structure of the SM. Particle content and Lagrangian of the SM are presented. We discuss the spontaneous symmetry breaking and the Higgs mechanism to generate the masses for weak gauge bosons, quarks and leptons. We also discuss the flavor mixing and CP violation in the quark sector. Observational problems on the SM, in particular, the neutrino oscillation phenomena and the existence of dark matter are introduced. In Chapter 4, we review the minimal $U(1)$ extended SM as a simple extension of the SM to incorporate the neutrino masses and flavor mixings. We first discuss the minimal $B-L$ model, and give detailed structure of the model. Next, we generalize the $B-L$ model to the minimal $U(1)_X$ model. In Chapter 5, LHC physics is briefly reviewed. We present the cross section formula of a process to produce a dilepton final state l^+l^- at the LHC. Chapter 6 and 7 are our original works in [45, 46]. In Chapter 6, we discuss one of the main topics in this thesis: Z'_{B-L} portal dark matter in the minimal $B-L$ extended SM. We discuss a complementarity between the cosmological and the LHC constraints, and identify the allowed parameter region. In Chapter 7, the other main topic is discussed: Z' portal dark matter in the minimal $U(1)_X$ extended SM. Here, we generalize the $B-L$ gauge symmetry to the $U(1)_X$ gauge symmetry. We discuss a complementarity between the cosmological and the LHC constraints, and identify the allowed parameter region. Chapter 8 is devoted to conclusions and future plans. In Appendix A, we discussed the rephasing of quarks to eliminate unphysical degrees of freedom from the quark mass matrices.

Chapter 2

Particle cosmology

2.1 Big Bang cosmology

Edwin Powell Hubble measured the distances and the red shifts of spectra for twenty four galaxies, and led to the so-called Hubble law in 1929 [47]:

$$v = H_0 d, \tag{2.1.1}$$

where v and d are recession velocity and distance of a galaxy, and the constant of proportionality H_0 is called the Hubble constant. This is the discovery of the expanding universe and also suggests the universe is isotropic and homogeneous. The Hubble law is well described by the Big Bang cosmology, the standard cosmological model of the expanding universe, developed in the twentieth century. Based on the theory, the early universe was in an extremely hot and dense state, and the present universe, which is cold and dilute, is a result from the expansion. In the following, we briefly review the Big Bang cosmology.

The evolution of the universe is described by the Einstein equation given by (for a review, see, for example, [48])

$$R_{\mu\nu} - \frac{1}{2} g_{\mu\nu} R + \Lambda g_{\mu\nu} = 8\pi G T_{\mu\nu}, \tag{2.1.2}$$

where $R_{\mu\nu}$, R, $g_{\mu\nu}$ and $T_{\mu\nu}$ are the Ricci tensor, the scalar curvature, the metric and the energy-momentum tensor, respectively. $G = 1/M_{pl}^2$ is the gravitational constant with the Planck mass ($M_{pl} = 1.22 \times 10^{19}$ GeV) and Λ is a cosmological constant. The left-hand side of (2.1.2) describes a geometry of the universe, which is determined by the energy-momentum tensor.

Since the universe is observed to be isotropic and homogeneous in large scales over 100 Mpc [49], we adopt the Friedmann-Robertson-Walker metric in the spherical coordinates [48],

$$ds^2 = dt^2 - a(t)^2 \left[\frac{dr^2}{1 - Kr^2} + r^2 d\Omega^2 \right], \tag{2.1.3}$$

and solve (2.1.2). Here, $a(t)$ is the so-called scale factor, which parametrizes the size of the universe, K is the curvature constant ($K = +1,\ 0,\ -1$ correspond to open, flat, closed universe, respectively), and $d\Omega$ is the solid angle, $d\Omega^2 = d\theta^2 + \sin^2\theta d\phi^2$. In the following, we set $K = 0$ according to the observational results that our universe is very flat [17]. In the perfect fluid approximation, the energy-momentum tensor is given by

$$T^\mu_\nu = \mathrm{diag}(\rho, -p, -p, -p), \tag{2.1.4}$$

where ρ and p are the energy density and the pressure of the universe, respectively.

Non-vanishing components in (2.1.2) turn out to be the (0,0)- and (i, i)-components. The (0,0)-component leads to the Friedmann equation,

$$\left(\frac{\dot{a}}{a}\right)^2 = H^2 = \frac{1}{3M_p^2}\rho + \frac{\Lambda}{3}, \tag{2.1.5}$$

where H is the expansion rate called the Hubble parameter, and $M_p = M_{pl}/\sqrt{8\pi} \simeq 2.44 \times 10^{18}$ GeV is the reduced Planck mass. The (i, i)-components ($i = 1, 2, 3$) lead to

$$2\left(\frac{\ddot{a}}{a}\right) + \left(\frac{\dot{a}}{a}\right)^2 = -\frac{1}{M_p^2}p + \Lambda. \tag{2.1.6}$$

Combining (2.1.5) and (2.1.6), we obtain the energy conservation law,

$$\frac{d\rho}{dt} + 3H(\rho + p) = 0. \tag{2.1.7}$$

(2.1.5) and (2.1.7) are the fundamental equations for the Big Bang cosmology.

We define the critical density as

$$\rho_{\mathrm{crit}} = 3M_p^2 H^2, \tag{2.1.8}$$

which coincides with the total energy density of the flat universe. Using the critical density, the density parameter of a state X (X = radiation, matter and cosmological constant) is defined by

$$\Omega_X \equiv \frac{\rho_X}{\rho_{\mathrm{crit}}}, \tag{2.1.9}$$

radiation	$w = 1/3$	$\rho \propto a^{-4}$	$a \propto t^{\frac{1}{2}}$
matter	$w = 0$	$\rho \propto a^{-3}$	$a \propto t^{\frac{2}{3}}$
cosmological constant	$w = -1$	$\rho =$ constant	$a \propto \mathrm{e}^{H_i t}$

Table 2.1: Solutions to the Friedman equation (2.1.5), when the total energy density is dominated by one state with $w = 1/3, 0, -1$.

where ρ_X is the energy density of X. We suppose that the total energy density of the universe consists of the energy densities of radiation ($\rho_{\rm rad}$), matter ($\rho_{\rm matter}$) and cosmological constant ($\rho_{\rm cc} = \Lambda M_p^2$) such that

$$\rho_{\rm total} = \rho_{\rm rad} + \rho_{\rm matter} + \rho_{\rm cc}, \tag{2.1.10}$$

and then we express the Friedmann equation (2.1.5) in terms of the density parameters as

$$\Omega_{\rm rad} + \Omega_{\rm matter} + \Omega_{\rm cc} = 1. \tag{2.1.11}$$

2.2 Thermal history

We specify an equation of state by

$$p = w\rho \tag{2.2.1}$$

with a constant w. Substituting (2.2.1) into (2.1.7), we obtain

$$\rho a^{3(1+w)} = \text{constant} \quad \rightarrow \quad \rho \propto a^{-3(1+w)}. \tag{2.2.2}$$

The values of $w = 1/3$, 0 and -1 correspond to the equation of state for radiation, matter and cosmological constant, respectively. When the total energy density is dominated by only one state with a fixed w, we can easily find a solution to the Friedmann equation as $a \propto \mathrm{e}^{H_i t}$ ($w = -1$), where $H_i = \sqrt{\Lambda/3}$, and $a \propto t^{\alpha}$ ($w \neq -1$) with

$$\alpha = \frac{2}{3(1+w)}. \tag{2.2.3}$$

These results are summarized in Table 2.1.

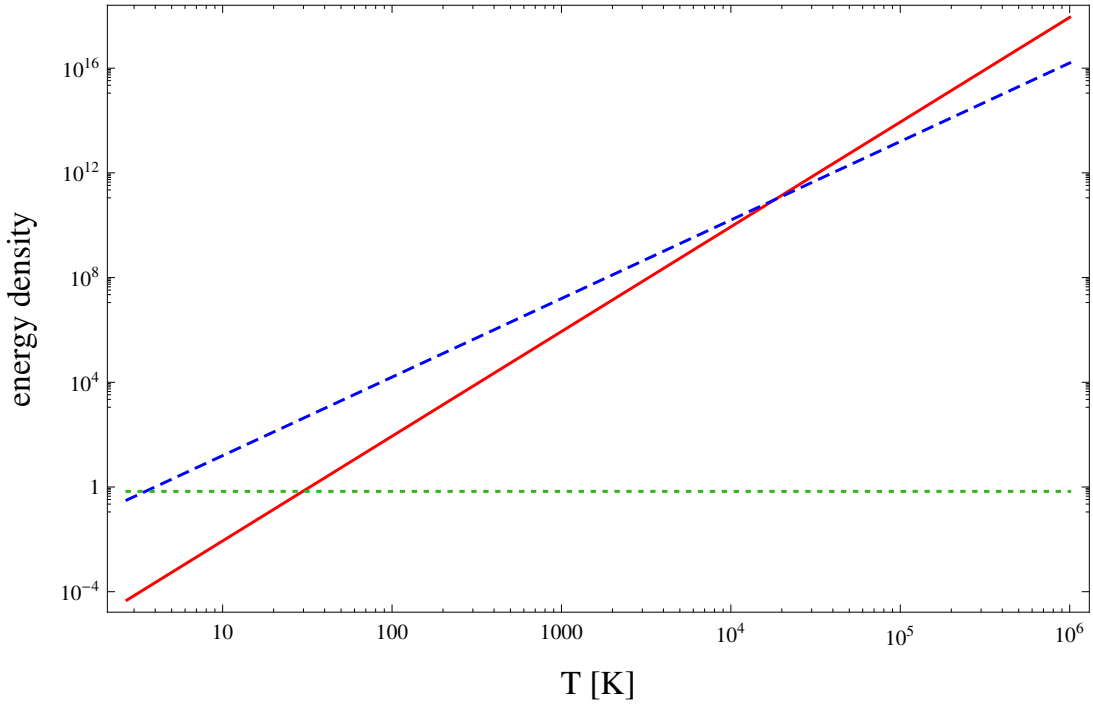

Figure 2.1: The evolutions of the energy densities of radiation (solid line), matter (dashed line) and cosmological constant (horizontal dotted line), as a function of temperature of the universe.

From Table 2.1, the energy densities in the early universe are given by

$$\begin{aligned} \rho_{\rm cc} &= \rho^0_{\rm cc}, \\ \rho_{\rm matter} &= \rho^0_{\rm matter}\left(\frac{a_0}{a}\right)^3, \\ \rho_{\rm rad} &= \rho^0_{\rm rad}\left(\frac{a_0}{a}\right)^4, \end{aligned} \tag{2.2.4}$$

where quantities with subscript/superscript 0 are the values in the present universe. From the results of the Planck satellite observation (Planck 2015 results) [50], the ratio of the energy densities in the present universe is determined as

$$\rho^0_{\rm cc} : \rho^0_{\rm matter} : \rho^0_{\rm rad} \simeq 0.68 : 0.32 : 4.8 \times 10^{-5}. \tag{2.2.5}$$

According to (2.2.4), the relations among $\rho_{\rm rad}$, $\rho_{\rm matter}$ and $\rho_{\rm cc}$ evolve from the early time to the present as follows:

1. $\rho_{\rm rad} \gg \rho_{\rm matter} \gg \rho_{\rm cc}$

2. $\rho_{\rm rad} = \rho_{\rm matter} \gg \rho_{\rm cc}$

3. $\rho_{\rm matter} \gg \rho_{\rm rad} \gg \rho_{\rm cc}$

4. $\rho_{\rm matter} \gg \rho_{\rm rad} = \rho_{\rm cc}$

5. $\rho_{\rm matter} \gg \rho_{\rm cc} \gg \rho_{\rm rad}$

6. $\rho_{\rm matter} = \rho_{\rm cc} \gg \rho_{\rm rad}$

7. $\rho_{\rm cc} > \rho_{\rm matter} \gg \rho_{\rm rad}$ (at present)

Since a becomes smaller back in time, it is clear from (2.2.4) that $\rho_{\rm rad}$ dominates in the very early time. This era between 1 to 2 is called the radiation dominated era. After the so-called equal epoch, 2, the era between 2 to 6 is called the matter dominated era. The present universe is in the epoch 7 (see (2.2.5)), and the expansion is accelerated. Figure 2.1 shows the evolution of the energy densities.

2.2.1 Equilibrium thermodynamics

As mentioned previously, the early universe was in a very hot and dense thermal plasma state, where all SM particles were in thermal equilibrium. In the following, let us discuss the properties of thermodynamic variables of a particle X in thermal equilibrium: number density, energy density, pressure and entropy density.

The phase space distribution of the particle X is given by

$$f(\vec{p}) = \frac{1}{{\rm e}^{\frac{E-\mu}{T}} \pm 1}, \tag{2.2.6}$$

where E and μ are the energy and the chemical potential of the particle X, T is the temperature of the system, and the $+$ and $-$ signs are for fermions and bosons, respectively. In the following discussion, we neglect the chemical potential μ, since $E \gg |\mu|$ in the early universe. The number density (n_X), energy density (ρ_X) and pressure (p_X) of the particle X are given in terms of $f(\vec{p})$:

$$\begin{aligned} n_X &= \frac{g_X}{(2\pi)^3} \int d^3p f(\vec{p}), \\ \rho_X &= \frac{g_X}{(2\pi)^3} \int d^3p E(\vec{p}) f(\vec{p}), \\ p_X &= \frac{g_X}{(2\pi)^4} \int d^3p \frac{|\vec{p}|^2}{3E(\vec{p})} f(\vec{p}). \end{aligned} \tag{2.2.7}$$

Here, g_X is the number of degrees of freedom of the particle X. For example, $g_X = 2$ for photon, and $g_X = 1$ for a real scalar. Rewriting $d^3p = 4\pi\sqrt{E^2 - m_X^2}EdE$, we have

$$\begin{aligned} n_X &= \frac{g_X}{2\pi^2}\int_{m_X}^{\infty} EdE\frac{\sqrt{E^2 - m_X^2}}{\mathrm{e}^{\frac{E}{T}} \pm 1}, \\ \rho_X &= \frac{g_X}{2\pi^2}\int_{m_X}^{\infty} E^2dE\frac{\sqrt{E^2 - m_X^2}}{\mathrm{e}^{\frac{E}{T}} \pm 1}, \\ p_X &= \frac{g_X}{6\pi^2}\int_{m_X}^{\infty} dE\frac{(\sqrt{E^2 - m_X^2})^3}{\mathrm{e}^{\frac{E}{T}} \pm 1}. \end{aligned} \tag{2.2.8}$$

In the relativistic limit, $T \gg m_X$,

$$\begin{aligned} n_X &= \begin{cases} \dfrac{\zeta(3)}{\pi^2}g_XT^3 & \text{(Bose-Einstein)} \\ \dfrac{3}{4}\dfrac{\zeta(3)}{\pi^2}g_XT^3 & \text{(Fermi-Dirac)}, \end{cases} \\ \rho_X &= \begin{cases} \dfrac{\pi^2}{30}g_XT^4 & \text{(Bose-Einstein)} \\ \dfrac{7}{8}\dfrac{\pi^2}{30}g_XT^4 & \text{(Fermi-Dirac)}, \end{cases} \\ p_X &= \frac{1}{3}\rho_X, \end{aligned} \tag{2.2.9}$$

where $\zeta(3)$ is the Riemann zeta function at 3 given by $\zeta(3) \simeq 1.20206$. In non-relativistic limit, $T \ll m_X$,

$$\begin{aligned} n_X &= g_X\left(\frac{m_XT}{2\pi}\right)^{\frac{3}{2}}\mathrm{e}^{-\frac{m_X}{T}}, \\ \rho_X &= m_Xn_X, \\ p_X &= n_XT. \end{aligned} \tag{2.2.10}$$

Using the fundamental thermodynamic relation for an equilibrium system,

$$dU = TdS - pdV, \tag{2.2.11}$$

where U, S and V are the total energy, the total entropy and the volume of the system, respectively, we have

$$d\rho - Tds = (Ts - \rho - p)\frac{dV}{V}. \tag{2.2.12}$$

Here, $\rho = U/V$ and $s = S/V$ are the energy density and the entropy density, respectively. Since $\rho(T)$ and $s(T)$ are functions of T, the left-hand side is proportional to dT,

$$d\rho - Tds \propto dT. \tag{2.2.13}$$

On the other hand, the right-hand side is proportional to dV independent of dT, and hence (2.2.12) can be satisfied only if the coefficients of dT (left-hand side) and dV (right-hand side) vanish. Thus, we express the entropy density as

$$s = \frac{\rho + p}{T} = \frac{2\pi^2}{45} g_* T^3, \tag{2.2.14}$$

where in the last equality we have used (2.2.9) in the radiation dominated era, and g_* is the effective number of degrees of freedom given by

$$g_* = \sum_i g_B^i + \frac{7}{8} \sum_i g_F^i. \tag{2.2.15}$$

Here, g_B^i and g_F^i are the degrees of freedom of bosons and fermions of i species, respectively. For the SM, $g_* = 106.75$ when all the SM particles are in the relativistic limit. Taking a variation of (2.2.11) with respect to t,

$$\begin{aligned} \frac{dS}{dt} &= \frac{1}{T}\left(\frac{dU}{dt} + p\frac{dV}{dt}\right) \\ &= \frac{V}{T}\left(\frac{d\rho}{dt} + 3H(\rho + p)\right) = 0, \end{aligned} \tag{2.2.16}$$

where in the last equality, we have used (2.1.7). Therefore, the total entropy of the universe is conserved. Combining $S \propto sa^3 =$ constant with (2.2.14), we find a relation between the scale factor (a) and the temperature of a radiation (T) such that $a \propto T^{-1}$, and the temperature decreases along with the expansion of the universe. Using this relation, the scale of the universe can be measured by the temperature of a radiation, for example, photon, independently of what dominates the energy density of the universe.

2.2.2 Era of dark matter physics

Since we have found $a \propto T^{-1}$ (from now on, T is the temperature of photon), we consider the evolution of the universe in terms of the photon temperature of the universe. Using the ratio of the energy densities (2.2.5) and the temperature ($T_0 = 2.73$ K$= 2.35 \times 10^{-4}$ eV) [51] in the present universe, let us calculate the temperature at typical epochs in the thermal history of the universe. At the epoch of $\rho_{\rm matter} = \rho_{\rm cc}$, we find $T = 3.50$ K$= 3.02 \times 10^{-4}$ eV, while $T = 29.7$ K$= 2.56 \times 10^{-3}$ eV at the epoch of $\rho_{\rm rad} = \rho_{\rm cc}$. The equal epoch is defined as $\rho_{\rm rad}(T_e) = \rho_{\rm matter}(T_e)$, at which $T_e = 1.82 \times 10^4$ K$= 1.56$ eV.

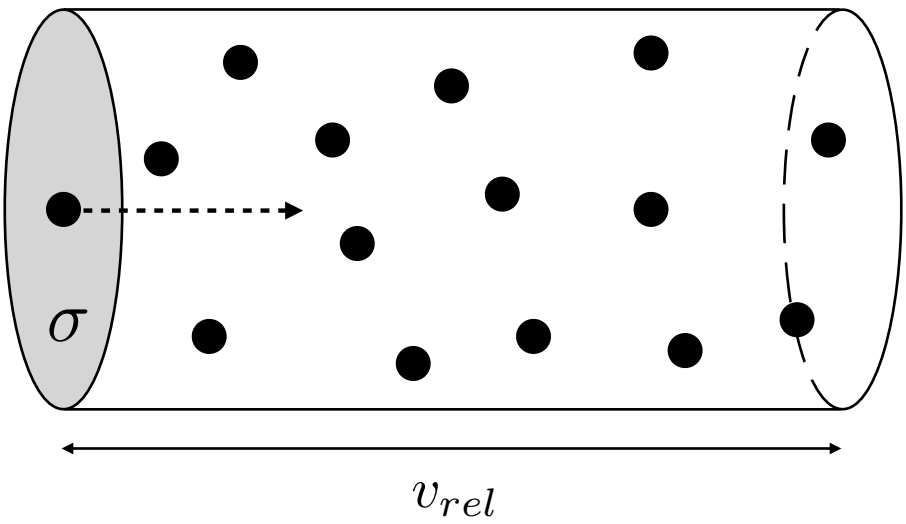

Figure 2.2: Schematic picture of the annihilation rate of X particles (black dots). The leftmost X particle moves to the right with a velocity v_{rel} in the frame where the others are at rest. Here, σ (shaded area) is the annihilation cross section of X particle, and v_{rel} is a traveling distance of X per unit time. The leftmost X collides (annihilates) with Xs inside the cylinder per unit time.

In this thesis, we consider the radiation dominated era ($T > T_e$) for discussion about Weakly Interacting Massive Particle (WIMP) dark matter, since a typical scale of WIMP dark matter physics is around the TeV scale (see the following sections). The total energy density of the universe in the radiation dominated era is approximately

$$\rho_{\text{total}} = \rho_{\text{rad}} = \frac{\pi^2}{30} g_* T^4, \tag{2.2.17}$$

and hence the Friedmann equation is given by

$$H^2 = \frac{\pi^2}{90} g_* \frac{T^4}{M_p^2}. \tag{2.2.18}$$

2.3 Decoupling from the equilibrium system

In the radiation dominated era at a very high temperature, particles are in thermal equilibrium. Due to the expansion, the temperature of the universe goes down and some

particles decouple from the equilibrium system. This phenomenon is called "decoupling". Here, we discuss the physics of decoupling.

We consider a thermal equilibrium system of particles X and Y in an expanding universe. When X and Y are in thermal equilibrium, the pair annihilation/creation processes $XX \to YY$ and $YY \to XX$ arise as the same rate. To simplify our discussion, suppose X is heavy with a mass of, say, $m_X = 1$ TeV, while Y is massless. Along with the expansion, the temperature of the universe and the number densities of X and Y are decreasing. In particular, for temperature $T < m_X$ the particle X becomes non-relativistic, and the number density of X is exponentially suppressed by the Boltzmann factor $\mathrm{e}^{-m_X/T}$.

Certain temperature (T_D) at which a particle decouples from the thermal equilibrium system is called "decoupling temperature." It is well known that the decoupling temperature is roughly estimated by [48]

$$\Gamma_X(T_D) = H(T_D). \tag{2.3.1}$$

Here, $\Gamma_X(T_D)$ is the pair annihilation rate of X, and $H(T_D)$ is the Hubble parameter at the temperature T_D. Γ_X is given by

$$\Gamma_X = n_X \langle \sigma v_{\mathrm{rel}} \rangle, \tag{2.3.2}$$

where n_X is the number density of X, v_{rel} is a relative velocity (the traveling distance of X per unit time), and $\langle \sigma v_{\mathrm{rel}} \rangle$ is the thermal average of the annihilation cross section times relative velocity. Thus, $\langle \sigma v_{\mathrm{rel}} \rangle$ is the volume of the cylinder in Figure 2.2). The leftmost X particle collides (annihilates) with X particles inside the cylinder, and Γ_X is the number of collisions of leftmost X per unit time. Since $t_H = 1/H$ is a typical time scale of the expansion universe (an age of the universe estimated by the expansion rate), (2.3.1) means that the number of collisions (N_X) for time interval t_H is 1.

Let us see what happens before or after the decoupling. Since $\Gamma_X(T) = n_X \langle \sigma v_{\mathrm{rel}} \rangle \propto \mathrm{e}^{-m_X/T}$ in the non-relativistic limit ($T < m_X$) and $H(T) \propto T^2$ (see (2.2.10) and (2.2.18)), $\Gamma_X(T)$ decreases more rapidly than $H(T)$ as the temperature goes down. In an early time ($T > T_D$), the annihilation rate is greater than the Hubble parameter, $\Gamma_X(T) > H(T)$, which means $N_X > 1$ and thus X and Y are in the thermal equilibrium system. The temperature goes down along with the expansion of the universe, then Γ_X becomes

comparable with H at the temperature T_D, the decoupling temperature, at which $N_X \sim 1$. After the decoupling ($T < T_D$), $\Gamma_X(T) < H(T)$, which means $N_X < 1$ and thus X particles no longer annihilate.

2.4 Dark matter physics

In 1930s, Fritz Zwicky estimated the mass of the Coma Cluster. Assuming the Coma Cluster is in a mechanical equilibrium, we can estimate the mass of the cluster from the velocity distribution of galaxies in the cluster. We can also estimate the mass from the brightness of galaxies. Zwicky found that the mass from the velocity distribution was smaller than the one from the brightness. The total mass of the optically observed galaxies was not enough to cause the observed revolutions of galaxies in the cluster. This is the so-called missing mass problem. In order to solve this problem, Zwicky proposed a matter that we can not optically observe, "dark matter" [52]. Dark matter carries the missing mass.

2.4.1 Evidences of dark matter

One of the clear evidences for the existence of dark matter is the galaxy rotation curve, which is a relation between distances of stars from the galactic center and their speeds of revolution. In 1980s, galaxy rotation curves were measured for various galaxies. From Newtonian mechanics, a circular velocity $v_c(r)$ of a star is given by

$$v_c(r) = \sqrt{\frac{GM(r)}{r}}, \tag{2.4.1}$$

where r and $M(r)$ are a radius from the center of galaxy and the total mass inside the radius (enclosed mass), respectively. If the mass is concentrated in the galactic disk, the enclosed mass $M(r)$ is constant for r greater than the radius of the galactic disk. In this case, the circular velocity is given by

$$v_c(r) \propto r^{-1/2}. \tag{2.4.2}$$

However, the observed results show that the circular velocity is almost constant (see Figure 2.3). This discrepancy between the observational results and the expectation is called the galactic rotation problem. The observational results suggest

$$M(r) \propto r, \tag{2.4.3}$$

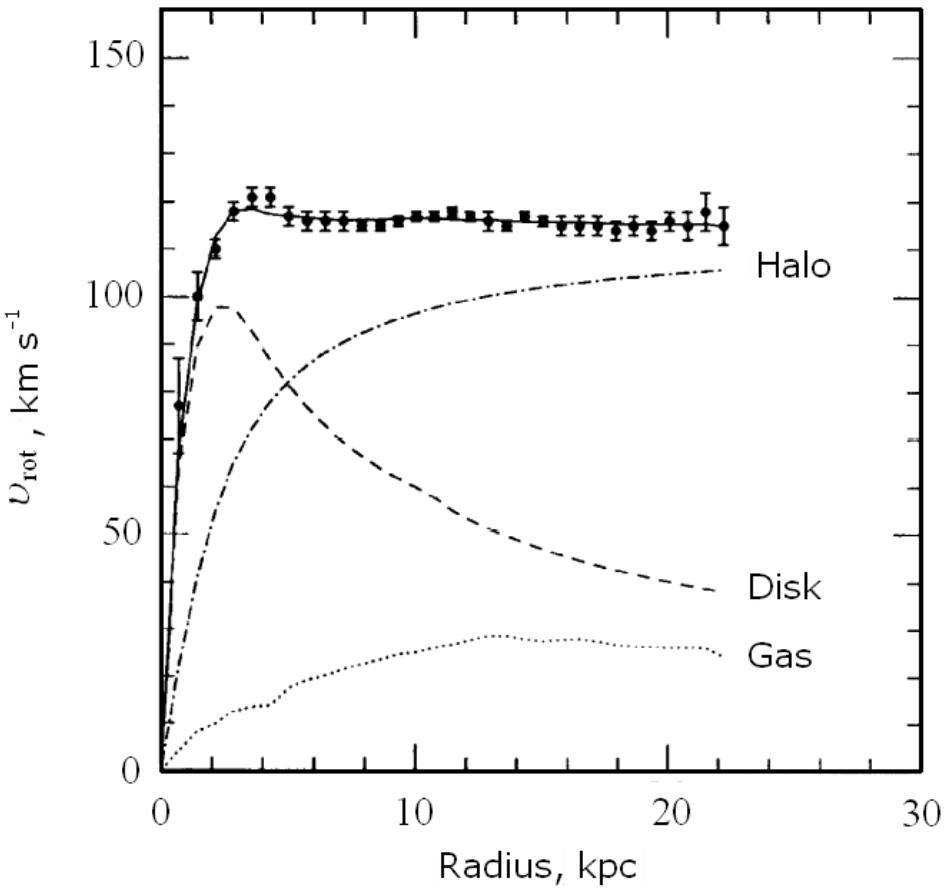

Figure 2.3: The rotation curve of galaxy NGC 6503 [53]. The dark matter halo contribution is shown by the dashed-dotted line.

which implies that optically unobservable matters exist beyond the radius of the galactic disk. This is an evidence of dark matter.

Another evidence of the dark matter has been seen in the observations in the anisotropy of the cosmic microwave back ground (CMB). Since the power spectrum of the CMB relates the energy budget of the universe, precise measurements can reveal the existence of the dark matter. The Cosmic Background Explorer (COBE) [51] is the first satellite for precision measurements of the CMB. The COBE observed that the energy distribution of the CMB obeys the Planck distribution for $T_0 = 2.73$ K in the accuracy of 10^{-4}. It also measured the anisotropy of the CMB and found that the fluctuation of the temperature of the CMB is extremely small, $\delta T_0/T_0 \simeq 10^{-5}$, but non-zero. The COBE satellite

experiment is the pioneer of precision cosmology. To determine the energy budget of the dark matter, more precise measurements were necessary. After the COBE satellite, the Wilkinson Microwave Anisotropy Probe (WMAP) [15] and the Planck satellite [16] measured the CMB anisotropy with greatly improved resolutions and sensitivities, and determined the energy budget very precisely. The energy budget of the present universe is determined to be composed of 73% dark energy, 23% cold dark matter and only 4% from baryonic matter [17].

2.4.2 Weakly Interacting Massive Particle as dark matter candidate

It is a prime question in particle physics and cosmology to identify the properties of the dark matter particle. One of the most promising candidates for the dark matter in the present universe is the so-called Weakly Interacting Massive Particle (WIMP), which was in thermal equilibrium in the early universe and its relic density is determined by the interactions with the SM particles. In this thesis, we consider a WIMP as the cold dark matter.

In the next subsection, we will evaluate the thermal relic density of a dark matter. We will see that the scale of the interactions of dark matter with SM particles is around the weak scale to reproduce the observed dark matter density.

2.4.3 Thermal relic density of WIMP

In order to evaluate the dark matter relic density, we need to know a time-evolution of the total number of dark matter particle in the universe ($N_{\rm DM}$). The time-evolution is described by the Boltzmann equation expressed as

$$\frac{dN_{\rm DM}(t)}{dt} = V(t)\Lambda_{\rm DM}(t) - \Gamma_{\rm DM}(t)N_{\rm DM}(t), \tag{2.4.4}$$

where V is the volume of the universe, and $\Lambda_{\rm DM}$ and $\Gamma_{\rm DM}$ are the creation and annihilation rates of the dark matter particles, respectively. When dark matter particles are in thermal equilibrium with SM particles in the early universe, dark matter pair annihilation/creation is comparable in rate to SM particle pair creation/annihilation,

$$V\Lambda_{\rm DM} = \Gamma^{\rm eq}_{\rm DM}N^{\rm eq}_{\rm DM}. \tag{2.4.5}$$

Here, $N_{\rm DM}^{\rm eq}$ is the total number of dark matter particles in the thermal equilibrium, and $\Gamma_{\rm DM}^{\rm eq}$ is the annihilation rate in the thermal equilibrium, which can be expressed $\Gamma_{\rm DM}^{\rm eq} = n_{\rm DM}^{\rm eq}\langle\sigma v_{\rm rel}\rangle$ with $n_{\rm DM}^{\rm eq} = N_{\rm DM}^{\rm eq}/V$ being the number density of dark matter in thermal equilibrium. Using

$$\Lambda_{\rm DM} = \Gamma_{\rm DM}^{\rm eq}\frac{N_{\rm DM}^{\rm eq}}{V} = (n_{\rm DM}^{\rm eq})^2\langle\sigma v_{\rm rel}\rangle, \tag{2.4.6}$$

the Boltzmann equation is rewritten as

$$\frac{dn_{\rm DM}}{dt} + 3Hn_{\rm DM} = -\langle\sigma v_{\rm rel}\rangle(n_{\rm DM}^2 - (n_{\rm DM}^{\rm eq})^2), \tag{2.4.7}$$

where we have used $V \propto a(t)^3$ and $dV/dt = 3HV$. We further rewrite the Boltzmann equation. The relation $s \propto a^{-3}$ leads to

$$\frac{ds}{dt} = -3sH. \tag{2.4.8}$$

We define the dimensionless quantities

$$x \equiv \frac{m_{\rm DM}}{T}, \tag{2.4.9}$$

$$Y_{\rm DM} \equiv \frac{n_{\rm DM}}{s}, \tag{2.4.10}$$

where $m_{\rm DM}$ is the dark matter mass, and $Y_{\rm DM}$ is the so-called yield, which means a comoving number density. The relation $T \propto a^{-1}$ leads to

$$\frac{d}{dt} = \frac{dx}{dt}\frac{d}{dx} = xH\frac{d}{dx}. \tag{2.4.11}$$

Using (2.4.8)-(2.4.11), we rewrite (2.4.7) to

$$\frac{dY_{\rm DM}}{dx} = -\frac{s\langle\sigma v_{\rm rel}\rangle}{xH}(Y_{\rm DM}^2 - (Y_{\rm DM}^{\rm eq})^2). \tag{2.4.12}$$

Since $H \propto T^2$ and $s \propto T^3$, we express

$$\begin{aligned} H(T) &= \frac{H(m_{\rm DM})}{x^2}, \\ s(T) &= \frac{s(m_{\rm DM})}{x^3} \end{aligned} \tag{2.4.13}$$

and obtain the final expression:

$$\frac{dY_{\rm DM}}{dx} = -\frac{s(m_{\rm DM})\langle\sigma v_{\rm rel}\rangle}{x^2H(m_{\rm DM})}(Y_{\rm DM}^2 - (Y_{\rm DM}^{\rm eq})^2). \tag{2.4.14}$$

Now we approximately solve the Boltzmann equation (2.4.14) for the dark matter particle which decouples in the non-relativistic regime, $x > 1$ (such a dark matter particle is called "cold dark matter"). For simplicity, we parametrize

$$\langle \sigma v_{\rm rel} \rangle = \sigma_n x^{-n}, \tag{2.4.15}$$

where σ_n is a constant, and $n = 0$ and 1 correspond to dark matter pair annihilation processes through the s-wave and the p-wave, respectively, and obtain

$$\frac{dY_{\rm DM}}{dx} = \frac{\lambda_n}{x^{n+2}}(Y_{\rm DM}^2 - (Y_{\rm DM}^{\rm eq})^2) \tag{2.4.16}$$

with

$$\begin{aligned} \lambda_n &= \frac{s(m_{\rm DM})}{H(m_{\rm DM})}\sigma_n \\ &= \frac{\frac{2\pi^2}{45} g_* m_{\rm DM}^3}{\sqrt{\frac{1}{3M_p^2}\frac{\pi^2}{30} g_* m_{\rm DM}^4}}\sigma_n \simeq 1.32\sqrt{g_*} M_p m_{\rm DM} \sigma_n. \end{aligned} \tag{2.4.17}$$

From (2.2.10) and (2.2.14),

$$Y_{\rm DM}^{\rm eq} = \frac{n_{\rm DM}^{\rm eq}}{s} \simeq 0.145 \frac{g_{\rm DM}}{g_*} x^{3/2} {\rm e}^{-x}, \tag{2.4.18}$$

where $g_{\rm DM}$ is the degrees of freedom of dark matter particle.

We first consider a small deviation of $Y_{\rm DM}$ from its thermal equilibrium value,

$$Y_{\rm DM} = Y_{\rm DM}^{\rm eq} + \Delta \quad (\Delta \ll Y_{\rm DM}^{\rm eq}). \tag{2.4.19}$$

The first derivative of $Y_{\rm DM}$ with respect to x is approximately given by

$$\frac{dY_{\rm DM}}{dx} = \frac{dY_{\rm DM}^{\rm eq}}{dx} + \frac{d\Delta}{dx} \simeq \frac{dY_{\rm DM}^{\rm eq}}{dx} \simeq -Y_{\rm DM}^{\rm eq}, \tag{2.4.20}$$

where we have used $Y_{\rm DM}^{\rm eq} \sim {\rm e}^{-x}$. The Boltzmann equation (2.4.16) is approximately

$$-Y_{\rm DM}^{\rm eq} \simeq -\frac{\lambda_n}{x^{n+2}} 2 Y_{\rm DM}^{\rm eq} \Delta, \tag{2.4.21}$$

and hence

$$\Delta \simeq \frac{x^{n+2}}{2\lambda_n}. \tag{2.4.22}$$

The small deviation Δ grows as x becomes larger, or equivalently the universe evolves.

Next, we define x_d (the value of x at the decoupling) by $\Delta(x_d) = Y_{\rm DM}^{\rm eq}(x_d)$. For $x > x_d$, $\Delta(x) \gg Y_{\rm DM}^{\rm eq}(x)$ and the Boltzmann equation is simplified as

$$\frac{d\Delta}{dx} \simeq -\frac{\lambda_n}{x^{n+2}}\Delta^2, \tag{2.4.23}$$

and integrating from x_d to x, we find

$$\frac{1}{\Delta(x)} - \frac{1}{\Delta(x_d)} \simeq \frac{\lambda_n}{n+1}\left(\frac{1}{x_d^{n+1}} - \frac{1}{x^{n+1}}\right). \tag{2.4.24}$$

In the limit $x \to \infty$, we obtain the final expression of the approximate solution to the Boltzmann equation:

$$\begin{aligned} \Delta(\infty) \simeq Y_{\rm DM}(\infty) &\simeq \frac{(n+1)x_d^{n+1}}{\lambda_n} \\ &= \frac{(n+1)x_d^{n+1}}{1.32\sqrt{g_*}M_p m_{\rm DM}\langle\sigma v_{\rm rel}\rangle_{x_d}}. \end{aligned} \tag{2.4.25}$$

The energy density of dark matter in the present universe is given by

$$\begin{aligned} \rho_{\rm DM}(T_0) &= m_{\rm DM} n_{\rm DM}(T_0) \\ &\simeq m_{\rm DM} Y(\infty) s_0 \\ &\simeq \frac{(n+1)x_d s_0}{1.32\sqrt{g_*}M_p\langle\sigma v_{\rm rel}\rangle_{x_d}}. \end{aligned} \tag{2.4.26}$$

We express the thermal relic density in terms of the density parameter,

$$\begin{aligned} \Omega_{\rm DM}h^2 &= \frac{\rho_{\rm DM}(T_0)}{\rho_{\rm crit}^0}h^2 \\ &= 8.7\times 10^{-11}[{\rm GeV}^{-2}] \times \frac{(n+1)x_d}{\sqrt{g_*}\langle\sigma v_{\rm rel}\rangle_{x_d}}. \end{aligned} \tag{2.4.27}$$

Note that the thermal relic density of a dark matter particle is controlled by its annihilation cross section (in the following discussion, we will see $x_d \sim 20$ for a WIMP dark matter). For $g_* = 100$ and $n = 1$, we have

$$\Omega_{\rm DM}h^2 \simeq \frac{10^{-10}[{\rm GeV}^{-2}]}{\langle\sigma v_{\rm rel}\rangle} \tag{2.4.28}$$

In order to reproduce the observed dark matter relic density, $\Omega_{\rm DM}h^2 \simeq 0.1$ [50], the annihilation cross section is found to be

$$\begin{aligned} \langle\sigma v_{\rm rel}\rangle &\simeq 10^{-9}[{\rm GeV}^{-2}] \\ &\simeq 1 \text{ pb}. \end{aligned} \tag{2.4.29}$$

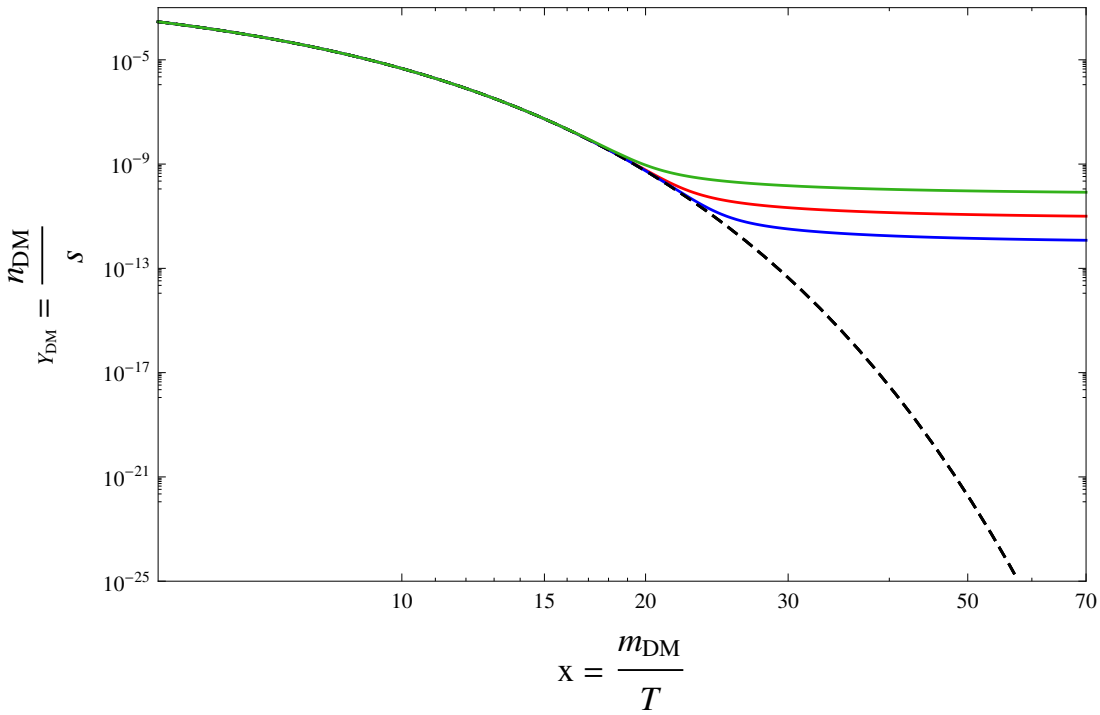

Figure 2.4: Numerical solutions for σ_0 [GeV^{-2}] $= 10^{-10}$ (upper (green) solid line), 10^{-9} (middle (red) solid line), and 10^{-8} (lower (blue) solid line), respectively, along with $Y_{\rm DM}^{\rm eq}$ (dashed line).

We may parametrize the annihilation cross section as

$$\langle \sigma v_{\rm rel} \rangle \simeq \frac{1}{16\pi} \left(\frac{1}{\Lambda_{\rm DM}} \right)^2 . \tag{2.4.30}$$

Note that a typical scale of the physics of the dark matter annihilation is roughly $\Lambda_{\rm DM} \simeq 1$ TeV, which is close to the weak scale. This is the reason why we call this cold dark matter "WIMP."

Let us now calculate the dark matter relic density by numerically solving the Boltzmann equation (2.4.14). For simplicity, we take

$$\begin{aligned} \langle \sigma v_{\rm rel} \rangle &= \sigma_0, \\ m_{\rm DM} &= 1 \text{ TeV}, \\ g_* &= 106.75, \\ g_{\rm DM} &= 2. \end{aligned} \tag{2.4.31}$$

In Figure 2.4, we show the numerical solutions for σ_0 [GeV^{-2}] $= 10^{-10}$ (upper (green) solid line), 10^{-9} (middle (red) solid line), and 10^{-8} (lower (blue) solid line), respectively, along with $Y_{\rm DM}^{\rm eq}$ (dashed line). For small x values, the yield $Y_{\rm DM}(x)$ traces $Y_{\rm DM}^{\rm eq}$, the yield starts deviating from its equilibrium value at $x = x_d \sim 20$ (decoupling), and it eventually becomes constant. As the annihilation cross section increases, the resultant relic density decreases. From our numerical results, we can see (2.4.25) is a good approximation and $Y_{\rm DM}(\infty) \propto 1/\langle \sigma v_{\rm rel} \rangle$.

Chapter 3

The Standard Model

3.1 Particle content and Lagrangian

In Nature, there are four fundamental interactions, namely, strong, weak, electromagnetic and gravitational interactions. The strong interaction is mediated by gluons, and confines quarks to make up a nucleon. The weak interaction is mediated by weak bosons, by which a neutron decays into a proton, an electron and an anti-neutrino (beta-decay). Particles which posses electric charges interact with each other through the exchange of photons. This is the electromagnetic interaction. Gravitation is well described by Einstein's theory of general relativity. In the particle physics point of view, the gravitational interaction is mediated by "graviton."

The Standard Model (SM) is the best theory that describes elementary particles and the three (strong, weak, and electromagnetic) interactions among them. Theoretical framework of the SM is based on the gauge field theory, where the SM gauge groups and elementary particle content are introduced, and invariance of Lagrangian density under gauge (local) transformations is required (gauge principle). The SM is based on the gauge group $SU(3)_C \times SU(2)_L \times U(1)_Y$. Here $SU(3)_C$, $SU(2)_L$ and $U(1)_Y$ correspond to Quantum Chromodynamics, weak interaction and hypercharge interaction, respectively. The SM particle content is given in Table 3.2.

Lagrangian of the SM, which is required to be gauge invariant under the SM gauge

interaction	gauge boson	gauge symmetry
strong	gluon	$SU(3)_C$
weak	$W^{\pm}, Z$ boson	$SU(2)_L \times U(1)_Y$
electromagnetic	photon	

Table 3.1: Fundamental interactions in the Standard Model. The strong interaction is mediated by gluons, and confines quarks to make up a nucleon. The weak interaction is mediated by weak bosons, by which a neutron decays into a proton, an electron and an anti-neutrino (beta-decay). Particles which posses electric charges interact with each other through the exchange of photons. This is the electromagnetic interaction.

	$SU(3)_C$	$SU(2)_L$	$U(1)_Y$
$q_L^i = \begin{pmatrix} u_L^i \\ d_L^i \end{pmatrix}$	**3**	**2**	1/6
u_R^i	**3**	**1**	2/3
d_R^i	**3**	**1**	-1/3
$l_L^i = \begin{pmatrix} \nu_L^i \\ e_L^i \end{pmatrix}$	**1**	**2**	-1/2
e_R^i	**1**	**1**	-1
$H = \begin{pmatrix} H^0 \\ H^- \end{pmatrix}$	**1**	**2**	-1/2

Table 3.2: Particle content of the Standard Model. $i = 1, 2, 3$ is the generation index. q_L and l_L are left-handed quark and lepton $SU(2)_L$ doublets, respectively. u_R and d_R are, respectively, right-handed up-type and down-type quarks, while e_R is right-handed charged lepton. The $SU(2)_L$ Higgs doublet scalar is denoted as H.

transmations, is given by

$$\begin{aligned}
\mathcal{L}_{\rm SM} &= -\frac{1}{2}\mathrm{tr}[G^{\mu\nu}G_{\mu\nu}] - \frac{1}{2}\mathrm{tr}[F^{\mu\nu}F_{\mu\nu}] - \frac{1}{4}B^{\mu\nu}B_{\mu\nu} \\
&+ \overline{q_L^i} i\gamma^\mu \mathcal{D}_\mu q_L^i + \overline{l_L^i} i\gamma^\mu \mathcal{D}_\mu l_L^i \\
&+ \overline{u_R^i} i\gamma^\mu \mathcal{D}_\mu u_R^i + \overline{d_R^i} i\gamma^\mu \mathcal{D}_\mu d_R^i + \overline{e_R^i} i\gamma^\mu \mathcal{D}_\mu e_R^i \\
&+ (\mathcal{D}^\mu H)^\dagger (\mathcal{D}_\mu H) - \lambda \left(H^\dagger H - \frac{1}{2}v^2 \right)^2 \\
&- \{Y_u^{ij} \overline{q_L^i} H u_R^j + Y_d^{ij} \overline{q_L^i} \tilde{H} d_R^j + Y_e^{ij} \overline{l_L^i} \tilde{H} e_R^j + H.c.\},
\end{aligned} \tag{3.1.1}$$

where $G_{\mu\nu}$, $F_{\mu\nu}$ and $B_{\mu\nu}$ are field strengths of $SU(3)_C$, $SU(2)_L$ and $U(1)_Y$ gauge bosons

respectively,

$$\begin{aligned} G_{\mu\nu} &= \partial_\mu G_\nu - \partial_\nu G_\mu - i g_3 [G_\mu, G_\nu], \\ F_{\mu\nu} &= \partial_\mu A_\nu - \partial_\nu A_\mu - i g_2 [A_\mu, A_\nu], \\ B_{\mu\nu} &= \partial_\mu B_\nu - \partial_\nu B_\mu, \end{aligned} \tag{3.1.2}$$

and g_3, g_2 and g_1 are $SU(3)_C$, $SU(2)_L$ and $U(1)_Y$ gauge coupling constants, respectively. Here, Y_f^{ij} (i, $j = 1, 2, 3$ are the generation indices, and $f = u, d, e$) is the Yukawa coupling constant, $\tilde{H} \equiv -i\sigma_2 H$, and summation convention is assumed for the repeated indices i, j. Note that gauge bosons are massless because of the gauge invariance. However, the weak gauge bosons are known to be massive by experiments [3, 4]. In the next section, we discuss the Higgs mechanism, which generates masses for gauge bosons. The SM fermions acquire their masses from Higgs field as well.

3.2 Higgs mechanism

We first discuss a global $U(1)$ model with a complex scalar, whose $U(1)$ charge is Q. The Lagrangian invariant under the global $U(1)$ transformation, $\Phi \to \mathrm{e}^{iQ\alpha}\Phi$ (α is a constant phase), is given by

$$\mathcal{L}_{\text{scalar}} = (\partial^\mu \Phi)^\dagger (\partial_\mu \Phi) - V(\Phi), \tag{3.2.1}$$

where

$$V(\Phi) = \lambda \left(\Phi^\dagger \Phi - \frac{1}{2} v^2 \right)^2. \tag{3.2.2}$$

Here, λ is a positive coupling constant, and v is a positive constant with mass dimension one.

Potential minimum appears along $|\Phi| = v/\sqrt{2}$, and we choose the vacuum of our theory as

$$\langle \Phi \rangle = \frac{v}{\sqrt{2}}, \tag{3.2.3}$$

by which the global $U(1)$ symmetry is spontaneously broken. Introducing the physical real scalars (ϕ and χ) around the vacuum,

$$\Phi = \frac{1}{\sqrt{2}} (v + \phi + i\chi), \tag{3.2.4}$$

we rewrite the Lagrangian as

$$\mathcal{L}_{\text{scalar}} = \frac{1}{2}(\partial^\mu \phi)(\partial_\mu \phi) + \frac{1}{2}(\partial^\mu \chi)(\partial_\mu \chi) - V(\phi, \chi), \tag{3.2.5}$$

where

$$V(\phi, \chi) = \frac{1}{2}(2\lambda v^2)\phi^2 + \frac{\lambda}{4}(\phi^2 + \chi^2)^2 + \lambda v \phi(\phi^2 + \chi^2). \tag{3.2.6}$$

Note that the scalar ϕ has mass $\sqrt{2\lambda}v$ while χ is massless. The massless χ is nothing but the Nambu-Goldstone (NG) boson [54, 55, 56].

Spontaneous symmetry breaking in the context of a $U(1)$ gauge theory was proposed by Peter Higgs in 1964 [57], where the mass of the $U(1)$ gauge boson is generated (Higgs mechanism). We extend the previous global $U(1)$ model to its local version. The scalar Lagrangian, which is invariant under local $U(1)$ gauge transformation $\Phi \to \mathrm{e}^{iQ\alpha(x)}\Phi$, is given by

$$\mathcal{L}_{\text{scalar}} = (\mathcal{D}^\mu \Phi)^\dagger (\mathcal{D}_\mu \Phi) - V(\Phi). \tag{3.2.7}$$

Here, the covariant derivative $\mathcal{D}_\mu$ is defined by

$$\mathcal{D}_\mu = \partial_\mu - iQgB_\mu, \tag{3.2.8}$$

where B_μ and g are the $U(1)$ gauge boson and the gauge coupling, respectively. Note that a mass term of $U(1)$ gauge boson $(1/2)M_B^2 B_\mu B^\mu$ is forbidden because it is not invariant under the gauge transformation $B_\mu \to B_\mu + \partial_\mu \alpha$.

We choose the vacuum as

$$\langle \Phi \rangle = \frac{v}{\sqrt{2}} \tag{3.2.9}$$

by which the $U(1)$ gauge symmetry is spontaneously broken. We parametrize the scalar field around the vacuum as

$$\Phi = \frac{1}{\sqrt{2}}(v + \phi(x))\mathrm{e}^{i\zeta(x)}, \tag{3.2.10}$$

where $\zeta(x)$ is the so-called would-be NG boson.

We consider a gauge transformation with the gauge parameter to be $Q\alpha(x) = -\zeta(x)$, so that we can eliminate $\zeta(x)$ from the theory,

$$\Phi = \frac{1}{\sqrt{2}}(v + \phi(x)). \tag{3.2.11}$$

This gauge choice is the so-called unitary gauge. The physical real scalar $\phi(x)$ is the physical Higgs boson with the mass of

$$m_\phi = \sqrt{2\lambda}v. \tag{3.2.12}$$

Let us now calculate the mass of gauge field B_μ. In the unitary gauge,

$$(\mathcal{D}^\mu\Phi)^\dagger(\mathcal{D}_\mu\Phi) = \frac{1}{2}(\partial^\mu\phi(x))(\partial_\mu\phi(x)) + \frac{1}{2}(Qg)^2 B^\mu B_\mu(v+\phi(x))^2. \tag{3.2.13}$$

Therefore, the gauge field acquires its mass $m_B = Qgv$. In addition to the two degrees of freedom corresponding to the transverse modes, the massive gauge boson has one more degree of freedom corresponding to its longitudinal mode, which is supplied by the degree of freedom of the would-be NG boson. This is called the Higgs mechanism.

We should note here that the vacuum expectation value (VEV) of Higgs field plays a role of giving masses to the fermions, as will be seen in the next section.

3.3 Spontaneous symmetry breaking in the Standard Model

3.3.1 Weak gauge boson masses

In the SM, the electroweak gauge symmetry, $SU(2)_L \times U(1)_Y$, is spontaneously broken to the electromagnetic $U(1)_{em}$ gauge symmetry. We apply the previous discussion about the Higgs mechanism to the SM and calculate the weak gauge boson masses.

Lagrangian of the Higgs field

$$H = \begin{pmatrix} H^0 \\ H^- \end{pmatrix}, \tag{3.3.1}$$

$SU(2)_L$ doublet field, is given by

$$\mathcal{L}_{\text{Higgs}} = (\mathcal{D}^\mu H)^\dagger(\mathcal{D}_\mu H) - V(H). \tag{3.3.2}$$

Here, the covariant derivative is

$$\begin{aligned} \mathcal{D}_\mu &= \partial_\mu - ig_2 A_\mu - ig_1\left(-\frac{1}{2}\right)B_\mu \\ &= \begin{pmatrix} \partial_\mu + \frac{i}{2}(-g_2 A^3_\mu + g_1 B_\mu) & -\frac{i}{2}g_2(A^1_\mu - iA^2_\mu) \\ -\frac{i}{2}g_2(A^1_\mu + iA^2_\mu) & \partial_\mu + \frac{i}{2}(g_2 A^3_\mu + g_1 B_\mu) \end{pmatrix} \end{aligned} \tag{3.3.3}$$

where $A_\mu = (1/2)\sigma^i A^i_\mu (i = 1, 2, 3)$ with the Pauli matrices σ^i is the $SU(2)_L$ gauge boson, B_μ is the $U(1)_Y$ gauge boson, and g_1 (g_2) is the $U(1)_Y$ ($SU(2)_L$) gauge coupling constant. We define the charged vector bosons as complex combinations of A^1_μ and A^2_μ,

$$\begin{aligned} W^+_\mu &\equiv \frac{1}{\sqrt{2}}(A^1_\mu - iA^2_\mu), \\ (W^+_\mu)^* &= \frac{1}{\sqrt{2}}(A^1_\mu + iA^2_\mu) \equiv W^-_\mu. \end{aligned} \tag{3.3.4}$$

Furthermore the electric-charge neutral vector bosons are defined as

$$\begin{aligned} Z_\mu &\equiv A^3_\mu \cos\theta_W - B_\mu \sin\theta_W, \\ A^0_\mu &\equiv A^3_\mu \sin\theta_W + B_\mu \cos\theta_W, \end{aligned} \tag{3.3.5}$$

where

$$\cos\theta_W = \frac{g_2}{g_Z}, \quad \sin\theta_W = \frac{g_1}{g_Z}, \tag{3.3.6}$$

$g_Z \equiv \sqrt{g_1^2 + g_2^2}$, and θ_W is the weak mixing angle. Then we rewrite the covariant derivative as

$$\mathcal{D}_\mu = \begin{pmatrix} \partial_\mu - \frac{i}{2} g_Z Z_\mu & -\frac{i}{\sqrt{2}} g_2 W^+_\mu \\ -\frac{i}{\sqrt{2}} g_2 W^-_\mu & \partial_\mu + \frac{i}{2} g_Z (Z_\mu \cos 2\theta_W + A^0_\mu \sin 2\theta_W) \end{pmatrix}. \tag{3.3.7}$$

Choosing a VEV of Higgs boson as

$$\langle H \rangle = \frac{1}{\sqrt{2}} \begin{pmatrix} v \\ 0 \end{pmatrix}, \tag{3.3.8}$$

by which the electroweak symmetry is broken down to the electromagnetic symmetry ($SU(2)_L \times U(1)_Y \to U(1)_{em}$), we have

$$\mathcal{D}_\mu \langle H \rangle = \frac{1}{2} \begin{pmatrix} \frac{i}{\sqrt{2}} g_Z Z_\mu v \\ -i g_2 W^-_\mu v \end{pmatrix}, \tag{3.3.9}$$

$$(\mathcal{D}^\mu H)^\dagger (\mathcal{D}_\mu H) \supset \frac{1}{8} g_Z^2 v^2 Z^\mu Z_\mu + \frac{1}{4} g_2^2 v^2 W^{-\mu} W^+_\mu. \tag{3.3.10}$$

Here, $v = 246$ GeV [58], and $\supset$ means that the left-hand side includes terms of the right-hand side. Hence W boson and Z boson masses are identified as

$$\begin{aligned} m_W &= \frac{1}{2} g_2 v, \\ m_Z &= \frac{1}{2} g_Z v, \end{aligned} \tag{3.3.11}$$

respectively. The gauge boson A^0_μ is still massless, which is nothing but the photon, the $U(1)_{\rm em}$ gauge boson.

The weak gauge bosons were discovered in 1983 [3, 4], and their masses are currently measured very precisely [58]:

$$\begin{aligned} m_W &= 80.385 \pm 0.015 \text{ GeV}, \\ m_Z &= 91.1876 \pm 0.0021 \text{ GeV}. \end{aligned} \tag{3.3.12}$$

The weak mixing angle θ_W is also measured as

$$\sin^2\theta_W = 0.23129 \pm 0.00005. \tag{3.3.13}$$

3.3.2 Fermion sector

quark sector

After the electroweak symmetry breaking, we rewrite the fermion Lagrangian with the massive weak gauge bosons and photon. First, we consider the quark sector, whose Lagrangian is given by

$$\begin{aligned} \mathcal{L}_{\rm quark} &= \overline{q^i_L} i\gamma^\mu(\mathcal{D}^q_\mu q^i_L) + \overline{u^i_R} i\gamma^\mu(\mathcal{D}^u_\mu u^i_R) + \overline{d^i_R} i\gamma^\mu(\mathcal{D}^d_\mu d^i_R) \\ &\quad -\{Y^{ij}_u \overline{q^i_L} H u^j_R + Y^{ij}_d \overline{q^i_L} \tilde{H} d^j_R + H.c.\}. \end{aligned} \tag{3.3.14}$$

The covariant derivatives of quarks are

$$\begin{aligned} \mathcal{D}^q_\mu &= \partial_\mu - ig_2 A_\mu - ig_1 \left(\frac{1}{6}\right) B_\mu - ig_3 G_\mu \\ &= \begin{pmatrix} \mathcal{D}^q_{11} & \mathcal{D}^q_{12} \\ \mathcal{D}^q_{21} & \mathcal{D}^q_{22} \end{pmatrix} - ig_3 G_\mu, \\ \mathcal{D}^u_\mu &= \partial_\mu - ig_1 \left(\frac{2}{3}\right) B_\mu - ig_3 G_\mu \\ &= \partial_\mu + i\frac{2}{3} g_1 (Z_\mu \sin\theta_W - A^0_\mu \cos\theta_W) - ig_3 G_\mu, \\ \mathcal{D}^d_\mu &= \partial_\mu - ig_1 \left(-\frac{1}{3}\right) B_\mu - ig_3 G_\mu \\ &= \partial_\mu + i\left(-\frac{1}{3}\right) g_1 (Z_\mu \sin\theta_W - A^0_\mu \cos\theta_W) - ig_3 G_\mu, \end{aligned} \tag{3.3.15}$$

where

$$
\begin{aligned}
\mathcal{D}^q_{11} &= \partial_\mu - ig_Z\left(-\frac{1}{2}-\frac{2}{3}\sin^2\theta_W\right)Z_\mu - ig_Z\left(\frac{2}{3}\right)\cos\theta_W\sin\theta_W A^0_\mu \\
\mathcal{D}^q_{12} &= -\frac{i}{\sqrt{2}}g_2 W^+_\mu \\
\mathcal{D}^q_{21} &= -\frac{i}{\sqrt{2}}g_2 W^-_\mu \\
\mathcal{D}^q_{22} &= \partial_\mu - ig_Z\left(-\frac{1}{2}-\frac{2}{3}\sin^2\theta_W\right)Z_\mu - ig_Z\left(-\frac{1}{3}\right)\cos\theta_W\sin\theta_W A^0_\mu. \quad (3.3.16)
\end{aligned}
$$

Hence the kinetic terms, the first line of the right-hand side of (3.3.14), are written as

$$
\begin{aligned}
\mathcal{L}^{\rm kin}_{\rm quark} &= \overline{u^i_L}i\gamma^\mu(\partial_\mu u^i_L) + \overline{d^i_L}i\gamma^\mu(\partial_\mu d^i_L) \\
&\quad + \overline{u^i_R}i\gamma^\mu(\partial_\mu u^i_R) + \overline{d^i_R}i\gamma^\mu(\partial_\mu d^i_R) \\
&\quad + J^\mu_- W^+_\mu + J^\mu_+ W^-_\mu + J^\mu_Z Z_\mu + J^\mu_{\rm em} A^0_\mu. \quad (3.3.17)
\end{aligned}
$$

Here, $J^\mu_\pm$, J^μ_Z and $J^\mu_{\rm em}$ are the charged, neutral and electromagnetic currents, respectively:

$$
\begin{aligned}
J^\mu_- &= \frac{g_2}{\sqrt{2}}(\overline{u^i_L}\gamma^\mu d^i_L), \\
J^\mu_+ &= \frac{g_2}{\sqrt{2}}(\overline{d^i_L}\gamma^\mu u^i_L) = (J^\mu_-)^\dagger, \\
J^\mu_Z &= g_Z\left\{\frac{1}{2}(\overline{u^i_L}\gamma^\mu u^i_L) + \left(-\frac{1}{2}\right)(\overline{d^i_L}\gamma^\mu d^i_L) - \sin^2\theta_W\left(\frac{2}{3}(\overline{u^i}\gamma^\mu u^i) + \left(-\frac{1}{3}\right)(\overline{d^i}\gamma^\mu d^i)\right)\right\}, \\
J^\mu_{\rm em} &= e\left\{\frac{2}{3}(\overline{u^i}\gamma^\mu u^i) + \left(-\frac{1}{3}\right)(\overline{d^i}\gamma^\mu d^i),\right\}, \quad (3.3.18)
\end{aligned}
$$

where $u^i = (u^i_L\ u^i_R)^T$ (T denotes to take transpose), $d^i = (d^i_L\ d^i_R)^T$, and the electromagnetic coupling constant is defined as $e \equiv g_1 g_2/g_Z$. In general, the neutral current J^μ_Z is written by

$$
J^\mu_Z = g_Z\overline{f_L}\left(\frac{1}{2}T^f_3 - Q^f_{\rm em}\sin^2\theta_W\right)f_L + g_Z\overline{f_R}(-Q^f_{\rm em}\sin^2\theta_W)f_R \quad (3.3.19)
$$

for left-handed and right-handed fermions (f_L and f_R), where T^f_3 and $Q^f_{\rm em}$ are the isospin and the electric charge of fermion f, respectively.

The quark masses are also generated by the electroweak symmetry breaking through the Yukawa couplings. Substituting $\langle H\rangle = (v/\sqrt{2}\ 0)^T$, we have

$$
\begin{aligned}
\mathcal{L}^{\rm mass}_{\rm quark} &= -Y^{ij}_u\frac{v}{\sqrt{2}}\overline{u^i_L}u^j_R - Y^{ij}_d\frac{v}{\sqrt{2}}\overline{d^i_L}d^j_R + H.c. \\
&= -M^{ij}_u\overline{u^i_L}u^j_R - M^{ij}_d\overline{d^i_L}d^j_R + H.c., \quad (3.3.20)
\end{aligned}
$$

where M_u^{ij} and M_d^{ij} are mass matrices for the up-type and the down-type quarks, respectively.

lepton sector

Next, we consider the lepton sector with the Lagrangian given by

$$\mathcal{L}_{\text{lepton}} = \bar{l_L^i} i\gamma^\mu(\mathcal{D}_\mu^l l_L^i) + \bar{e_R^i} i\gamma^\mu(\mathcal{D}_\mu^e e_R^i) - \{Y_e^{ij}\overline{l_L^i}\tilde{H}e_R^j + H.c.\}. \tag{3.3.21}$$

The covariant derivatives of leptons are

$$\begin{aligned}
\mathcal{D}_\mu^l &= \partial_\mu - ig_2 A_\mu - ig_1\left(-\frac{1}{2}\right)B_\mu \\
&= \begin{pmatrix} \partial_\mu + \frac{i}{2}(-g_2 A_\mu^3 + g_1 B_\mu) & -\frac{i}{2}g_2(A_\mu^1 - iA_\mu^2) \\ -\frac{i}{2}g_2(A_\mu^1 + iA_\mu^2) & \partial_\mu + \frac{i}{2}(g_2 A_\mu^3 + g_1 B_\mu) \end{pmatrix} \\
&= \begin{pmatrix} \partial_\mu + \frac{i}{2}g_Z Z_\mu & -\frac{i}{\sqrt{2}}g_2 W_\mu^+ \\ -\frac{i}{\sqrt{2}}g_2 W_\mu^- & \partial_\mu + \frac{i}{2}g_Z(Z_\mu \cos 2\theta_W + A_\mu^0 \sin 2\theta_W) \end{pmatrix}, \\
\mathcal{D}_\mu^e &= \partial_\mu - ig_1(-1)B_\mu \\
&= \partial_\mu + ig_1(\sin\theta_W Z_\mu - \cos\theta_W A_\mu^0).
\end{aligned} \tag{3.3.22}$$

Hence the kinetic terms are written as

$$\begin{aligned}
\mathcal{L}_{\text{lepton}}^{\text{kin}} &= \overline{\nu_L^i} i\gamma^\mu(\partial_\mu \nu_L^i) + \overline{e_L^i} i\gamma^\mu(\partial_\mu e_L^i) + \overline{e_R^i} i\gamma^\mu(\partial_\mu e_R^i) \\
&\quad + J_-^\mu W_\mu^+ + J_+^\mu W_\mu^- + J_Z^\mu Z_\mu + J_{\text{em}}^\mu A_\mu^0.
\end{aligned} \tag{3.3.23}$$

For the leptons, the charged, neutral and electromagnetic currents are given by

$$\begin{aligned}
J_-^\mu &= \frac{g_2}{\sqrt{2}}(\overline{\nu_L}\gamma^\mu e_L) \\
J_+^\mu &= \frac{g_2}{\sqrt{2}}(\overline{e_L}\gamma^\mu \nu_L) = (J_-^\mu)^\dagger \\
J_Z^\mu &= \frac{1}{2}g_Z((\overline{\nu_L}\gamma^\mu \nu_L) - (\overline{e_L}\gamma^\mu e_L)) + g_Z \sin^2\theta_W(\bar{e}\gamma^\mu e) \\
J_{\text{em}}^\mu &= -e(\bar{e}\gamma^\mu e),
\end{aligned} \tag{3.3.24}$$

where $e = (e_L\ e_R)^T$.

The lepton masses are also generated by the electroweak symmetry breaking through the Yukawa couplings. Substituting $\langle H\rangle = (v/\sqrt{2}\ 0)^T$, we have

$$\begin{aligned}
\mathcal{L}_{\text{lepton}}^{\text{mass}} &= -Y_e^{ij}\frac{v}{\sqrt{2}}\overline{e_L^i}e_R^j + H.c. \\
&= -M_e^{ij}\overline{e_L^i}e_R^j + H.c.,
\end{aligned} \tag{3.3.25}$$

where M_e^{ij} is a mass matrix for the charged leptons. Note that there is no the neutrino mass term in the SM, because right-handed neutrinos are not included in the SM particle content in contrast to the other fermions.

3.4 Quark flavor mixing and CP violation

Without mixings between generations (flavor mixings), u-quark can only couple to d-quark in the charged current. However, flavor mixing phenomena are observed by experiments (for example, see [59]). Here we discuss the origin of the quark flavor mixings.

In (3.3.20) we see that the quark mass matrices are not diagonalized in general. We need to rewrite the Lagrangian of quark sector in terms of quark mass eigenstates. Without loss of generality, we work on a basis where the up-type quark mass matrix (M_u) is diagonal (see Appendix A), while the down-type quark mass matrix (M_d) is needed to be diagonalized. Let us first consider two generation case.

3.4.1 Cabibbo angle

In the two generation case, flavor eigenstates are related to mass eigenstates through a 2×2 orthogonal matrix as

$$\begin{pmatrix} d' \\ s' \end{pmatrix} = V \begin{pmatrix} d \\ s \end{pmatrix}, \tag{3.4.1}$$

where d and s are the mass eigenstates, d' and s' are the flavor eigenstates, and

$$V = \begin{pmatrix} V_{ud} & V_{us} \\ V_{cd} & V_{cs} \end{pmatrix} = \begin{pmatrix} \cos\theta_C & \sin\theta_C \\ -\sin\theta_C & \cos\theta_C \end{pmatrix}. \tag{3.4.2}$$

Here θ_C is the Cabibbo angle [60].

Now we express the charged, neutral and electromagnetic currents in terms of the mass eigenstates.

$$\begin{aligned}
J_-^\mu &= \frac{g_2}{\sqrt{2}}(\overline{u_L^i}\gamma^\mu d_L'^i) = \frac{g_2}{\sqrt{2}}\{\overline{u_L}\gamma^\mu(\cos\theta_C d_L + \sin\theta_C s_L) + \overline{c_L}\gamma^\mu(-\sin\theta_C d_L + \cos\theta_C s_L)\}, \\
J_Z^\mu &= g_Z\left\{\frac{1}{2}(\overline{u_L^i}\gamma^\mu u_L^i) + \left(-\frac{1}{2}\right)(\overline{d_L^i}\gamma^\mu d_L^i) - \sin^2\theta_W\left(\frac{2}{3}(\overline{u^i}\gamma^\mu u^i) + \left(-\frac{1}{3}\right)(\overline{d^i}\gamma^\mu d^i)\right)\right\}, \\
J_{em}^\mu &= e\left\{\frac{2}{3}(\overline{u^i}\gamma^\mu u^i) + \left(-\frac{1}{3}\right)(\overline{d^i}\gamma^\mu d^i),\right\}.
\end{aligned} \tag{3.4.3}$$

The flavor mixings only appear in the charged currents, while the neutral and electromagnetic currents are flavor diagonal, because $\overline{d'^i}\gamma^\mu d'^i = \overline{d^i}\gamma^\mu d^i$.

	creation	weak interaction	detection	mixing matrix
quark	mass eigenstate	flavor eigenstate	mass eigenstate	CKM matrix
	creation	propagation	detection	mixing matrix
neutrino	flavor eigenstate	mass eigenstate	flavor eigenstate	MNS matrix

Table 3.3: Flavor physics of quarks and neutrinos. In flavor mixing phenomena among quarks, quarks are created and detected as mass eigenstates, while the weak interaction occurs for flavor eigenstates. In neutrino oscillation phenomena, neutrinos are created and detected as flavor eigenstates, while they propagate as mass eigenstates.

3.4.2 Cabibbo-Kobayashi-Maskawa matrix

Now we consider three generations case. Flavor eigenstates are related to mass eigenstates through a 3×3 unitary matrix as

$$\begin{pmatrix} d \\ s \\ b \end{pmatrix} = V \begin{pmatrix} d' \\ s' \\ b' \end{pmatrix}. \tag{3.4.4}$$

3×3 unitary matrix has nine degrees of freedom, out of which we can eliminate five diagonal phases by redefinition the phases of down-type quarks (see Appendix A). As a result, the physical degrees of freedom of V are four (three mixing angles and one CP phase). An explicit form of V is given by

$$\begin{aligned} V_{CKM} &= \begin{pmatrix} V_{ud} & V_{us} & V_{ub} \\ V_{cd} & V_{cs} & V_{cb} \\ V_{td} & V_{ts} & V_{tb} \end{pmatrix} \\ &= \begin{pmatrix} 1 & 0 & 0 \\ 0 & c_{23} & s_{23} \\ 0 & -s_{23} & c_{23} \end{pmatrix} \begin{pmatrix} c_{13} & 0 & s_{13}\mathrm{e}^{-i\delta} \\ 0 & 1 & 0 \\ -s_{13}\mathrm{e}^{i\delta} & 0 & c_{13} \end{pmatrix} \begin{pmatrix} c_{12} & s_{12} & 0 \\ -s_{12} & c_{12} & 0 \\ 0 & 0 & 1 \end{pmatrix} \\ &= \begin{pmatrix} c_{12}c_{13} & s_{12}c_{13} & s_{13}\mathrm{e}^{-i\delta} \\ -s_{12}c_{23} - c_{12}s_{23}s_{13}\mathrm{e}^{i\delta} & c_{12}c_{23} - s_{12}s_{23}s_{13}\mathrm{e}^{i\delta} & s_{23}c_{13} \\ s_{12}s_{23} - c_{12}c_{23}s_{13}\mathrm{e}^{i\delta} & -c_{12}s_{23} - s_{12}c_{23}s_{13}\mathrm{e}^{i\delta} & c_{23}c_{13} \end{pmatrix}, \end{aligned} \tag{3.4.5}$$

where $c_{ij} = \cos\theta_{ij}$, $s_{ij} = \sin\theta_{ij}$, $\theta_{ij}(i, j = 1, 2, 3,\ i \neq j)$ are the mixing angles, and δ is the CP-violating phase. This matrix V_{CKM} is called the Cabbibo-Kobayashi-Maskawa (CKM) matrix [61]. The magnitudes of the CKM matrix elements are measured by

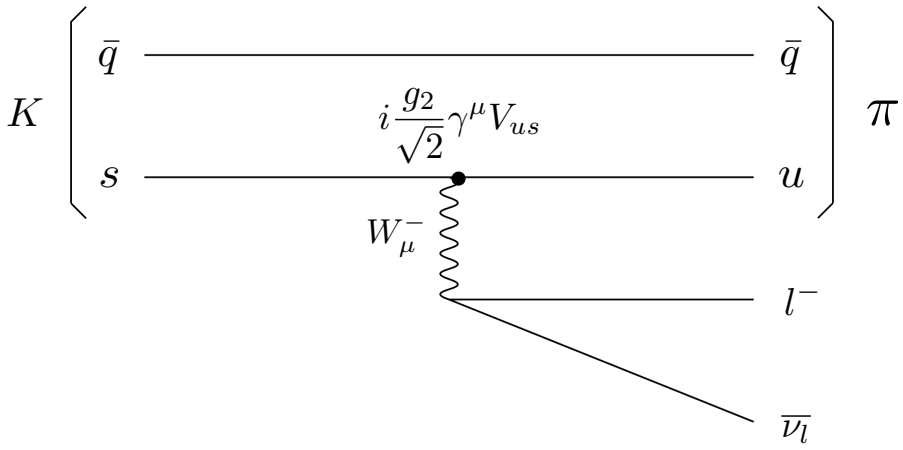

Figure 3.1: K meson decay process ($K \to \pi l^- \overline{\nu_l}$) through $|V_{us}|$. $\overline{q}$ denotes anti-up or down quark.

experiments [58] as

$$
\begin{aligned}
|V_{ud}| &= 0.97417 \pm 0.00021, \\
|V_{us}| &= 0.2248 \pm 0.0006, \\
|V_{ub}| &= (4.09 \pm 0.39) \times 10^{-3}, \\
|V_{cd}| &= 0.220 \pm 0.005, \\
|V_{cs}| &= 0.995 \pm 0.016, \\
|V_{cb}| &= (40.5 \pm 1.5) \times 10^{-3}, \\
|V_{td}| &= (8.2 \pm 0.6) \times 10^{-3}, \\
|V_{ts}| &= (40.0 \pm 2.7) \times 10^{-3}, \\
|V_{tb}| &= 1.009 \pm 0.031. \qquad (3.4.6)
\end{aligned}
$$

As an example, we show a K meson decay process ($K \to \pi l^- \overline{\nu_l}$) in Figure 3.1. The element $|V_{us}|$ in the CKM matrix is determined through this process in the experiments.

The generations of quarks are distinguished by observed (their bound state) mass eigenvalues. In flavor mixing phenomena among quarks, quarks are created and detected

as mass eigenstates, while the weak interaction occurs for flavor eigenstates (Table 3.3).

3.5 Observational problems

Although the SM is a very successful theory, there are some observational results that the SM cannot account for. In this section, we discuss such observational problems on the SM, in particular, neutrino oscillation phenomena and the existence of dark matter in the universe.

3.5.1 Neutrino masses and mixings

Neutrino oscillation between neutrino and anti-neutrino is first proposed by Bruno Pontecorvo in 1957 [62]. Neutrino oscillation phenomena among three neutrino flavors have been confirmed by the Super-Kamiokande experiments in 1998 [8], and the Sudbury Neutrino Observatory (SNO) in 2001 [9]. Neutrino oscillation phenomena require neutrino masses and mixings, however neutrinos are massless fermions in the SM. In the following, we will briefly review the neutrino oscillation and see that neutrino masses and mixings are essential for the neutrino oscillation phenomena to occur.

Neutrino oscillation phenomena originate from the discrepancy between the flavor and mass eigenstates (Table 3.3). Suppose neutrinos have masses. We define the neutrino flavor eigenstates ν_α ($\alpha = e, \mu, \tau$) as the states paired with corresponding charged leptons in the charged currents. While a neutrino generated through the charged current interaction is the flavor eigenstate, it propagates as the mass eigenstate, and is detected as the flavor eigenstate. As we have discussed in the previous section, the neutrino mass eigenstates do not coincide with the flavor eigenstates in general.

Let us consider neutrino oscillation in two generation case. The neutrino mass eigenstates $|\nu_m^i(t)\rangle$ ($i = 1, 2$) obey the Schrödinger equation:

$$i\frac{d}{dt}|\nu_m^i(t)\rangle = H|\nu_m^i(t)\rangle. \tag{3.5.1}$$

Since neutrino mass eigenvalues are much smaller than energies of propagating neutrinos,

Hamiltonian is approximated as

$$\begin{aligned} H = E &= \sqrt{|\vec{p}|^2 + m^2} \\ &\simeq |\vec{p}| \left(1 + \frac{1}{2}\frac{m^2}{|\vec{p}|^2} + \cdots\right) \\ &\simeq E\left(1 + \frac{1}{2}\frac{m^2}{E^2} + \cdots\right) \simeq E + \frac{1}{2}\frac{m^2}{E}. \end{aligned} \tag{3.5.2}$$

The solution of the Schrödinger equation (3.5.1) is given by

$$\begin{aligned} |\nu_m^i(t)\rangle &= \mathrm{e}^{-iHt}|\nu_m^i(0)\rangle \\ &= \mathrm{e}^{-iE_it}\mathrm{e}^{-i\frac{m_i^2}{2E_i}t}|\nu_m^i(0)\rangle. \end{aligned} \tag{3.5.3}$$

We express the flavor eigenstates by a superposition of the mass eigenstates,

$$\begin{aligned} |\nu_\alpha(t)\rangle &= U_{\alpha i}|\nu_m^i(t)\rangle \\ &= U_{\alpha i}\mathrm{e}^{-iEt}\mathrm{e}^{-i\frac{m_i^2}{2E}t}|\nu_m^i(0)\rangle, \end{aligned} \tag{3.5.4}$$

where we have taken $E_1 = E_2 = E$ since $E \gg m_1,\ m_2$, and U is the mixing matrix,

$$U = \begin{pmatrix} \cos\theta & \sin\theta \\ -\sin\theta & \cos\theta \end{pmatrix}. \tag{3.5.5}$$

The flavor eigenstates at time t are given by

$$\begin{aligned} \begin{pmatrix} |\nu_e(t)\rangle \\ |\nu_\mu(t)\rangle \end{pmatrix} &= \mathrm{e}^{-iEt}\begin{pmatrix} \cos\theta & \sin\theta \\ -\sin\theta & \cos\theta \end{pmatrix}\begin{pmatrix} \mathrm{e}^{-i\frac{m_1^2}{2E}t} & 0 \\ 0 & \mathrm{e}^{-i\frac{m_2^2}{2E}t} \end{pmatrix}\begin{pmatrix} |\nu_m^1(0)\rangle \\ |\nu_m^2(0)\rangle \end{pmatrix} \\ &= \mathrm{e}^{-iEt}\mathrm{e}^{-i\frac{m_1^2}{2E}t}\begin{pmatrix} \cos\theta & \sin\theta \\ -\sin\theta & \cos\theta \end{pmatrix}\begin{pmatrix} 1 & 0 \\ 0 & \mathrm{e}^{-i\frac{\Delta m_{21}^2}{2E}t} \end{pmatrix} \\ &\quad \times \begin{pmatrix} \cos\theta & -\sin\theta \\ \sin\theta & \cos\theta \end{pmatrix}\begin{pmatrix} |\nu_e(0)\rangle \\ |\nu_\mu(0)\rangle \end{pmatrix}, \end{aligned} \tag{3.5.6}$$

where $\Delta m_{21}^2 = m_2^2 - m_1^2$. Suppose ν_e is created at $t = 0$, namely

$$\begin{pmatrix} |\nu_e(0)\rangle \\ |\nu_\mu(0)\rangle \end{pmatrix} = \begin{pmatrix} 1 \\ 0 \end{pmatrix}, \tag{3.5.7}$$

we find the flavor states at t such that

$$\begin{pmatrix} |\nu_e(t)\rangle \\ |\nu_\mu(t)\rangle \end{pmatrix} = \mathrm{e}^{-i(Et+\frac{m_1^2}{2E})}\begin{pmatrix} \cos^2\theta + \mathrm{e}^{-i\frac{\Delta m_{21}^2}{2E}t}\sin^2\theta \\ (1 - \mathrm{e}^{-i\frac{\Delta m_{21}^2}{2E}t})\sin\theta\cos\theta \end{pmatrix}. \tag{3.5.8}$$

Thus, the probability to detect the flavor eigenstate ν_μ at t is obtained as

$$\begin{aligned} P(\nu_e \to \nu_\mu) &= |\langle \nu_\mu(t)|\nu_e(0)\rangle|^2 \\ &= \sin^2 2\theta \sin^2\left(\frac{\Delta m_{21}^2}{4E}t\right). \end{aligned} \tag{3.5.9}$$

Therefore, the conversion probability of $\nu_e \to \nu_\mu$ can be non-zero, if both of the mixing angle and the mass squared difference are non-zero. This is the neutrino oscillation.

It is straightforward to extend our discussion to the realistic three generation case, where the above mixing matrix U is extended to a 3×3 unitary matrix, the so-called Maki-Nakagawa-Sakata(MNS) matrix [63],

$$U_{MNS} = \begin{pmatrix} 1 & 0 & 0 \\ 0 & c_{23} & s_{23} \\ 0 & -s_{23} & c_{23} \end{pmatrix} \begin{pmatrix} c_{13} & 0 & s_{13}\mathrm{e}^{-i\delta_{CP}} \\ 0 & 1 & 0 \\ -s_{13}\mathrm{e}^{i\delta_{CP}} & 0 & c_{13} \end{pmatrix} \begin{pmatrix} c_{12} & s_{12} & 0 \\ -s_{12} & c_{12} & 0 \\ 0 & 0 & 1 \end{pmatrix}, \tag{3.5.10}$$

where $c_{ij} = \cos\theta_{ij}$, $s_{ij} = \sin\theta_{ij}$, θ_{ij} $(i, j = 1, 2, 3)$ are the mixing angles, and δ_{CP} is CP-violating phase. The recent neutrino oscillation data from a variety of experiments are listed bellow [58]: for the mass squared differences,

$$\begin{aligned} \Delta m_{12}^2 &= (7.53 \pm 0.18) \times 10^{-5}\ \mathrm{eV}^2, \\ |\Delta m_{23}^2| &= (2.44 \pm 0.06) \times 10^{-3}\ \mathrm{eV}^2 \text{ (normal mass hierarchy)}, \\ & (2.51 \pm 0.06) \times 10^{-3}\ \mathrm{eV}^2 \text{ (inverted mass hierarchy)}. \end{aligned} \tag{3.5.11}$$

Here, $\Delta m_{12}^2 \equiv m_2^2 - m_1^2$, $\Delta m_{23}^2 \equiv m_3^2 - m_2^2$, and the normal mass hierarchy means the mass spectrum $m_1 < m_2 < m_3$, while $m_3 < m_1 < m_2$ for the inverted mass hierarchy. For the mixing angles,

$$\begin{aligned} \sin^2\theta_{12} &= 0.304 \pm 0.014, \\ \sin^2\theta_{23} &= 0.51 \pm 0.05 \text{ (normal mass hierarchy)}, \\ & 0.50 \pm 0.05 \text{ (inverted mass hierarchy)}, \\ \sin^2\theta_{13} &= (2.19 \pm 0.12) \times 10^{-2}. \end{aligned} \tag{3.5.12}$$

Note that observed neutrino oscillation phenomena require an extension of the SM to incorporate neutrino masses.

The so-called seesaw mechanism [10, 11, 12, 13, 14] is a simple and natural way to generate small neutrino masses and flavor mixings. For simplicity, we first consider one

generation case to discuss the essence of the seesaw mechanism. We introduce a right-handed neutrino (N_R) to the SM, which is totally singlet under the SM gauge groups, and new terms to the SM Lagrangian,

$$\mathcal{L}^{\text{mass}}_{\text{neutrino1}} = -Y_D \overline{l_L} H N_R - \frac{1}{2} M \overline{N_R^C} N_R + H.c., \tag{3.5.13}$$

where Y_D is the Dirac Yukawa coupling constant, and M is a Majorana mass. Note that since N_R is totally singlet, we can add the Majorana mass term. After the electroweak symmetry breaking, we have a neutrino mass matrix,

$$M_{\text{neutrino1}} = \begin{pmatrix} 0 & m_D \\ m_D & M \end{pmatrix}, \tag{3.5.14}$$

where $m_D = Y_D v/\sqrt{2}$ is the Dirac mass. Then, mass eigenvalues are given by

$$\lambda_\pm = \frac{M \pm \sqrt{M^2 + 4m_D^2}}{2}. \tag{3.5.15}$$

Let us consider a limit $m_D \ll M$, we obtain

$$\begin{aligned} \lambda_+ &\sim M, \\ \lambda_- &\sim -\frac{m_D^2}{M} = -m_D \left(\frac{m_D}{M}\right). \end{aligned} \tag{3.5.16}$$

Therefore, the light mass eigenvalue λ_- is highly suppressed by $|m_D/M| \ll 1$. This is the seesaw mechanism. For example, if we take $m_D \sim m_e = 5 \times 10^{-4}$ GeV (electron mass) and $M \sim \mathcal{O}(1)$ TeV, we obtain $\lambda_- \sim \mathcal{O}(10^{-2})$ eV, which is a natural neutrino mass scale, $\sqrt{|\Delta m_{23}^2|}$.

Next, we consider a realistic case, which can reproduce the neutrino oscillation data, (3.5.11) and (3.5.12). In the following, we discuss the so-called minimal seesaw [25, 26], in which only two generations of right-handed neutrinos are introduced. It turns out that two right-handed neutrinos are enough to reproduce the neutrino oscillation data. We introduce two right-handed neutrinos (N_R^j, $j = 1, 2$) to the SM, and new terms to the SM Lagrangian,

$$\mathcal{L}^{\text{mass}}_{\text{neutrino2}} = -Y_D^{ij} \overline{l_L^i} H N_R^j - \frac{1}{2} M^{kl} \overline{N_R^{kC}} N_R^l + H.c., \tag{3.5.17}$$

where Y_D^{ij} ($i = 1, 2, 3$, $j = 1, 2$) is the Dirac Yukawa coupling constant, and M^{kl} ($k, l = 1, 2$) is a Majorana mass matrix for two right-handed neutrinos. For simplicity, we take

$M^{11} = M^{22} = M$ and $M^{12} = M^{21} = 0$. After the electroweak symmetry breaking, we have a neutrino mass matrix,

$$M_{\text{neutrino2}} = \begin{pmatrix} 0 & m_D \\ m_D^T & M\mathbf{1}_{2\times 2} \end{pmatrix}, \tag{3.5.18}$$

where m_D is 3×2 matrix defined as $m_D^{ij} = Y_D^{ij} v/\sqrt{2}$, and $\mathbf{1}_{2\times 2}$ is the 2×2 unit matrix. Assuming $m_D^{ij} \ll M$, we can approximately block-diagonalize this matrix as

$$M_{\text{neutrino2}} \to \begin{pmatrix} m_\nu & 0 \\ 0 & M\mathbf{1}_{2\times 2} \end{pmatrix}, \tag{3.5.19}$$

where m_ν is a 3×3 symmetric mass matrix of the light neutrinos:

$$m_\nu \simeq -m_D M^{-1} m_D^T. \tag{3.5.20}$$

The rank of m_ν is 2, and it has one zero and two nonzero mass eigenvalues. Therefore, two mass squared differences of the neutrino oscillation data (3.5.11) can be reproduced. Note that if we introduce only one right-handed neutrino, the rank of m_ν is 1, and two mass squared differences cannot be reproduced. Since m_D is 3×2 complex matrix, it has twelve degrees of freedom. Three degrees of freedom can be removed by rephasing with three left-handed neutrinos as we have discussed in the quark sector (see Appendix A), and as a result nine degrees of freedom are left, which are enough to reproduce six observables (two mass squared differences, three mixing angles, and one CP-violating phase) of the neutrino oscillation data. The neutrino oscillation data can be reproduced by the seesaw mechanism with only two generations of right-handed neutrinos.

3.5.2 Dark matter

The necessary conditions for a particle to be a suitable dark matter candidate are [48]

1. electrically neutral.
2. stable.
3. cold dark matter.

The condition 1 is from the fact that the dark matter have not optically observed. The dark matter particle exists in the present universe, which means its lifetime is longer than the age of the universe, $\tau_U \simeq 10^{17}$ sec (condition 2). The structure of the universe is

generated by non-relativistic dark matter particles as seeds. The condition 3 is related with the structure of the present universe. We explain this below.

The minimum scale of the structure of the present universe is characterized by a temperature (T_{NR}) at which the dark matter particle becomes non-relativistic. According to [48], this scale is estimated as

$$L_{FS} \simeq 20 \left(\frac{T_{NR}}{30 \text{ eV}} \right)^{-1} \text{ Mpc.} \tag{3.5.21}$$

The scale of the galactic halo is about 100 kpc, and in order to create the structure of the halo, we obtain $T_{NR} > 1$ keV. A dark matter particle which satisfies this condition is called "cold dark matter" [48]. The SM neutrinos, once their masses are generated by some new physics (e.g. the seesaw mechanism), satisfy the conditions 1 and 2. However, the condition 3 is not satisfied because their typical mass scale is $\sqrt{|\Delta m_{23}^2|} = \mathcal{O}(10^{-2})$ eV, which is too small. Therefore, there is no suitable cold dark matter candidate in the SM, and we need to extend the SM so as to incorporate a cold dark matter candidate.

Chapter 4

The minimal $U(1)_X$ extended Standard Model

4.1 The minimal $B-L$ model

The SM Lagrangian at the tree-level is invariant under the global $U(1)_B$ and $U(1)_L$ transformations,

$$\begin{aligned} \psi &\rightarrow \psi' = \mathrm{e}^{iQ_B\theta_B}\psi, \\ \psi &\rightarrow \psi' = \mathrm{e}^{iQ_L\theta_L}\psi, \end{aligned} \tag{4.1.1}$$

where θ_B and θ_L are constant phases associated with the $U(1)_B$ and $U(1)_L$ transformations, and Q_B and Q_L are charges identified as a baryon number (B) and a lepton number (L) of the fermion ψ, respectively. The baryon number is a quantum number to characterize fermions. A quark (antiquark) has a baryon number $1/3$ ($-1/3$), while a SM lepton has 0. The lepton number is a quantum number similar to baryon number. A lepton (antilepton) has a lepton number 1 (-1), while a quark has 0. Although these global $U(1)$ symmetries are anomalous under the SM gauge group, the combination of $B-L$ is anomaly free. The $B-L$ symmetry means that the SM Lagrangian is invariant under the global $U(1)_{B-L}$ transformation,

$$\psi \rightarrow \psi' = \mathrm{e}^{i(Q_B-Q_L)\theta_{B-L}}\psi, \tag{4.1.2}$$

where θ_{B-L} is a constant phase associated with the $U(1)_{B-L}$ transformation.

In the minimal $B-L$ model [19, 20, 21, 22, 23], this global $B-L$ symmetry in the SM is gauged, and hence the gauge group of the model is $SU(3)_C \times SU(2)_L \times U(1)_Y \times U(1)_{B-L}$.

	$SU(3)_C$	$SU(2)_L$	$U(1)_Y$	$U(1)_{B-L}$
q_L^i	**3**	**2**	$1/6$	$1/3$
u_R^i	**3**	**1**	$2/3$	$1/3$
d_R^i	**3**	**1**	$-1/3$	$1/3$
l_L^i	**1**	**2**	$-1/2$	-1
N_R^i	**1**	**1**	0	-1
e_R^i	**1**	**1**	-1	-1
H	**1**	**2**	$-1/2$	0
Φ	**1**	**1**	0	2

Table 4.1: Particle content of the minimal $B-L$ model.

Three right-handed neutrinos (N_R^i, $i = 1, 2, 3$ is a generation index) are introduced to make the theory gauge anomaly free, while an SM singlet scalar field (Φ) are introduced to break the $U(1)_{B-L}$ gauge symmetry. The particle content of the minimal $B-L$ model is listed in Table 4.1.

4.1.1 Gauge sector

Lagrangian of gauge bosons in the $B-L$ model is generally given by

$$\mathcal{L}_{\text{gauge}}^{B-L} = -\frac{1}{2}\text{tr}[G_{\mu\nu}G^{\mu\nu}] - \frac{1}{2}\text{tr}[F_{\mu\nu}F^{\mu\nu}] - \frac{1}{4}B_{\mu\nu}B^{\mu\nu} - \frac{1}{4}B'_{\mu\nu}B'^{\mu\nu} - c_{\text{mix}}B_{\mu\nu}B'^{\mu\nu}, \quad (4.1.3)$$

where

$$B'_{\mu\nu} = \partial_\mu(Z'_{B-L})_\nu - \partial_\nu(Z'_{B-L})_\mu \quad (4.1.4)$$

is the field strength for the new neutral gauge boson (Z'_{B-L}) associated with $U(1)_{B-L}$. Note that in general, we can introduce the last term for a kinetic mixing between the $U(1)_Y$ and the $U(1)_{B-L}$ gauge bosons. In the following, we define the minimal $B-L$ model with $c_{\text{mix}} = 0$ at the scale of the $B-L$ symmetry breaking.

4.1.2 Scalar sector

Lagrangian of the scalar sector in the $B-L$ model is given by

$$\mathcal{L}_{\text{scalar}}^{B-L} = (\mathcal{D}^\mu H)^\dagger(\mathcal{D}_\mu H) + (\mathcal{D}^\mu \Phi)^\dagger(\mathcal{D}_\mu \Phi) - V(H, \Phi), \quad (4.1.5)$$

where H and Φ are the SM Higgs field and the SM singlet scalar field ($B-L$ Higgs), respectively, and the scalar potential is given by

$$\begin{aligned} V(H,\Phi) &= \lambda_H \left(H^\dagger H - \frac{v^2}{2} \right)^2 + \lambda_\Phi \left(\Phi^\dagger \Phi - \frac{v_{B-L}^2}{2} \right)^2 \\ &\quad + \lambda_{\rm mix} \left(H^\dagger H - \frac{v^2}{2} \right) \left(\Phi^\dagger \Phi - \frac{v_{B-L}^2}{2} \right). \end{aligned} \tag{4.1.6}$$

Here, λ_H (>0), λ_Φ (>0) and $\lambda_{\rm mix}$ are real coupling constants, $v = 246$ GeV [58], and v_{B-L} is a real and positive constant. We will derive a condition for $\lambda_{\rm mix}$ to make the potential bounded from below. In this scalar potential, the SM Higgs doublet and $U(1)_{B-L}$ Higgs field develop the VEVs,

$$\begin{aligned} \langle H \rangle &= \frac{1}{\sqrt{2}} \begin{pmatrix} v \\ 0 \end{pmatrix}, \\ \langle \Phi \rangle &= \frac{v_{B-L}}{\sqrt{2}}. \end{aligned} \tag{4.1.7}$$

We expand the Higgs fields around the VEVs such that

$$\begin{aligned} H &= \frac{1}{\sqrt{2}} \begin{pmatrix} v + h \\ 0 \end{pmatrix}, \\ \Phi &= \frac{v_{B-L} + h'}{\sqrt{2}}, \end{aligned} \tag{4.1.8}$$

where h, h' are physical Higgs bosons. Substituting this expansion into the scalar potential (4.1.6), we read out the mass terms of the Higgs bosons as

$$\begin{aligned} V(H,\Phi) &\supset \lambda_H v^2 h^2 + \lambda_\Phi v_{B-L}^2 h'^2 + \lambda_{\rm mix} v v_{B-L} h h' \\ &= \frac{1}{2} (h \ h') \begin{pmatrix} 2\lambda_H v^2 & \lambda_{\rm mix} v v_{B-L} \\ \lambda_{\rm mix} v v_{B-L} & 2\lambda_\Phi v_{B-L}^2 \end{pmatrix} \begin{pmatrix} h \\ h' \end{pmatrix} \\ &= \frac{1}{2} (h \ h') M_{\rm scalar} \begin{pmatrix} h \\ h' \end{pmatrix}. \end{aligned} \tag{4.1.9}$$

In order for the scalar potential to be bounded from below, the mass matrix $M_{\rm scalar}$ must be positive definite, in particular,

$$\det[M_{\rm scalar}] = (4\lambda_H \lambda_\Phi - \lambda_{\rm mix}^2) v^2 v_{B-L}^2 > 0, \tag{4.1.10}$$

and hence $|\lambda_{mix}| < 2\sqrt{\lambda_H \lambda_\Phi}$. Now we diagonalize the mass matrix by

$$\begin{pmatrix} h \\ h' \end{pmatrix} = \begin{pmatrix} \cos\alpha & \sin\alpha \\ -\sin\alpha & \cos\alpha \end{pmatrix} \begin{pmatrix} h_1 \\ h_2 \end{pmatrix}, \tag{4.1.11}$$

where h_1, h_2 are mass eigenstates, and the mixing angle is given by

$$\tan 2\alpha = -\frac{\lambda_{\rm mix} v v_{B-L}}{\lambda_H v^2 - \lambda_\Phi v_{B-L}^2}. \tag{4.1.12}$$

The mass eigenstates are given by

$$\begin{aligned} m_{h_1}^2 &= \lambda_H v^2 + \lambda_\Phi v_{B-L}^2 + \sqrt{(\lambda_H v^2 - \lambda_\Phi v_{B-L}^2)^2 + (\lambda_{\rm mix} v v_{B-L})^2}, \\ m_{h_2}^2 &= \lambda_H v^2 + \lambda_\Phi v_{B-L}^2 - \sqrt{(\lambda_H v^2 - \lambda_\Phi v_{B-L}^2)^2 + (\lambda_{\rm mix} v v_{B-L})^2}. \end{aligned} \tag{4.1.13}$$

For simplicity, we assume a very small $\lambda_{\rm mix}$, so that one mass eigenstate is an SM-like Higgs boson, and the other is almost a $B-L$ Higgs boson.

Let us now calculate the mass of the $B-L$ gauge boson Z'_{B-L}. The kinetic term of the $B-L$ Higgs field is given by

$$\mathcal{L}_{\rm scalar}^{B-L\ \rm kin} = (\mathcal{D}_\mu \Phi)^\dagger (\mathcal{D}^\mu \Phi), \tag{4.1.14}$$

where the covariant derivative is

$$\mathcal{D}_\mu = \partial_\mu - 2 i g_{B-L} (Z'_{B-L})_\mu, \tag{4.1.15}$$

and g_{B-L} is the coupling constant of $U(1)_{B-L}$ gauge interaction. Substituting $\Phi \to \langle \Phi \rangle$, the Z'_{B-L} gauge boson mass is found to be

$$M_{Z'} = 2 g_{B-L} v_{B-L}. \tag{4.1.16}$$

4.1.3 Yukawa sector

Lagrangian of the Yukawa sector in the $B-L$ model is given by

$$\mathcal{L}_{\rm Yukawa}^{B-L} \supset -\sum_{i=1}^{3}\sum_{j=1}^{3} Y_D^{ij} \overline{l_L^i} H N_R^j - \frac{1}{2}\sum_{k=1}^{3} Y_N^k \Phi \overline{N_R^{kC}} N_R^k + H.c., \tag{4.1.17}$$

where Y_D^{ij} and Y_N^k are Dirac Yukawa coupling constant and Majorana Yukawa coupling constant. A non-zero VEV of the $B-L$ Higgs field Φ breaks the $B-L$ gauge symmetry and generates the Majorana masses for the right-handed neutrinos through the Majorana Yukawa coupling. The seesaw mechanism is automatically implemented in the model after the electroweak symmetry breaking. Neutrino mass matrix is given by

$$M_{\rm neutrino} = \begin{pmatrix} 0 & m_D \\ m_D^T & M \end{pmatrix}. \tag{4.1.18}$$

	$SU(3)_C$	$SU(2)_L$	$U(1)_Y$	$U(1)_X$
q_L^i	**3**	**2**	$1/6$	$(1/6)x_H + (1/3)x_\Phi$
u_R^i	**3**	**1**	$2/3$	$(2/3)x_H + (1/3)x_\Phi$
d_R^i	**3**	**1**	$-1/3$	$-(1/3)x_H + (1/3)x_\Phi$
l_L^i	**1**	**2**	$-1/2$	$-(1/2)x_H - x_\Phi$
N_R^i	**1**	**1**	0	$-x_\Phi$
e_R^i	**1**	**1**	-1	$-x_H - x_\Phi$
H	**1**	**2**	$-1/2$	$-(1/2)x_H$
Φ	**1**	**1**	0	$2x_\Phi$

Table 4.2: Particle content of the minimal $U(1)_X$ model. The $U(1)_X$ charges of fields are determined by two real parameters, x_H and x_Φ. Without loss of generality we fix $x_\Phi = 1$ throughout this thesis.

Here, m_D and M are Dirac and Majorana mass matrices, respectively, which are given by

$$\begin{aligned} m_D &= \frac{Y_D}{\sqrt{2}} v, \\ M &= \frac{Y_N}{\sqrt{2}} v_{B-L}. \end{aligned} \tag{4.1.19}$$

Assuming $|m_D^{ij}| \ll M^k$, we can block diagonalize the mass matrix M_{neutrino} to be

$$\begin{pmatrix} 0 & m_D \\ m_D^T & M \end{pmatrix} \rightarrow \begin{pmatrix} -m_D^T M^{-1} m_D & 0 \\ 0 & M \end{pmatrix}. \tag{4.1.20}$$

As we have discussed in Section 3.5.1, when we consider only one generation, the mass eigenvalues are simply

$$\begin{aligned} m_{\nu_l} &\simeq -\frac{m_D^2}{M}, \\ m_{\nu_h} &\simeq M. \end{aligned} \tag{4.1.21}$$

Because of the seesaw mechanism, a huge mass hierarchy between the light eigenstate (ν_l) and the heavy eigenstate (ν_h).

4.2 The minimal $U(1)_X$ model

We can generalize the minimal $B - L$ model to the minimal $U(1)_X$ model [44]. This is the most general extension of the SM with an extra anomaly-free $U(1)$ gauge symmetry. The particle content is listed in Table 4.2. The fermions and scalars have suitable $U(1)_X$

charges as linear combinations of their $U(1)_Y$ and $U(1)_{B-L}$ charges, and hence the $U(1)_X$ charges of fields are determined by two real parameters, x_H and x_Φ. Except for the $U(1)_X$ charge assignments, the particle content of this model is the same as the minimal $B-L$ model. Note that in the model the charge x_Φ always appears as a product with the $U(1)_X$ gauge coupling and it is not an independent free parameter. Hence, without loss of generality we fix $x_\Phi = 1$ throughout this thesis. In this way, we reproduce the minimal $B-L$ model with the conventional charge assignment as the limit of $x_H \to 0$. The limit of $x_H \to +\infty(-\infty)$ indicates that the $U(1)_X$ is (anti-)aligned to the $U(1)_Y$ direction, which is the so-called "hypercharge oriented $U(1)_X$ model" [64]. The anomaly structure of the model is the same as the minimal $B-L$ model and the model is free from all gauge and gravitational anomalies in the presence of the three right-handed neutrinos.

4.2.1 Scalar sector and Yukawa sector

Lagrangian of the scalar sector in the $U(1)_X$ model is given by

$$\mathcal{L}^X_{\text{scalar}} = (\mathcal{D}^H_\mu H)^\dagger(\mathcal{D}^{H\mu} H) + (\mathcal{D}^\Phi_\mu \Phi)^\dagger(\mathcal{D}^{\Phi\mu}\Phi) - V(H,\Phi), \tag{4.2.1}$$

where H and Φ are the SM Higgs field and the $U(1)_X$ Higgs field, respectively, and the scalar potential $V(H,\Phi)$ is identical to (4.1.6). In this scalar potential, the SM Higgs doublet and $U(1)_X$ Higgs field develop the VEVs,

$$\begin{aligned} \langle H \rangle &= \frac{1}{\sqrt{2}} \begin{pmatrix} v \\ 0 \end{pmatrix}, \\ \langle \Phi \rangle &= \frac{v_X}{\sqrt{2}}. \end{aligned} \tag{4.2.2}$$

The discussion about the Higgs boson mass spectrum is the same as the $B-L$ case with the replacement of $v_{B-L} \to v_X$.

Let us now calculate the mass of the $U(1)_X$ gauge boson (Z' boson). The kinetic terms of the SM Higgs and the $U(1)_X$ Higgs fields are given by

$$\mathcal{L}^{X\ \text{kin}}_{\text{scalar}} = (\mathcal{D}^H_\mu H)^\dagger(\mathcal{D}^{H\mu} H) + (\mathcal{D}^\Phi_\mu \Phi)^\dagger(\mathcal{D}^{\Phi\mu}\Phi), \tag{4.2.3}$$

where the covariant derivatives with respect to the $U(1)_X$ gauge symmetry are

$$\begin{aligned} \mathcal{D}^H_\mu &= \partial_\mu - i\left(-\frac{1}{2}x_H\right) g_X Z'_\mu, \\ \mathcal{D}^\Phi_\mu &= \partial_\mu - 2ig_X Z'_\mu, \end{aligned} \tag{4.2.4}$$

and g_X is the coupling constant of $U(1)_X$ gauge interaction. Substituting $H \to \langle H \rangle$ and $\Phi \to \langle \Phi \rangle$, the Z' gauge boson mass is found to be

$$M_{Z'} = g_X \sqrt{4v_X^2 + \frac{x_H^2 v^2}{4}} \simeq 2 g_X v_X, \tag{4.2.5}$$

where g_X is the $U(1)_X$ gauge coupling, and the Large Electron-Positron Collider (LEP) constraint [5, 6] $v_X^2 \gg v^2$ has been used. Because of the LEP constraint, the mass mixing of the Z' boson with the SM Z boson is very small, and we neglect it in our analysis in this thesis.

Lagrangian of the Yukawa sector in the $U(1)_X$ model is given by

$$\mathcal{L}^X_{\text{Yukawa}} \supset -\sum_{i=1}^{3}\sum_{j=1}^{3} Y_D^{ij} \overline{l_L^i} H N_R^j - \frac{1}{2}\sum_{k=1}^{3} Y_N^k \Phi \overline{N_R^{kC}} N_R^k + H.c., \tag{4.2.6}$$

which is identical to the Lagrangian of the Yukawa sector in the $B-L$ model. A non-zero VEV of the $U(1)_X$ Higgs field Φ breaks the $U(1)_X$ symmetry and generates the Majorana mass matrix (M) for the right-handed neutrinos:

$$M = \frac{Y_N}{\sqrt{2}} v_X. \tag{4.2.7}$$

All discussions about neutrino mass generation via the seesaw mechanism is the same as in the $B-L$ model.

Chapter 5

Large Hadron Collider physics

5.1 Overview of Large Hadron Collider

The Large Hadron Collider (LHC), which was built at the European Organization for Nuclear Research (CERN) between 1998 and 2008, is the most powerful proton-proton circular collider (see Figure 5.1 for the overall view). Its length is 26.7 kilometers, the design center of mass energy is 14 TeV, and the design luminosity is 10^{34} cm^{-2}s^{-1}. The first physics run (LHC Run-1) has been in operation during 2010-2013 at a center of mass energy of 7 to 8 TeV. After its upgrade of a center of mass energy from 8 TeV to 13 TeV, the second physics run (LHC Run-2) started in 2015 and is planned to continue until 2018. After the Run-2, the upgrade of its luminosity by a factor of 10 to reach 10^{35} cm^{-2}s^{-1} is planned, which is the so-called High Luminosity LHC.

Two general-purpose detectors, A Toroidal LHC Apparatus (ATLAS) experiment and the Compact Muon Solenoid (CMS) are constructed at the LHC to explore TeV scale particle physics, namely, testing the SM at the TeV scale and searching for new physics beyond the SM. In 2012, the ATLAS and CMS collaborations independently discovered the Higgs boson [1, 2], the last particle in the SM to be directly observed.

5.2 Basics of LHC physics

In order to discuss basics of LHC physics, let us consider a process to produce a dilepton final state l^+l^- from a pair annihilation of quark (q) and antiquark ($\overline{q}$) at the LHC. We assume that this process is mediated by an intermediate state X, $q\overline{q} \to X \to l^+l^-$, and express the cross section of this process as $\sigma_{q\overline{q}}(\hat{s})$, where $\sqrt{\hat{s}}$ is the center of mass energy

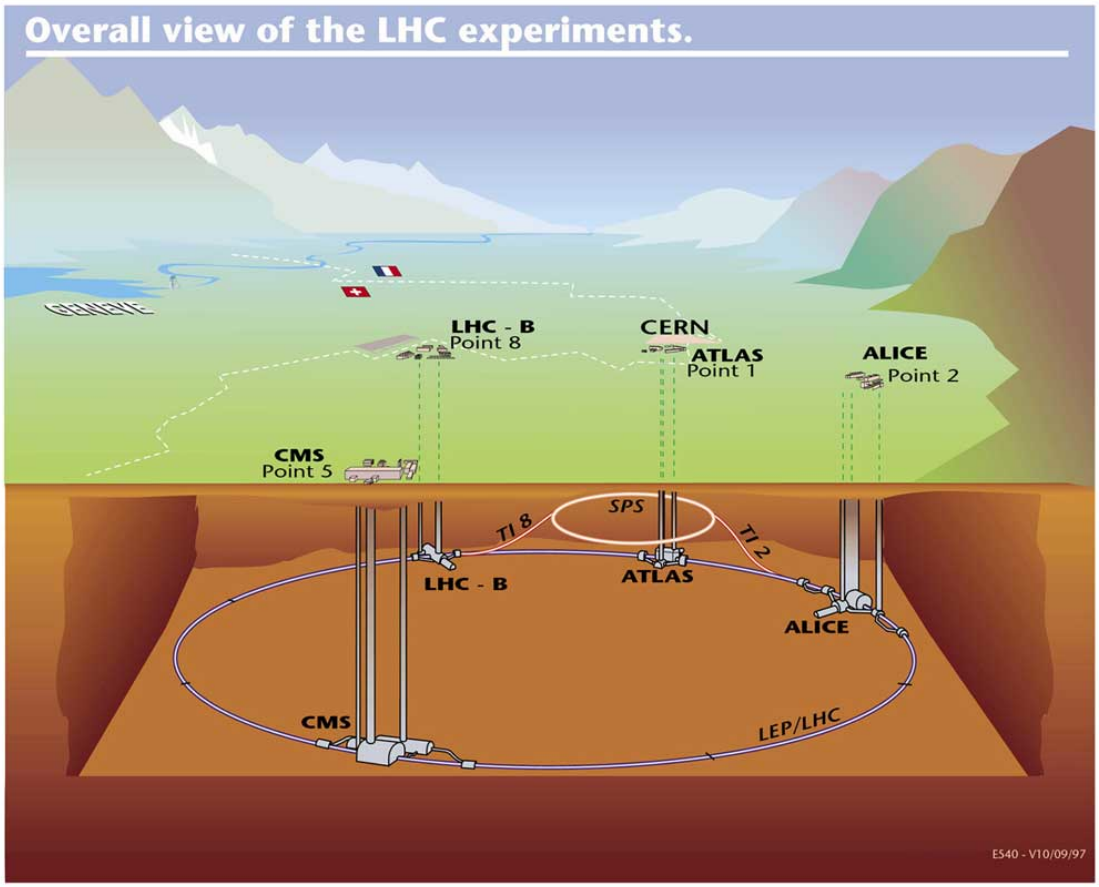

Figure 5.1: Overall view of the LHC [https://home.cern/].

for the initial state $q\overline{q}$, and $q\overline{q}$ can be $u\overline{u}$, $d\overline{d}$ and so on. Since the LHC is a proton-proton collider, we need to calculate the cross section of the process, $pp \to X \to l^+l^-$, by using $\sigma_{q\overline{q}}(\hat{s})$, such that

$$\sigma_{\rm LHC}(pp \to X \to l^+l^-) = 2\int_0^1 dx \int_0^1 dy \sum_{q,\overline{q}=u,\overline{u},\cdots} \left[f_q(x,Q)f_{\overline{q}}(y,Q)\sigma_{q\overline{q}}(\hat{s})\right]. \tag{5.2.1}$$

Here, $f_q(x,Q)$ is a parton distribution function (PDF) (see, for example, [65]), which is a probability to find a parton (quark in our case) with its energy $xE_{\rm proton}$ inside a proton with energy $E_{\rm proton}$, and Q is an energy transfer between partons in the process (we naturally take $Q = \sqrt{\hat{s}}$). Overall factor 2 is a combinatorial factor from choosing q in one proton or the other. The center of mass energy of $q\overline{q}$ is related to the LHC center of mass energy $\sqrt{s}$ as $\hat{s} = xys$ (for the LHC Run-2, $\sqrt{s} = 13$ TeV). From the energy conservation, $\sqrt{s} = M_{l^+l^-}$, where $M_{l^+l^-}$ is an invariant mass of the dilepton final state.

For later use, it is convenient to rewrite the cross section into the differential cross section, $d\sigma_{LHC}/dM_{l^+l^-}$. Using

$$\frac{d\sigma_{\rm LHC}}{dy} = \frac{xs}{2M_{l^+l^-}}\frac{d\sigma_{\rm LHC}}{dM_{l^+l^-}}, \tag{5.2.2}$$

we have

$$\frac{d\sigma_{\rm LHC}}{dM_{l^+l^-}} = 2\int_{x_{min}}^{1} dx \frac{2M_{l^+l^-}}{xs} f_q(x, M_{l^+l^-}) f_{\bar{q}}(\frac{M^2_{l^+l^-}}{xs}, M_{l^+l^-})\sigma(M^2_{l^+l^-}), \tag{5.2.3}$$

where $x_{min} = M^2_{l^+l^-}/s$. For example, the differential cross section shows a resonance peak at $M_{l^+l^-} = M_X$, where M_X is the mass of the intermediate state X. The ATLAS and CMS collaborations have been searching for such a resonance peak at the LHC.

Chapter 6

Z'_{B-L} portal dark matter in the minimal $B-L$ extended Standard Model

6.1 The minimal $B-L$ model with $\mathbf{Z}_2$ symmetry

As we have discussed in the previous chapter, the minimal $B-L$ extended Standard Model naturally incorporate the neutrino masses and mixings through the seesaw mechanism. However, a cold dark matter candidate is still missing in the model to be incorporated. Among a lot of possibilities, we consider a concise way of introducing a dark matter candidate to the model without extending its particle content [24]. We introduce a Z_2 symmetry: one right-handed neutrino N_R is assigned to be Z_2-odd, while the other fields are Z_2-even. The particle content listed on Table 6.1. Except for the introduction of the Z_2 symmetry and its assignments, the particle contents is identical to that of the minimal $B-L$ model in Table 4.1. The conservation of the Z_2 symmetry ensures the stability of the Z_2-odd N_R, and therefore, this right-handed neutrino is a unique dark matter candidate in the model [24].

With the Z_2 symmetry, the Yukawa sector of the minimal $B-L$ model is modified to be

$$\mathcal{L}^{B-L}_{\text{Yukawa}} \supset -\sum_{i=1}^{3}\sum_{j=1}^{2} Y_D^{ij}\overline{l_L^i} H N_R^j - \frac{1}{2}\sum_{k=1}^{2} Y_N^k \Phi \overline{N_R^{kC}} N_R^k - \frac{1}{2} Y_N \Phi \overline{N_R^C} N_R + H.c. \quad (6.1.1)$$

Note that because of the Z_2 symmetry, only the two generation right-handed neutrinos have the neutrino Dirac Yukawa coupling. The renormalizable scalar potential for the SM Higgs and the $B-L$ Higgs fields are the same as the minimal $B-L$ model, and the Higgs

	$SU(3)_C$	$SU(2)_L$	$U(1)_Y$	$U(1)_{B-L}$	Z_2
q_L^i	**3**	**2**	1/6	1/3	+
u_R^i	**3**	**1**	2/3	1/3	+
d_R^i	**3**	**1**	-1/3	1/3	+
l_L^i	**1**	**2**	-1/2	-1	+
N_R^j	**1**	**1**	0	-1	+
N_R	**1**	**1**	0	-1	-
e_R^i	**1**	**1**	-1	-1	+
H	**1**	**2**	-1/2	0	+
Φ	**1**	**1**	0	2	+

Table 6.1: The particle content of the minimal $B-L$ extended SM with Z_2 symmetry. We introduce the three right-handed neutrinos [N_R^j (j = 1, 2) and N_R] and the $B-L$ Higgs field (Φ) to the SM particle content (i = 1, 2, 3). Because of the Z_2 symmetry assignment shown here, the N_R is a unique (cold) dark matter candidate. Without loss of generality, we fix $x_\Phi = 1$ throughout this thesis.

fields develop their VEVs. Associated with the $B-L$ symmetry breaking, the Majorana neutrinos N_R^j (j = 1, 2), the dark matter particle N_R and the $B-L$ gauge boson (Z'_{B-L} boson) acquire their masses as

$$\begin{aligned} m_N^j &= \frac{Y_N^j}{\sqrt{2}} v_{B-L}, \\ m_{\rm DM} &= \frac{Y_N}{\sqrt{2}} v_{B-L}, \\ m_{Z'} &= 2 g_{B-L} v_{B-L}. \end{aligned} \tag{6.1.2}$$

The seesaw mechanism [10, 11, 12, 13, 14] is automatically implemented in the model after the electroweak symmetry breaking. Because of the Z_2 symmetry, only two generation right-handed neutrinos are relevant to the seesaw mechanism, and this so-called minimal seesaw [25, 26] has an enough number of free parameters in Y_D^{ij} and can reproduce the neutrino oscillation data.

The dark matter particle can communicate with the SM particles in two ways. One is through the Higgs bosons. In the Higgs potential of (4.1.6), the SM Higgs boson and the $B-L$ Higgs boson mix with each other in the mass eigenstates (see (4.1.11) and (4.1.12)), and this Higgs boson mass eigenstates mediate the interactions between the dark matter particle and the SM particles. Dark matter physics with the interactions mediated by the Higgs bosons have been investigated in [24, 27, 28]. The analysis involves four free

parameters: Yukawa coupling Y_N and three free parameters from the Higgs potential after two conditions of $v = 246$ GeV and the SM-like Higgs boson mass fixed to be 125 GeV are taken into account. The other way for the dark matter particle to communicate with the SM particles is through the $B - L$ gauge interaction with the Z'_{B-L} gauge boson. In this case, only three free parameters (g_{B-L}, $m_{Z'}$ and m_{DM}) are involved in dark matter physics analysis. In this thesis, we concentrate on dark matter physics mediated by the Z'_{B-L} boson, namely "Z' portal dark matter." When $|\lambda_{\rm mix}| \ll 1$ in the Higgs potential (4.1.6), the Higgs bosons mediated interactions are negligibly small, and the dark matter particle communicates with the SM particles only through the Z'_{B-L} boson. For example, this situation is realized in supersymmetric extension of our model [66], where $\lambda_{\rm mix}$ is forbidden by supersymmetry in the Higgs superpotential at the renormalizable level. When squarks and sleptons are all heavier than the dark matter particles, there is no essential difference in dark matter phenomenology between the nonsupersymmetric case and the supersymmetric case (see [66]). For a limited parameter choice, the Z'_{B-L} portal dark matter scenario has been investigated in [27, 28, 66].

6.2 Cosmological constraints on Z'_{B-L} portal dark matter

The dark matter relic density is measured at the 68% limit as [50]

$$\Omega_{\rm DM} h^2 = 0.1198 \pm 0.0015. \tag{6.2.1}$$

We now evaluate the relic density of the dark matter N_R and identify an allowed parameter region that satisfies the upper bound on the dark matter relic density of $\Omega_{\rm DM} h^2 \leq 0.1213$. The relic density of dark matter N_R is evaluated by solving the Boltzmann equation:

$$\frac{dY_{\rm DM}}{dx} = -\frac{s\langle \sigma v_{\rm rel}\rangle}{xH(m_{\rm DM})}(Y_{\rm DM}^2 - (Y_{\rm DM}^{\rm eq})^2), \tag{6.2.2}$$

where $Y_{\rm DM} = n_{DM}/s$ is the yield of the dark matter particle with the dark matter number density (n_{DM}) and the entropy density (s), Y_{DM} in thermal equilibrium is denoted as $Y_{\rm DM}^{\rm eq}$, $x \equiv m_{\rm DM}/T$ (T is temperature of the universe) is time normalized by the dark matter mass, $H(m_{\rm DM})$ is the Hubble parameter at $T = m_{\rm DM}$, and $\langle \sigma v_{\rm rel}\rangle$ is the thermal average of the cross section for dark matter annihilation process times relative velocity. We give

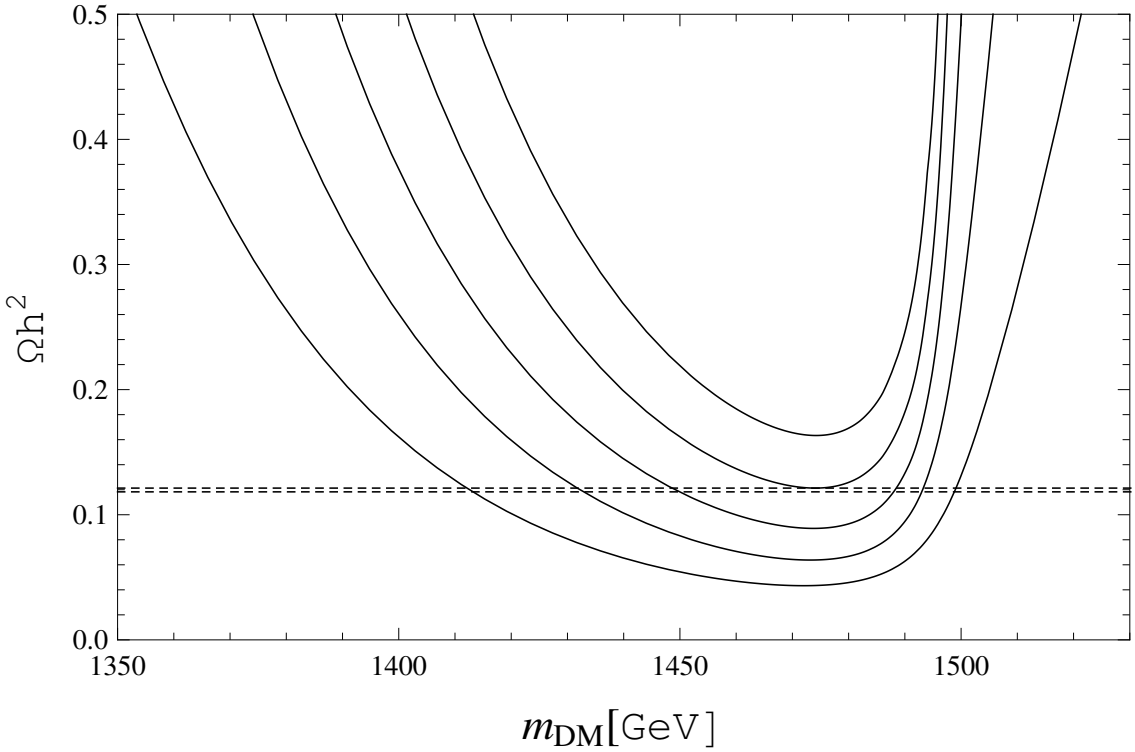

Figure 6.1: The relic density of the Z'_{B-L} portal right-hard neutrino dark matter as a function of the dark matter mass ($m_{\rm DM}$) for $m_{Z'} = 3$ TeV and various values of the gauge coupling $\alpha_{B-L} = 0.001,\ 0.0014,\ 0.002,\ 0.003$ and 0.005 (solid lines from top to bottom). The two horizontal lines denote the range of the observed dark matter relic density, $0.1183 \leq \Omega_{\rm DM} h^2 \leq 0.1213$.

explicit formulas of the quantities in the Boltzmann equation:

$$\begin{aligned} s &= \frac{2\pi^2}{45} g_* \frac{m_{\rm DM}^3}{x^3}, \\ H(m_{\rm DM}) &= \sqrt{\frac{4\pi^3}{45} g_*} \frac{m_{\rm DM}^2}{M_{pl}}, \\ sY_{\rm DM}^{\rm eq} &= \frac{g_{\rm DM}}{2\pi^2} \frac{m_{\rm DM}^3}{x} K_2(x), \end{aligned} \tag{6.2.3}$$

where $M_{pl} = 1.22 \times 10^{19}$ GeV is the Planck mass, g_* is the effective total degrees of freedom for SM particles in thermal equilibrium ($g_* = 106.75$ is employed in the following analysis), $g_{\rm DM} = 2$ is the degrees of freedom for the right-handed neutrino dark matter, and K_2 is the modified Bessel function of the second kind. In our Z'_{B-L} portal dark matter scenario, the dark matter particles pair-annihilate into the SM particles mainly through the s-channel Z'_{B-L} boson exchange (see the left panel of Figure 6.2). The thermal average

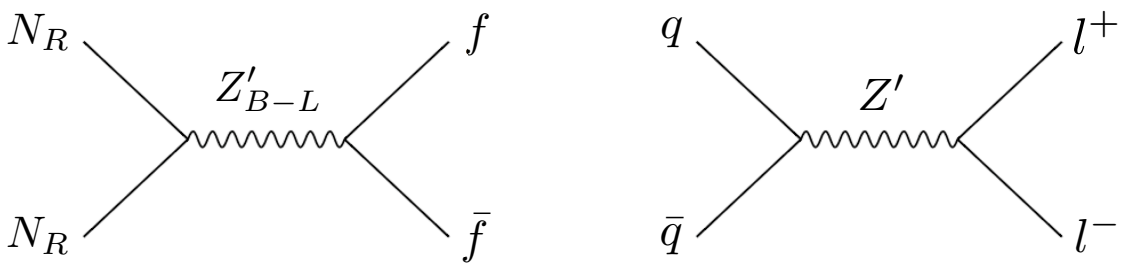

Figure 6.2: Left panel: Majorana neutrino dark matter (N_R) pair annihilation process into the SM fermions (f) through the Z'_{B-L} exchange in the s-channel, $N_R N_R \to Z'_{B-L} \to f\bar{f}$. Right panel: parton level process (quark (q) and anti-quark ($\bar{q}$) annihilation process) to produce a dilepton final state (l^+l^-) through an s-channel Z' exchange at the LHC.

of the annihilation cross section is calculated as

$$\langle \sigma v_{\rm rel} \rangle = (sY_{\rm DM}^{\rm eq})^{-2} g_{\rm DM}^2 \frac{m_{\rm DM}}{64\pi^4 x} \int_{4m_{\rm DM}^2}^{\infty} ds \hat{\sigma}(s) \sqrt{s} K_1 \left(\frac{x\sqrt{s}}{m_{\rm DM}} \right), \tag{6.2.4}$$

where $\hat{\sigma}(s) = 2(s - 4m_{\rm DM}^2)\sigma(s)$ is the reduced cross section with $\sigma(s)$ being the total annihilation cross section. The total cross section of the annihilation process $N_R N_R \to Z'_{B-L} \to f\bar{f}$ (f denotes an SM fermion) is calculated as

$$\sigma(s) = \pi \alpha_{B-L}^2 \frac{\sqrt{s(s - 4m_{\rm DM}^2)}}{(s - m_{Z'}^2)^2 + m_{Z'}^2 \Gamma_{Z'}^2} \left[\frac{37}{9} + \frac{1}{3}\beta_t \left(1 - \frac{1}{3}\beta_t^2 \right) \right], \tag{6.2.5}$$

with $\beta_t(s) = \sqrt{1 - 4m_t^2/s}$, top quark mass of $m_t = 173.34$ GeV [58] and the total decay width of Z'_{B-L} boson given by

$$\Gamma_{Z'} = \frac{\alpha_{B-L}}{6} m_{Z'} \left[\frac{37}{3} + \frac{\beta_t(m_{Z'}^2)}{3}(3 - \beta_t(m_{Z'}^2)^2) + \left(1 - \frac{4m_{\rm DM}^2}{m_{Z'}^2} \right)^{\frac{2}{3}} \theta \left(\frac{m_{Z'}^2}{m_{\rm DM}^2} - 4 \right) \right] \tag{6.2.6}$$

Here, we have taken $m_N^j > m_{Z'}/2$, for simplicity.

Solving the Boltzmann equation numerically, we evaluate the dark matter relic density by

$$\Omega_{\rm DM} h^2 = \frac{m_{\rm DM} s_0 Y(\infty)}{\rho_{crit}/h^2}, \tag{6.2.7}$$

where $Y(\infty)$ is the yield in the limit of $x \to \infty$, $s_0 = 2890$ cm^{-3} is the entropy density of the present universe, and $\rho_{\rm crit}/h^2 = 1.05 \times 10^{-5}$ GeV/cm^3 is the critical density. Note

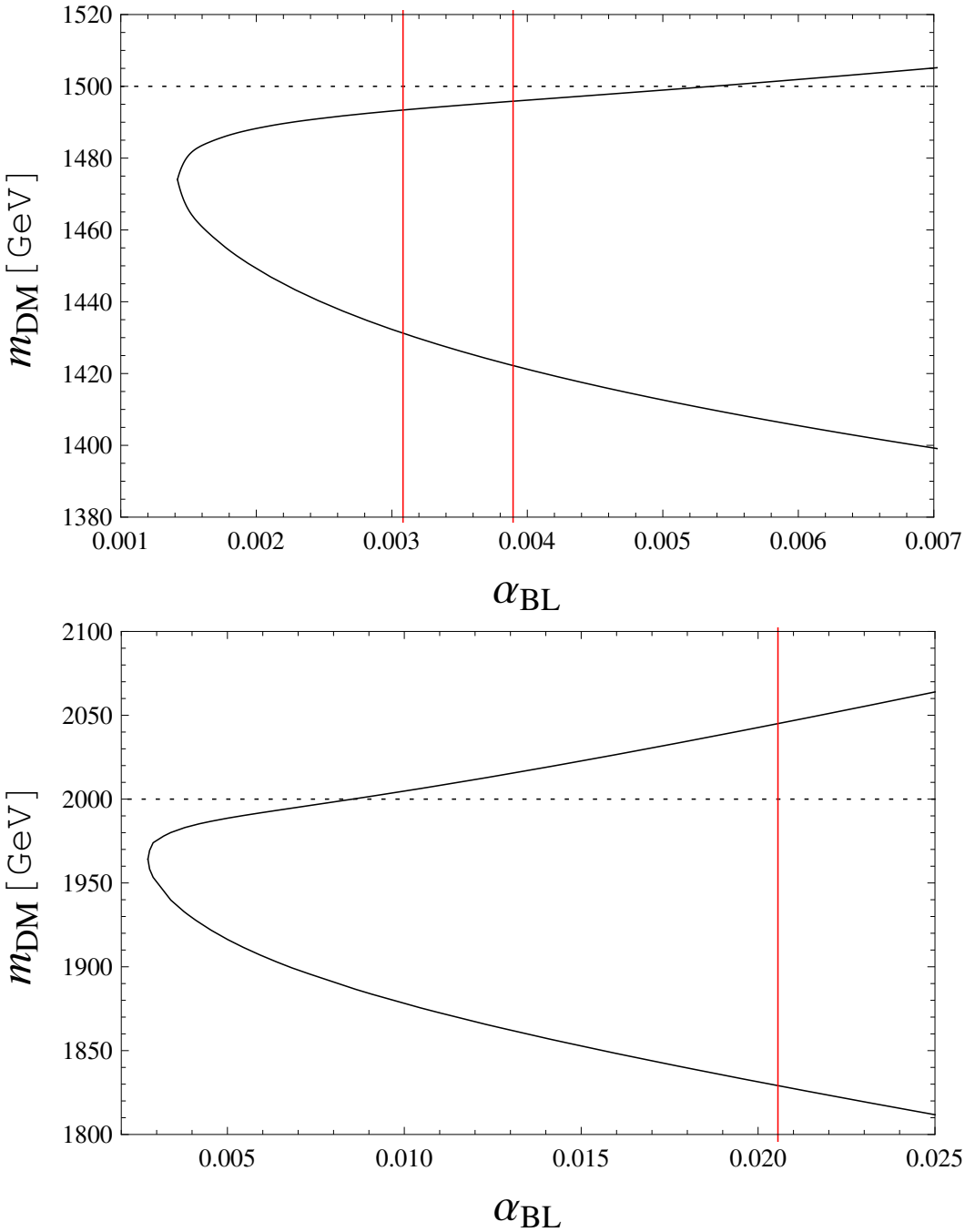

Figure 6.3: The dark matter mass as a function of α_{B-L} for $m_{Z'} = 3$ TeV (top panel) and 4 TeV (bottom panel). Along the solid (black) curve in each panel, $\Omega_{\rm DM}h^2 = 0.1198$ is satisfied. The dotted lines correspond to $m_{\rm DM} = m_{Z'}/2$. The vertical solid lines (in red) denote the upper bound on α_{B-L} obtained from the recent LHC Run-2 results (see Figures 6.5 and 6.6). In the top panel, the left vertical line represents the constraint from the ATLAS result [42], while the right one is from the CMS result [43]. In the bottom panel, the vertical line represents the constraint from the ATLAS result [42].

that we have only three parameters, $\alpha_{B-L} = g_{B-L}^2/(4\pi)$, $m_{Z'}$ and $m_{\rm DM}$, in our analysis. For $m_{Z'} = 3$ TeV and various values of the gauge coupling α_{B-L}, Figure 6.1 depicts the resultant dark matter relic density as a function of its mass $m_{\rm DM}$, along with the observed bounds $0.1183 \leq \Omega_{\rm DM}h^2 \leq 0.1213$ [50] (two horizontal dashed lines). The solid curves from top to bottom correspond to the results for $\alpha_{B-L} = 0.001,\ 0.0014,\ 0.002,\ 0.003$ and 0.005, respectively. We find that in order to reproduce the observed relic density, the dark matter mass must be close to half of the Z'_{B-L} boson mass. In other words, normal values of the dark matter annihilation cross section leads to overabundance, and it is necessary that an enhancement of the cross section through the Z'_{B-L} boson resonance in the s-channel annihilation process.

For a fixed $m_{\rm DM}$ in the Figure 6.1, the resultant relic density becomes larger as the gauge coupling α_{B-L} is lowered. As a result, there is a lower bound on α_{B-L} in order to satisfy the cosmological upper bound on the dark matter relic density $\Omega_{\rm DM}h^2 \leq 0.1213$. For an α_{B-L} value larger than the lower bound, we can find two values of m_{DM} which result in the center value of the observed relic density $\Omega_{\rm DM}h^2 = 0.1198$. In Figures 6.3, we show the dark matter mass yielding $\Omega_{\rm DM}h^2 = 0.1198$ as a function of α_{B-L}. The top panel shows the result for $m_{Z'} = 3$ TeV, while the corresponding result for $m_{Z'} = 4$ TeV is shown in the bottom panel. As a reference, we also show the dotted lines corresponding to $m_{\rm DM} = m_{Z'}/2$. In Figure 6.1, we see that the minimum relic density is achieved by a dark matter mass which is very close to, but smaller than $m_{Z'}/2$. Although the annihilation cross section of (6.2.5) has a peak at $\sqrt{s} = m_{Z'}$, the thermal averaged cross section given in (6.2.4) includes the integral of the product of the reduced cross section and the modified Bessel function K_1. Our results indicate that for $m_{\rm DM}$ taken to be slightly smaller than $m_{Z'}/2$, the thermal averaged cross section is larger than the one for $m_{\rm DM} = m_{Z'}/2$.

As mentioned above, for a fixed Z'_{B-L} boson mass, we can find a corresponding lower bound on the gauge coupling α_{B-L} in order for the resultant relic density not to exceed the cosmological upper bound $\Omega_{\rm DM}h^2 = 0.1213$. Figure 6.4 depicts the lower bound of α_{B-L} as a function of $m_{Z'}$ [solid (black) line]. Along this solid (black) line, we find that the dark matter mass is approximately given by $m_{\rm DM} \simeq 0.49 m_{Z'}$. The dark matter relic density exceeds the cosmological upper bound in the region below the solid (black) line. Along with the other constraints that will be obtained in the next section, Figure 6.4 is our main results in this chapter.

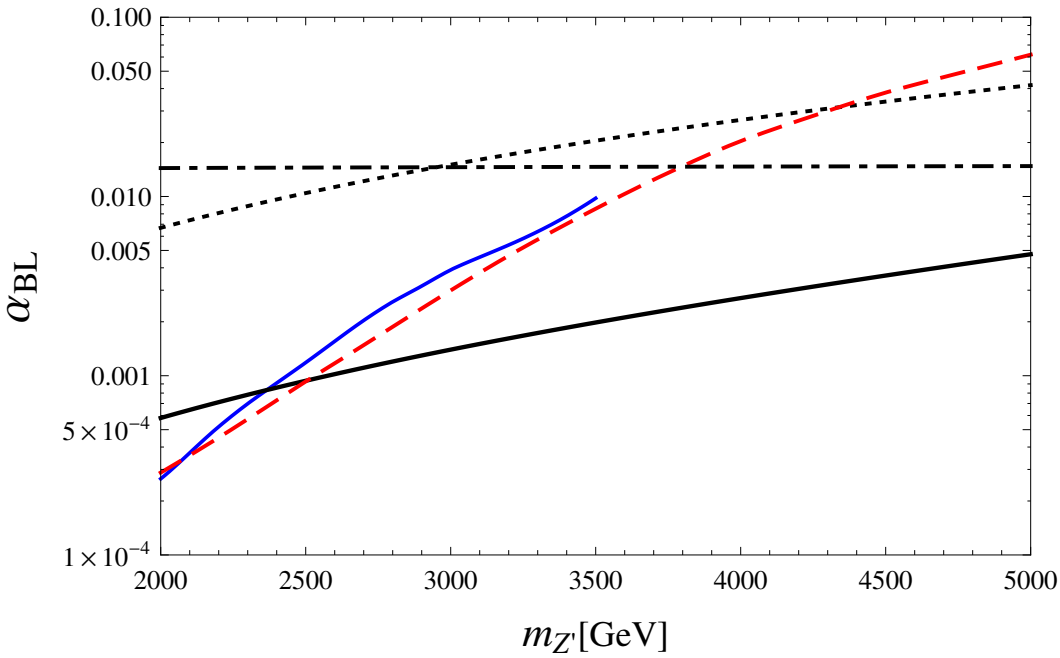

Figure 6.4: Allowed parameter region for the Z'_{B-L} portal dark matter scenario. The solid (black) line depicts the lower bound on α_{B-L} as a function of $m_{Z'}$ from the cosmological upper bound on the dark matter relic density. The dashed line (in red) shows the upper bound on α_{B-L} as a function of $m_{Z'}$ from the ATLAS results of the search for Z' boson resonance, while the (blue) diagonal line in the range of 2000 GeV $\leq m_{Z'} \leq$ 3500 GeV denotes the upper bound obtained from the result by the CMS collaboration. The LEP bound is depicted as the dotted line. The regions above these dashed, solid and dotted lines are excluded. We also show a theoretical upper bound on α_{B-L} to avoid the Landau pole of the running $B-L$ gauge coupling below the Planck mass M_{pl}.

6.3 LHC Run-2 constraints

Recently, the LHC Run-2 started its operation with a 13 TeV collider energy.[1] Preliminary results from the ATLAS and the CMS collaborations have been reported. The Run-2 results have provided constraints on new physics models. The ATLAS and the CMS collaborations continue search for Z' boson resonance with dilepton final states at the LHC Run-2 (see the right panel of Figure 6.2), and have improved the upper limits on the Z' boson production cross section from those in the LHC Run-1 [67, 68]. Employing the LHC Run-2 results, we will derive an upper bound on α_{B-L} as a function of $m_{Z'}$.

[1]This chapter is based on my original work [45], where the first LHC Run-2 results [42, 43] were employed in our analysis.

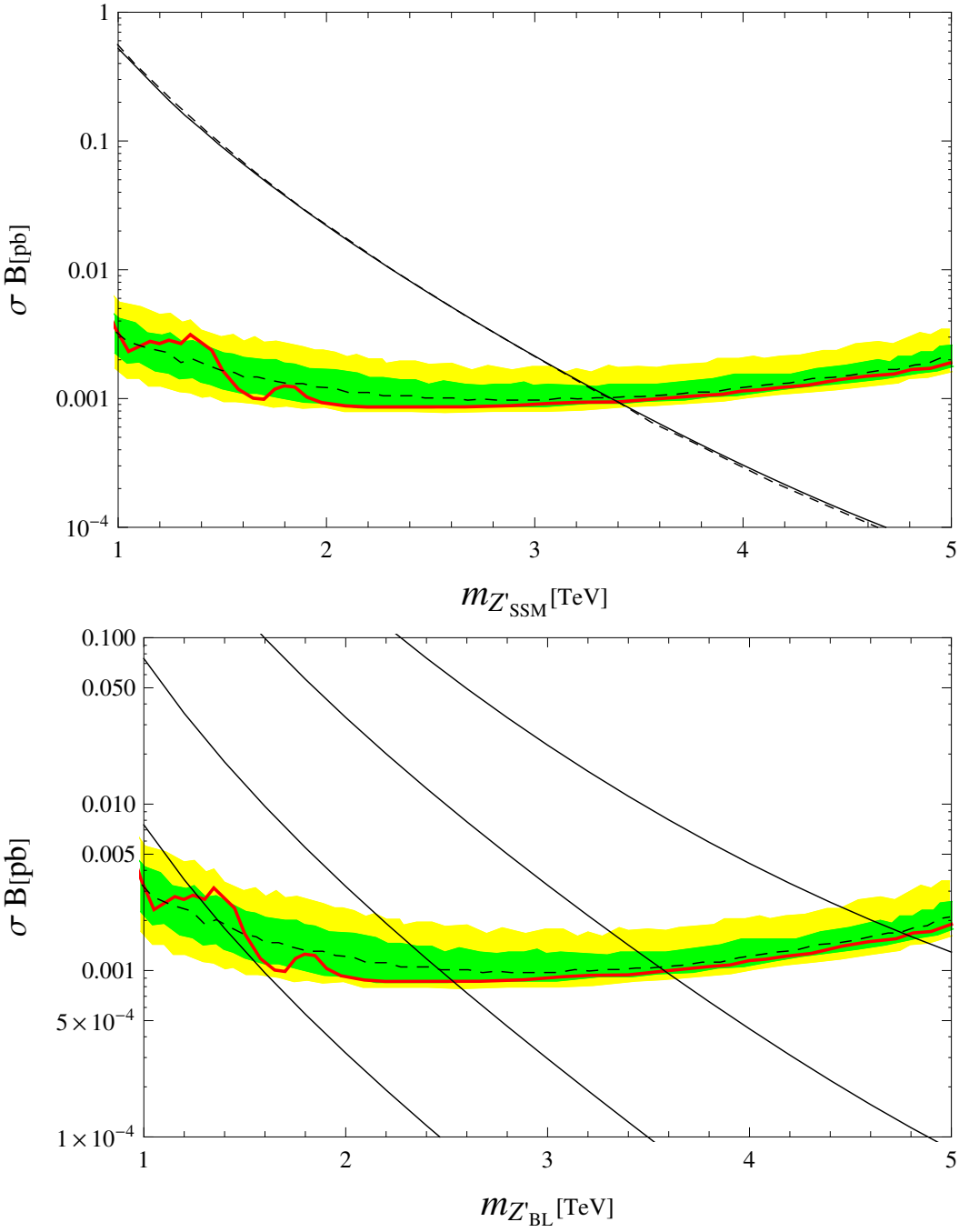

Figure 6.5: Top panel: the solid line shows the cross section as a function of the Z'_{SSM} mass for $k = 1.31$, along with the ATLAS result in [42]. Bottom panel: the cross sections calculated for various values of α_{B-L} with $k = 1.31$. The solid lines from left to right correspond to $\alpha_{B-L} = 0.0001$, 0.001, 0.01 and 0.05, respectively.

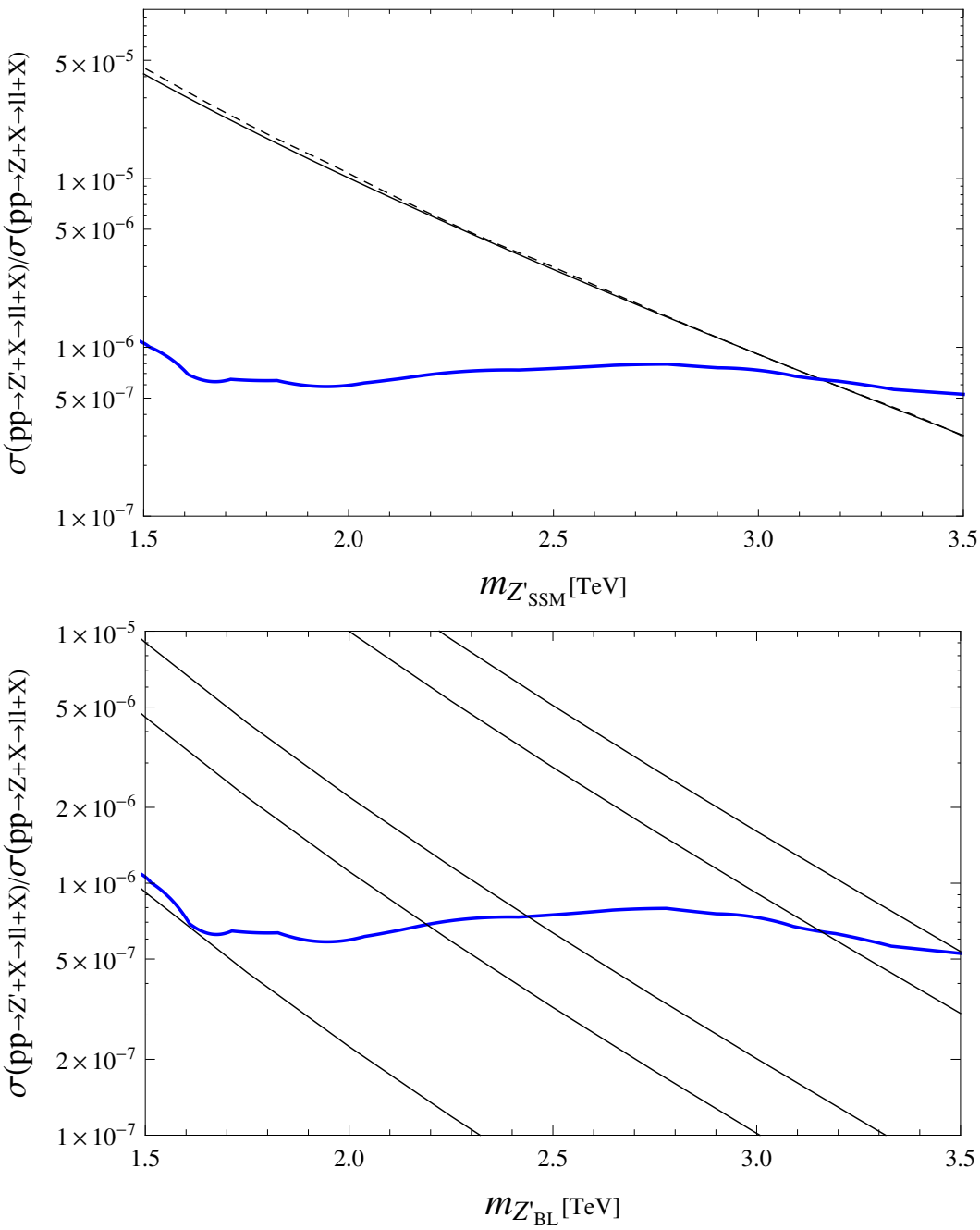

Figure 6.6: Top panel: The solid line shows the cross section as a function of the Z'_{SSM} mass for $k = 1.80$, along with the CMS result in [43]. Bottom panel: the cross section ratios calculated for various values of α_{B-L} with $k = 1.80$. The solid lines from left to right correspond to $\alpha_{B-L} = 0.0001$, 0.0005, 0.001, 0.005 and 0.01, respectively.

Since we have obtained in the previous section the lower bound on α_{B-L} as a function of $m_{Z'}$ from the constraint on the dark matter relic density, the LHC Run-2 results are complementary to the cosmological constraint. As a result, the parameter space of the Z'_{B-L} portal dark matter scenario is severally constrained once the two constraints are combined.

Let us consider the Z'_{B-L} boson production process, $pp \to Z'_{B-L} + X \to l^+l^- + X$, where X denotes hadron jets. The differential cross section is given by

$$\frac{d\sigma}{dM_{ll}} = \sum_{a,b} \int_{\frac{M_{ll}^2}{E_{\rm CM}^2}}^{1} dx \frac{2M_{ll}}{xE_{\rm CM}^2} f_a(x,Q^2) f_b\left(\frac{M_{ll}^2}{E_{\rm CM}^2}, Q^2\right) \hat{\sigma}(q\bar{q} \to Z'_{B-L} \to l^+l^-), \qquad (6.3.1)$$

where $E_{\rm CM} = 13$ TeV is the LHC Run-2 energy in the center-of-mass frame, M_{ll} is the invariant mass of the dilepton final state, and f_a is the PDF for a parton "a." For the PDFs we utilize CTEQ6L [69] with $Q = m_{Z'}$ as the factorization scale. Here, the cross section for the colliding partons is given by

$$\hat{\sigma} = \frac{4\pi\alpha_{B-L}^2}{81} \frac{M_{ll}^2}{(M_{ll}^2 - m_{Z'}^2)^2 + m_{Z'}^2\Gamma_{Z'}^2}. \qquad (6.3.2)$$

In calculating the total cross section, we set a range of M_{ll} that is used in the analysis by the ATLAS and the CMS collaborations, respectively. We compare our results of the total cross section with the upper limits of the ATLAS and CMS results.

The so-called sequential SM Z' (Z'_{SSM}) model [70] has been considered as a reference model in the analysis by the ATLAS and the CMS collaborations. In this model, the couplings of the Z'_{SSM} boson with quarks and leptons are exactly the same as those of the SM Z boson, while its mass is a free parameter. In order to examine the consistency of our analysis with those by the ATLAS collaboration, we first calculate the cross section $\sigma(pp \to Z'_{SSM} + X \to l^+l^- + X)$ for the sequential Z' boson like (6.3.1). By integrating the differential cross section for the region of 128 GeV $\leq M_{ll} \leq$ 6000 GeV [67], we obtain the total cross section as a function of Z'_{SSM} boson mass. The top panel on Figure 6.5 shows our result (diagonal solid line), along with the plot presented by the ATLAS collaboration [42] (diagonal dashed line). The ATLAS collaboration obtains the upper limit of the cross section of the process $pp \to Z' + X \to l^+l^- + X$ (red line in Figure 6.5). Comparing the limit with the theory prediction for the Z'_{SSM} boson production (diagonal dashed line), we obtain a lower bound of Z'_{SSM} boson mass as $m_{Z'_{\rm SSM}} \geq 3.4$ TeV. When we compare our theory calculation with the one by the ATLAS collaboration, we need to consider a

difference between PDFs used in two analysis and uncertainties from QCD corrections. Taking these factors into account, we have scaled our cross section to obtain the same bound of $m_{Z'_{\rm SSM}} \geq 3.4$ TeV. In the top panel on Figure 6.5, we have chosen this scaling factor to be $k = 1.31$. We see that the two lines from our calculation (diagonal solid line) and the ATLAS collaboration [42] (diagonal dashed line) are very well overlapping. We use this factor $k = 1.31$ in our LHC analysis for the Z'_{B-L} production. For various values of α_{B-L}, we calculate the cross section $\sigma(pp \to Z'_{B-L} + X \to l^+l^- + X)$. Our results are shown in the bottom panel of Figure 6.5, along with the plot in [42]. The diagonal solid lines from left to right correspond to $\alpha_{B-L} = 0.0001,\ 0.001,\ 0.01$ and 0.05, respectively. From the intersections of the horizontal curve and diagonal solid lines, we can read off a lower bound on the Z'_{B-L} boson mass for a fixed α_{B-L} value. In this way, we have obtained the upper bound on α_{B-L} as a function the Z'_{B-L} boson mass, which is depicted in Figure 6.4 [dashed (red) line].

We also consider the result by the CMS collaboration [43]. Corresponding to their analysis, we integrate the differential cross section for the range of $0.97 m_{Z'_{SSM}} \leq M_{ll} \leq 1.03 m_{Z'_{SSM}}$. The limits provided by the CMS collaboration are given as the ratio of the cross sections, $\sigma(pp \to Z'_{SSM} + X \to l^+l^- + X))/\sigma(pp \to Z + X \to l^+l^- + X)$, where $\sigma(pp \to Z + X \to l^+l^- + X) = 1928$ pb is the dilepton production cross section mediated by the Z/γ^* exchange in a mass window of 60 to 120 GeV. Our result is shown as a diagonal solid line in the top panel of Figure 6.6, along with the plot presented in [43]. The CMS collaboration obtains the upper limit of the ratio, $\sigma(pp \to Z'_{SSM} + X \to l^+l^- + X)/\sigma(pp \to Z + X \to l^+l^- + X)$ (blue line in Figure 6.6). Comparing the limit with the theory prediction for the Z'_{SSM} boson production (diagonal dashed line), we obtain a lower bound of Z'_{SSM} boson mass as $m_{Z'_{\rm SSM}} \geq 3.15$ TeV. In our calculation, we set a factor $k = 1.80$ to yield the same bound of $m_{Z'_{SSM}} \geq 3.15$ TeV. The top panel shows that our results are well-overlapping with the theoretical cross section presented in [43].

Using $k = 1.80$, we calculate $\sigma(pp \to Z'_{B-L} + X \to l^+l^- + X)$ for various values of α_{B-L}. Our results are shown in the bottom panel of Figure 6.6, along with the plot in [43]. The diagonal solid lines from left to right correspond to $\alpha_{B-L} = 0.0001,\ 0.0005,\ 0.001,\ 0.005$ and 0.01, respectively. From the intersections of the horizontal (blue) curve and diagonal solid lines, we can read off a lower bound on the Z'_{B-L} boson mass for a fixed α_{B-L} value. In Figure 6.4, the diagonal solid (blue) line in the range of 2000 GeV $\leq m_{Z'} \leq$ 3500 GeV

shows the upper bound on α_{B-L} as a function the Z' boson mass. The ATLAS and the CMS bounds are similar, and the ATLAS bound is slightly more severe than the CMS bound, and applicable to a higher mass range up to $m_{Z'} = 5000$ GeV.

In Figure 6.4, we also show the LEP bound (dotted line) on 4-Fermi interactions generated by the Z'_{B-L} boson exchange [71]. An updated limit with the final LEP 2 data [6] is found to be [72]

$$\frac{m_{Z'}}{g_{B-L}} \geq 6.9 \text{ TeV} \tag{6.3.3}$$

at 95% confidence level. We find that the ATLAS results at the LHC Run-2 provide more severe constraints than the LEP results for $m_{Z'} \leq 4.3$ TeV. In order to avoid the Landau pole of the running $B-L$ coupling $\alpha_{B-L}(\mu)$, below the Plank mass ($1/\alpha_{B-L}(M_{pl}) > 0$), we find

$$\alpha_{B-L} < \frac{\pi}{6 \ln \left[\frac{M_{pl}}{m_{Z'}}\right]}, \tag{6.3.4}$$

which is shown as the dashed-dotted line in Figure 6.4. Here, the gauge coupling α_{B-L} used in our analysis for dark matter physics and LHC physics is defined as the running gauge coupling $\alpha_{B-L}(\mu)$ at $\mu = m_{Z'}$, and we have employed the renormalization group equation at the one-loop level with $m_N^1 = m_N^2 = m_\Phi = m_{Z'}$, for simplicity.

Chapter 7

Z' portal dark matter in the minimal $U(1)_X$ extended Standard Model

7.1 The minimal $U(1)_X$ model with Z_2 symmetry

In this chapter, we generalize Z'_{B-L} portal dark matter in the minimal $B-L$ model to the minimal $U(1)_X$ model. This model is defined by the particle content listed on Table 7.1. The introduction of the Z_2 symmetry is crucial to incorporate a DM candidate in the model while keeping the minimality of the particle content. The conservation of the Z_2 symmetry ensures the stability of the Z_2-odd right-handed neutrino, and, therefore, it is a unique DM candidate in the model.

The Yukawa sector of the SM is extended to have

$$\mathcal{L}_{\text{Yukawa}} \supset -\sum_{i=1}^{3}\sum_{j=1}^{2} Y_D^{ij}\overline{l_L^i}HN_R^j - \frac{1}{2}\sum_{k=1}^{2} Y_N^k \Phi \overline{N_R^{kC}} N_R^k - \frac{1}{2} Y_N \Phi \overline{N_R^C} N_R + H.c., \quad (7.1.1)$$

where the first term in the right-hand side is the Dirac Yukawa coupling, and the second and third terms are the Majorana Yukawa couplings. Without loss of generality, the Majorana Yukawa couplings are diagonal. Note that because of the Z_2 symmetry, only the two-generation right-handed neutrinos have the neutrino Dirac Yukawa coupling. A nonzero VEV of the $U(1)_X$ Higgs field Φ breaks the $U(1)_X$ gauge symmetry and generates the Majorana masses for the right-handed neutrinos. Then, the seesaw mechanism is automatically implemented in the model after the electroweak symmetry breaking. Because of the Z_2 symmetry, only two-generation right-handed neutrinos are relevant to the seesaw mechanism. Even with two right-handed neutrinos, the Dirac Yukawa coupling constants Y_D^{ij} have an enough number of free parameters to reproduce the neutrino oscillation data.

	$SU(3)_C$	$SU(2)_L$	$U(1)_Y$	$U(1)_X$	Z_2
q_L^i	**3**	**2**	1/6	$(1/6)x_H + 1/3$	+
u_R^i	**3**	**1**	2/3	$(2/3)x_H + 1/3$	+
d_R^i	**3**	**1**	-1/3	$-(1/3)x_H + 1/3$	+
l_L^i	**1**	**2**	-1/2	$-(1/2)x_H - 1$	+
N_R^j	**1**	**1**	0	-1	+
N_R	**1**	**1**	0	-1	−
e_R^i	**1**	**1**	-1	$-x_H - 1$	+
H	**1**	**2**	-1/2	$-(1/2)x_H$	+
Φ	**1**	**1**	0	2	+

Table 7.1: The particle content of the minimal $U(1)_X$ extended SM with Z_2 symmetry. In addition to the SM particle content (i = 1, 2, 3), the three right-handed neutrinos [N_R^j (j = 1, 2) and N_R] and the $U(1)_X$ Higgs field (Φ) are introduced. Because of the Z_2 symmetry assignment shown here, the N_R is a unique (cold) dark matter candidate. The $U(1)_X$ charges of fields are determined by two real parameters, x_H and x_Φ. Without loss of generality, we fix $x_\Phi = 1$ throughout this thesis.

The baryon asymmetry in the universe can also be reproduced with the two right-handed neutrinos [25, 26] (see, for example, [73] for detailed analysis of leptogenesis at the TeV scale with two right-handed neutrinos).

The renormalizable scalar potential for the SM Higgs doublet (H) and the $U(1)_X$ Higgs fields is given by

$$V = \lambda_H \left(H^\dagger H - \frac{v^2}{2} \right)^2 + \lambda_\Phi \left(\Phi^\dagger \Phi - \frac{v_X^2}{2} \right)^2 + \lambda_{\rm mix} \left(H^\dagger H - \frac{v^2}{2} \right) \left(\Phi^\dagger \Phi - \frac{v_X^2}{2} \right), \quad (7.1.2)$$

where all quartic couplings are chosen to be positive. At the potential minimum, the Higgs fields develop their VEVs as

$$\begin{aligned} \langle H \rangle &= \begin{pmatrix} \frac{v}{\sqrt{2}} \\ 0 \end{pmatrix}, \\ \langle \Phi \rangle &= \frac{v_X}{\sqrt{2}}. \end{aligned} \quad (7.1.3)$$

In this thesis, we assume $\lambda_{mix} \ll 1$ and neglect the mixing between the SM Higgs boson and the $U(1)_X$ Higgs boson. Hence, right-handed neutrino dark matter communicates with the SM particles only through the Z' boson. Associated with the $U(1)_X$ symmetry breaking, the Majorana neutrinos N_R^j ($j = 1, 2$), the dark matter particle N_R, and the Z'

gauge boson acquire their masses as

$$
\begin{aligned}
m_N^j &= \frac{Y_N^j}{\sqrt{2}} v_X, \\
m_{\rm DM} &= \frac{Y_N}{\sqrt{2}} v_X, \\
m_{Z'} &= g_X \sqrt{4v_X^2 + \frac{x_H^2 v_X^2}{4}} \simeq 2 g_X v_X,
\end{aligned}
\tag{7.1.4}
$$

where g_X is the $U(1)_X$ gauge coupling, and the Large Electron-Positron Collider (LEP) constraint [5, 6] $v_X^2 \gg v^2$ has been used. Because of the LEP constraint, the mass mixing of the Z' boson with the SM Z boson is very small, and we neglect it in our analysis in the following. Assuming $\lambda_{\rm mix} \ll 1$, we focus on the Z'-portal nature of right-handed neutrino dark matter. In this case, only four free parameters (g_X, $m_{Z'}$, $m_{\rm DM}$, and x_H) are involved in our analysis. As we will discuss in the next section, it turns out that the condition of $m_{\rm DM} \simeq m_{Z'}/2$ must be satisfied to reproduce the observed dark matter relic density. Thus, $m_{\rm DM}$ does not work as an independent parameter, so that our results are described by only three free parameters.

7.2 Cosmological constraints on Z' portal dark matter

We evaluate the dark matter relic density and identify an allowed parameter region to satisfy the upper bound of $\Omega_{\rm DM} h^2 \leq 0.1213$ (see (6.2.1)). The dark matter relic density is evaluated by integrating the Boltzmann equation (6.2.2). In our Z' portal dark matter scenario, the dark matter particles pair-annihilate into the SM particles through the s-channel Z' boson exchange. The thermally averaged annihilation cross section is given by (6.2.4). In the minimal $U(1)_X$ model, the total cross section of the dark matter pair annihilation process $N_R N_R \to Z' \to f\overline{f}$ (f denotes the SM fermions) is calculated as

$$
\sigma(s) = \frac{\pi}{3} \alpha_X^2 \frac{\sqrt{s(s-4m_{\rm DM}^2)}}{(s-m_X^2)^2 + m_{Z'}^2 \Gamma_{Z'}^2} F(x_H),
\tag{7.2.1}
$$

where

$$
F(x_H) = 13 + 16 x_H + 10 x_H^2 = 10(x_H + 0.8)^2 + 6.6,
\tag{7.2.2}
$$

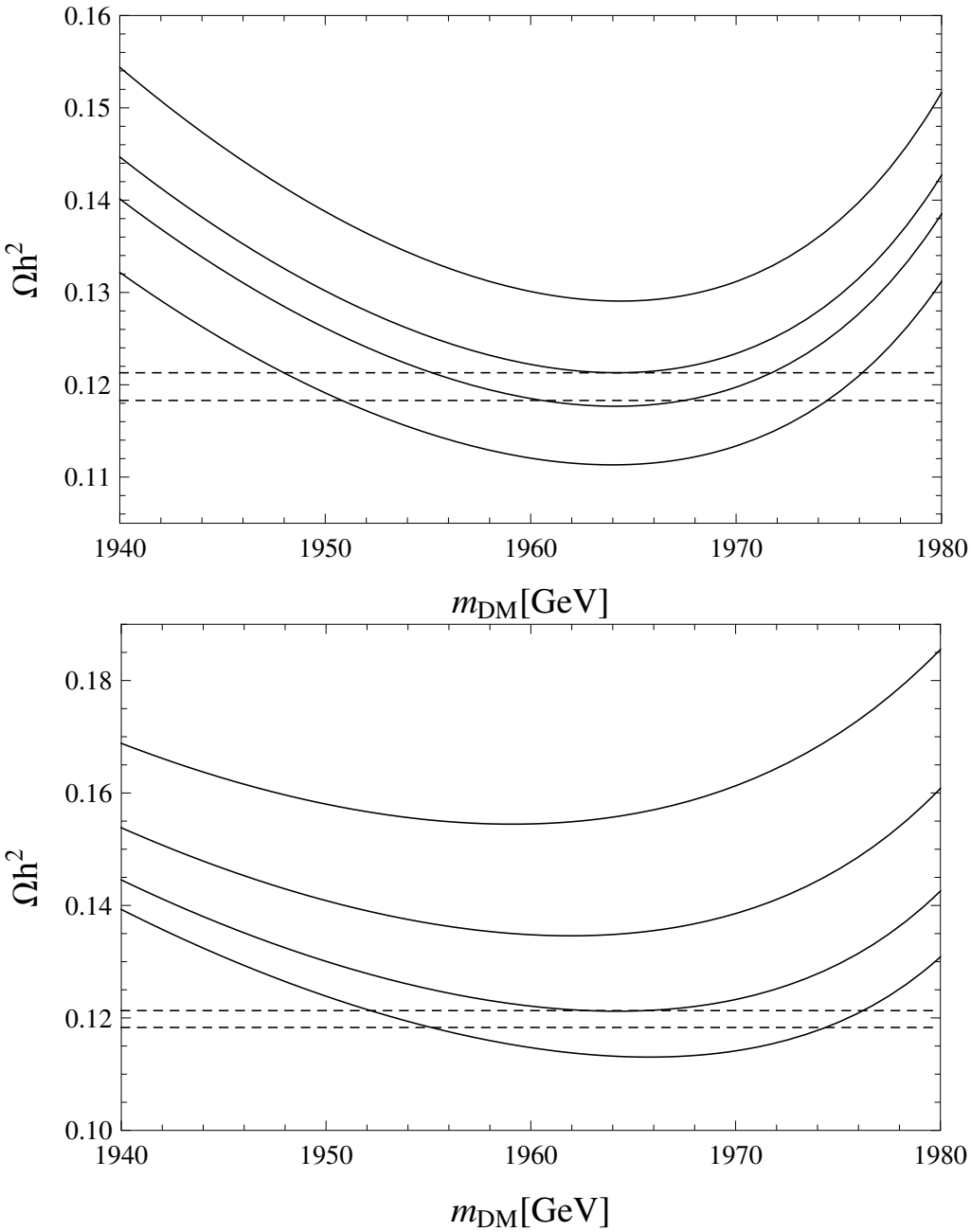

Figure 7.1: The relic density of the Z' portal right-handed neutrino dark matter is shown as a function of $m_{\rm DM}$ for $m_{Z'} = 4$ TeV. In the top panel, we have fixed $x_H = 0$ (the minimal $B - L$ model limit). The solid curves show the relic density for $\alpha_X = 0.0025$, 0.0027, 0.0028, and 0.0030, respectively, from top to bottom. In the bottom panel, we have fixed $\alpha_X = 0.0027$. The solid curves show the relic density for various values of $x_H = -0.8$, 0, 0.5, and 1.0, respectively, from bottom to top. The region in between two horizontal lines corresponds to the observed DM relic density, $0.1183 \leq \Omega_{\rm DM} h^2 \leq 0.1213$, in (6.2.1).

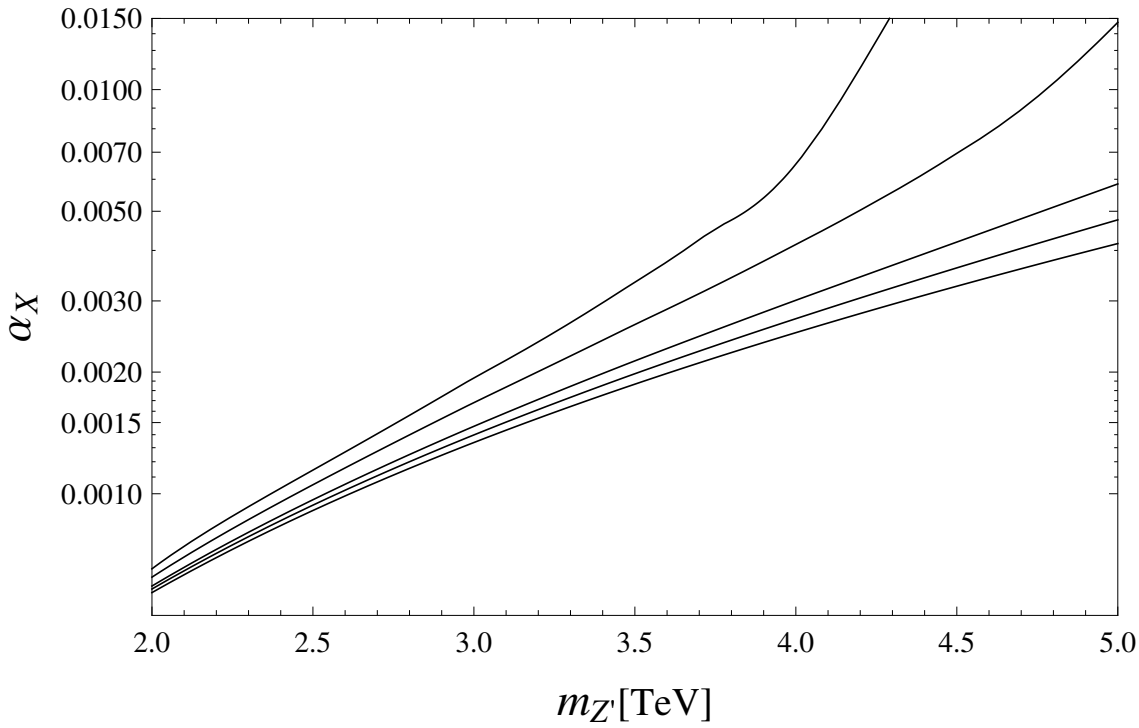

Figure 7.2: The lower bounds on α_X as a function of $m_{Z'}$ for various values of x_H, to satisfy the cosmological constraint of $0.1183 \leq \Omega_{\rm DM}h^2 \leq 0.1213$. The solid lines from top to bottom correspond to $x_H = -3$, $+1$, -2, 0, and -1, respectively. As the input x_H value is going away from the point of $x_H = -0.8$, the lower bound on α_X is increasing.

and the total decay width of Z' boson is given by

$$\Gamma_{Z'} = \frac{\alpha_X}{6} m_{Z'} \left[F(x_H) + \left(1 - \frac{4m_{\rm DM}^2}{m_{Z'}^2}\right)^{\frac{3}{2}} \theta\left(\frac{m_{Z'}^2}{m_{\rm DM}^2} - 4\right)\right]. \tag{7.2.3}$$

Here, we have neglected all SM fermion masses and assumed $m_N^j > m_{Z'}/2$, for simplicity.

Solving the Boltzmann equation numerically, we evaluate the dark matter relic density by

$$\Omega_{\rm DM}h^2 = \frac{m_{\rm DM} s_0 Y(\infty)}{\rho_{crit}/h^2}, \tag{7.2.4}$$

where $Y(\infty)$ is the yield in the limit of $x \to \infty$, $s_0 = 2890$ cm^{-3} is the entropy density of the present universe, and $\rho_{\rm crit}/h^2 = 1.05 \times 10^{-5}$ GeV/cm^3 is the critical density. Note that we have only four parameters, $\alpha_X = g_X^2/(4\pi)$, $m_{Z'}$, $m_{\rm DM}$ and x_H, in our analysis. For $m_{Z'} = 4$ TeV, our results are shown in Figure 7.1, along with the observed dark

matter relic density, $0.1183 \leq \Omega_{\rm DM}h^2 \leq 0.1213$ [50] (two horizontal dashed lines). In the top panel, we have fixed $x_H = 0$, which is the minimal $B - L$ model limit. The solid curves show the dark matter relic densities for $\alpha_X = 0.0025$, 0.0027, 0.0028, and 0.0030, respectively, from top to bottom. From the plots, we can see that the observed relic density can be reproduced only for $\alpha_X \geq 0.0027$. Furthermore, the cosmological constraint is satisfied for $m_{\rm DM} \simeq m_{Z'}/2$, which indicates that the dark matter annihilation cross section needs to be enhanced via the s-channel Z' boson resonance. The bottom panel shows our results for various values of x_H with the fixed $\alpha_X = 0.0027$. The solid curves correspond to the results for $x_H = -0.8$, 0, 0.5, and 1.0, respectively, from bottom to top. From (6.2.4) and (7.2.1)-(7.2.3), we can see that the dark matter annihilation cross section for $m_{\rm DM} \simeq m_{Z'}/2$ is proportional to $1/F(x_H)$. Therefore, the maximum annihilation cross section for the fixed values of α_X, $m_{Z'}$, and $m_{\rm DM} \simeq m_{Z'}/2$ is achieved for $x_H = -0.8$. Since the function $1/F(x_H)$ is symmetric about the point of $x_H = -0.8$, the results shown in the left panel indicate the constraint $-1.6 \leq x_H \leq 0$ to satisfy the cosmological bound for the fixed values of $m_{Z'} = 4$ TeV and $\alpha_X = 0.027$.

In Figure 7.2 we show the lower bounds on α_X as a function of $m_{Z'}$ for various values of x_H, to reproduce the observed dark matter relic density in the range of $0.1183 \leq \Omega_{\rm DM}h^2 \leq 0.1213$. The solid lines from top to bottom correspond to $x_H = -3$, $+1$, -2, 0, and -1, respectively. For fixed α_X and $m_{Z'}$, the dark matter annihilation cross section becomes maximum for $x_H = -0.8$ with the minimum Z' boson decay width. As an input x_H value goes away from the point of $x_H = -0.8$, the decay width becomes larger and the dark matter annihilation cross section reduces. As a result, the lower bound on the gauge coupling increases.

7.3 LHC Run-2 constraints

The recent results by the ATLAS and CMS collaborations with the combined 2015 and 2016 data were reported at the ICHEP 2016 conference. In this section, we will employ this recent LHC Run-2 results to derive LHC constraints on the model parameters, α_X, $m_{Z'}$, and x_H.

Let us calculate the cross section of the dilepton production, $pp \to Z' + X \to l^+l^- + X$, mediated by the Z' boson. Our analysis here is the same as that for the Z'_{B-L} case in the

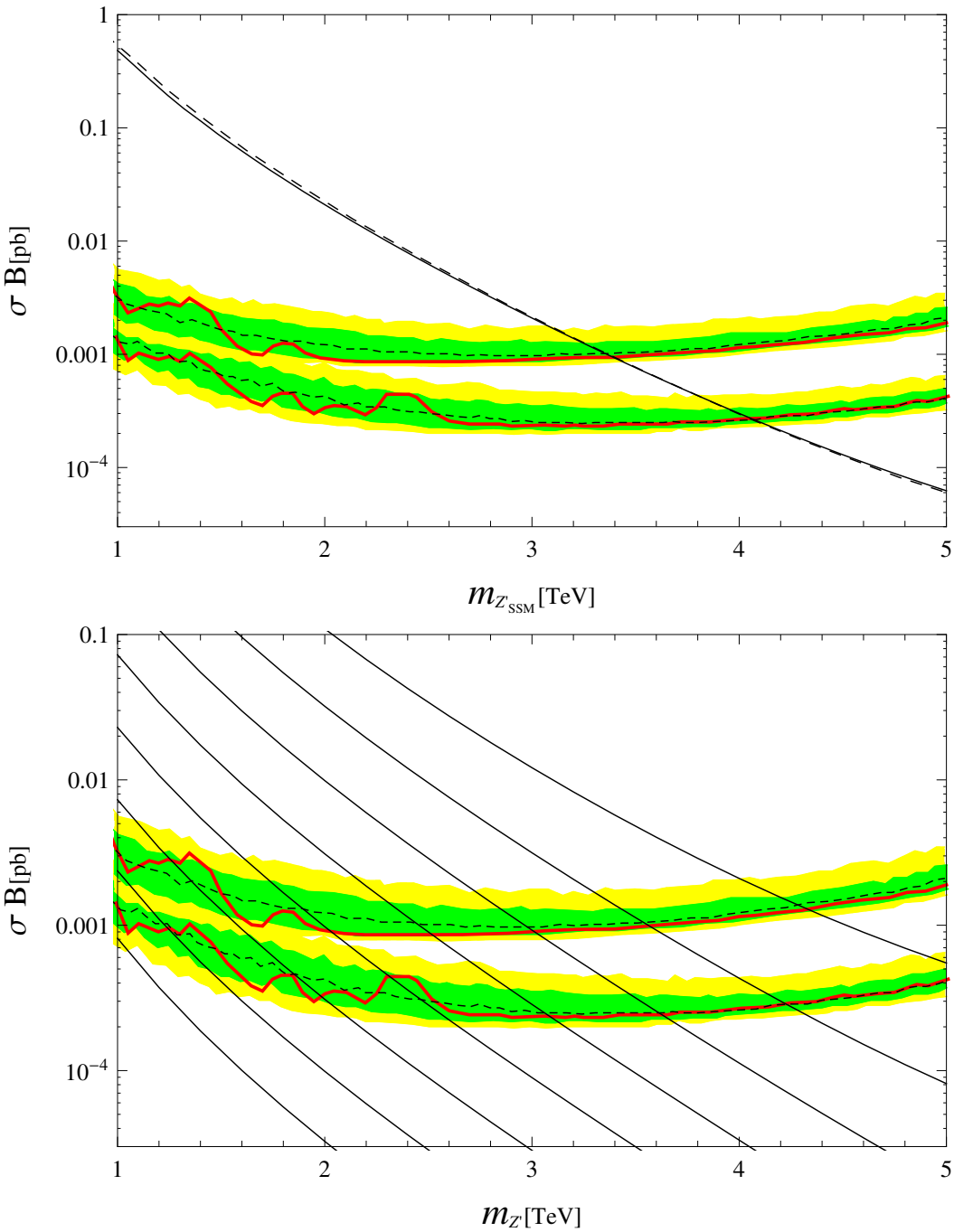

Figure 7.3: Top panel: The solid line shows the cross section as a function of the Z'_{SSM} mass for $k = 1.28$, along with the ATLAS results in 2015 [42] and 2016 [74]. Bottom panel: The cross sections calculated for various values of α_X with $k = 1.28$, for the minimal $B-L$ model limit ($x_H = 0$). The solid lines from left to right correspond to $\alpha_X = 10^{-5}$, $10^{-4.5}$, 10^{-4}, $10^{-3.5}$, 10^{-3}, $10^{-2.5}$, 10^{-2}, and $10^{-1.5}$, respectively.

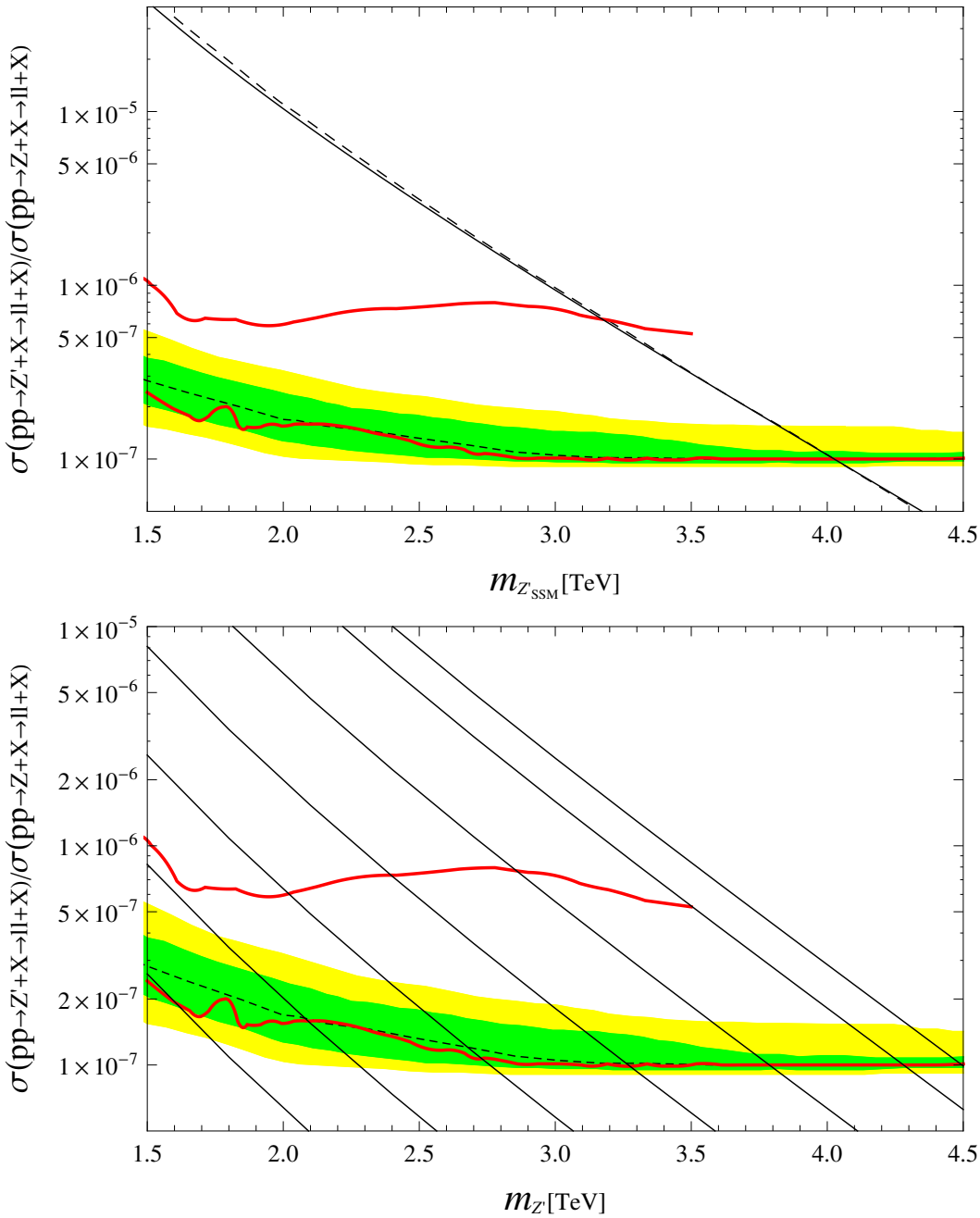

Figure 7.4: Top panel: The cross section ratio as a function of the Z'_{SSM} mass (solid line) with $k = 1.61$, along with the CMS results from 2015 [43] and 2016 [75] from the combined dielectron and dimuon channels. Bottom panel: The cross section ratios calculated for various values of α_X with $k = 1.61$ for the minimal $B - L$ model limit ($x_H = 0$). The solid lines from left to right correspond to $\alpha_X = 10^{-4.5}$, 10^{-4}, $10^{-3.5}$, 10^{-3}, $10^{-2.5}$, 10^{-2}, and $10^{-1.75}$, respectively.

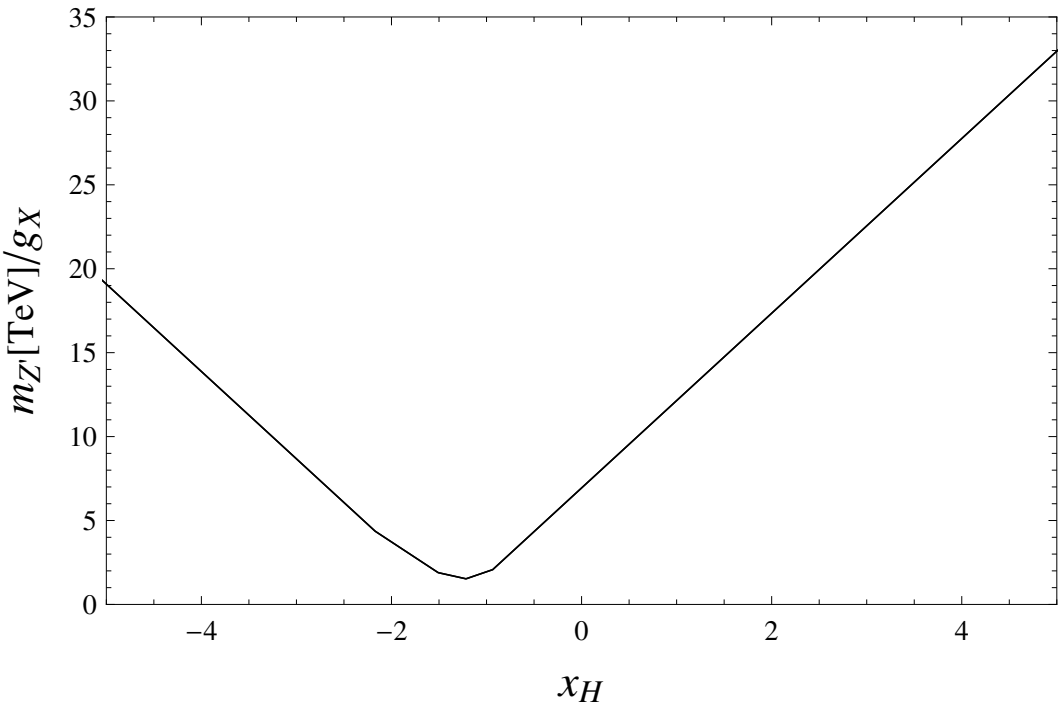

Figure 7.5: The lower bound on $m_{Z'}/g_X$ as a function of x_H. We have employed the final LEP 2 data [6] at the 95% confidence level.

previous chapter. The cross section for the colliding partons is given by

$$\hat{\sigma}(q\overline{q} \to Z' \to l^+l^-) = \frac{\pi}{1296}\alpha_X \frac{M_{ll}^2}{(M_{ll}^2 - m_{Z'}^2)^2 + m_{Z'}^2\Gamma_{Z'}^2} F_{ql}(x_H), \tag{7.3.1}$$

where the function $F_{ql}(x_H)$ is given by

$$\begin{aligned} F_{ul}(x_H) &= (8 + 20x_H + 17x_H^2)(8 + 12x_H + 5x_H^2), \\ F_{dl}(x_H) &= (8 - 4x_H + 5x_H^2)(8 + 12x_H + 5x_H^2) \end{aligned} \tag{7.3.2}$$

for q being the up-type (u) and down-type (d) quarks, respectively. In calculating the total cross section, we set a range of M_{ll} that is used in the analysis by the ATLAS and the CMS collaborations, respectively. We compare our results of the total cross section with the upper limits of the ATLAS and CMS results.

The sequential SM Z' (Z'_{SSM}) model [70] has been considered as a reference model in the analysis by the ATLAS and the CMS collaborations. In order to examine the consistency of our analysis with those by the ATLAS collaboration, we first calculate the cross section $\sigma(pp \to Z'_{SSM} + X \to l^+l^- + X)$ for the sequential Z' boson like (6.3.1).

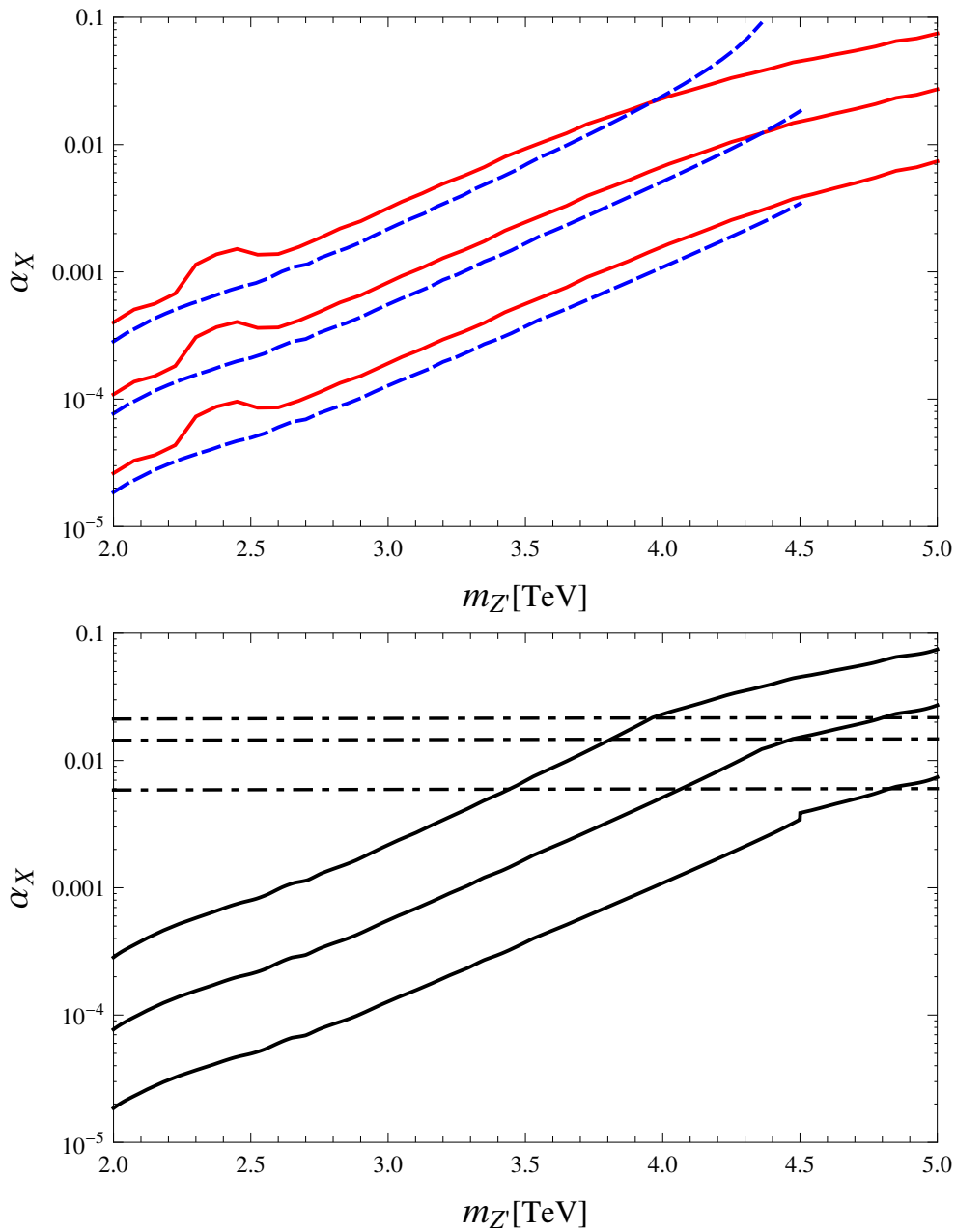

Figure 7.6: Top panel: The upper bounds on α_X as a function of $m_{Z'}$ = −1, 0, and +1 from top to bottom, respectively, for the solid and dashed lines. The solid lines denote the bounds from the ATLAS results [74] while the dashed lines denote the bounds from the CMS results [75]. Bottom panel: The upper bounds on α_X after combining the ATLAS and CMS results shown in the top panel. The solid lines correspond to the combined upper bounds for x_H = −1, 0, and +1 from top to bottom, respectively. The perturbativity bounds of (7.3.3) for x_H = −1, 0, and +1 are shown as the horizontal dashed-dotted lines from top to bottom, respectively.

By integrating the differential cross section for the region of 128 GeV $\leq M_{ll} \leq$ 6000 GeV [67], we obtain the total cross section as a function of Z'_{SSM} boson mass. The top panel on Figure 7.3 shows our result (diagonal solid line), along with the plot presented by the ATLAS collaboration [42, 74] (diagonal dashed line). The ATLAS collaboration obtains the upper limit of the cross section of the process $pp \to Z' + X \to l^+l^- + X$ (lower horizontal red line in Figure 7.3). Comparing the limit with the theory prediction for the Z'_{SSM} boson production (diagonal dashed line), we obtain a lower bound of Z'_{SSM} boson mass as $m_{Z'_{\rm SSM}} \geq 4.05$ TeV. Here, we have also shown the plot presented in [42] (upper horizontal red line). We can see the dramatic improvement from the 2015 results [42] to the 2016 results [74]. When we compare our theory calculation with the one by the ATLAS collaboration, we need to consider a difference between PDFs used in two analysis and uncertainties from QCD corrections. Taking these factors into account, we have scaled our cross section to obtain the same bound of $m_{Z'_{\rm SSM}} \geq 4.05$ TeV. In the top panel on Figure 7.3, we have chosen this scaling factor to be $k = 1.28$. We see that the two lines from our calculation (diagonal solid line) and the ATLAS collaboration [74] (diagonal dashed line) are very well overlapping. We use this factor $k = 1.28$ in our LHC analysis for the Z' production.

For various values of of α_X, $m_{Z'}$ and x_H, we calculate the cross section $\sigma(pp \to Z' + X \to l^+l^- + X)$. For $x_H = 0$ (the minimal $B - L$ model limit), we show our results in the bottom panel of Figure 7.3, along with the plots in the ATLAS papers [42, 74]. The diagonal solid lines from left to right correspond to $\alpha_X = 10^{-5}$, $10^{-4.5}$, 10^{-4}, $10^{-3.5}$, 10^{-3}, 10^{-2}, and $10^{-1.5}$. From the intersections of the lower horizontal curve (in red) and diagonal solid lines, we can read off the lower bounds on the Z' boson mass for the corresponding α_X values. For example, $m_{Z'} > 3.1$ TeV for $\alpha_X = 0.001$. In this way, we have obtained the upper bound on α_X as a function of the Z' boson mass. We do the same analysis for various values of x_H and find the upper bound.

We also consider the result by the CMS collaboration [75]. Corresponding to their analysis, we integrate the differential cross section for the range of $0.95 m_{Z'_{SSM}} \leq M_{ll} \leq 1.05 m_{Z'_{SSM}}$. The limits provided by the CMS collaboration are given as the ratio of the cross sections, $\sigma(pp \to Z'_{SSM} + X \to l^+l^- + X))/\sigma(pp \to Z + X \to l^+l^- + X)$, where $\sigma(pp \to Z+X \to l^+l^-+X) = 1928$ pb is the dilepton production cross section mediated by the Z/γ^* exchange in a mass window of 60 to 120 GeV. Our result is shown as a diagonal

solid line in the top panel of Figure 7.4, along with the plot presented in [75]. The CMS collaboration obtains the upper limit of the ratio, $\sigma(pp \to Z'_{SSM} + X \to l^+l^- + X)/\sigma(pp \to Z + X \to l^+l^- + X)$ (lower horizontal red line in Figure 7.4). Comparing the limit with the theory prediction for the Z'_{SSM} boson production (diagonal dashed line), we obtain a lower bound of Z'_{SSM} boson mass as $m_{Z'_{\rm SSM}} \geq 4.0$ TeV. Here, we have also shown the plot presented in [43] (upper horizontal red line). As in the top panel of Figure 7.4, we can see the dramatic improvement from the 2015 results [43] to the 2016 results [75]. In our calculation, we set a factor $k = 1.61$ to yield the same bound of $m_{Z'_{SSM}} \geq 4.0$ TeV. The top panel shows that our results are well-overlapping with the theoretical cross section presented in [75].

Using $k = 1.61$, we calculate $\sigma(pp \to Z' + X \to l^+l^- + X)$ for various values of α_X, $m_{Z'}$, and x_H. For the minimal $B - L$ model limit, we show our results in the bottom panel of Figure 7.4, along with the plots in the CMS papers [43, 75]. The diagonal solid lines from left to right correspond to $\alpha_X = 10^{-4.5}$, 10^{-4}, $10^{-3.5}$, 10^{-3}, $10^{-2.5}$, 10^{-2}, and $10^{-1.75}$. From the intersections of the lower horizontal curve and the diagonal solid lines, we can read off the lower bounds on the Z' boson mass for the corresponding α_X values. For example, $m_{Z'} > 3.8$ TeV is read off for $\alpha_X = 10^{-2.5}$. In this way, we have obtained the upper bound on α_X as a function of $m_{Z'}$. For various values of x_H we do the same analysis and find the upper bound.

Effective 4-Fermi interactions mediated by a Z' boson have been searched at the LEP [5, 6]. Following the analysis in [71], we employ the LEP 2 data [6] at the 95% confidence level and derive a lower bound on $m_{Z'}/g_X$ as a function of x_H. Our result is shown in Figure 7.5. We find that for any values of x_H, the LEP constraints are always weaker than the LHC Run-2 constraints for $m_{Z'} \leq 5$ TeV.

As a theoretical constraint, we may impose an upper bound on the $U(1)_X$ gauge coupling to avoid the Landau pole in its renormalization group evolution $\alpha_X(\mu)$ up to the Planck mass, $1/\alpha_X(M_{pl}) > 0$, where $M_{pl} = 1.22 \times 10^{19}$ GeV. Employing the renormalization group equation at the one-loop level with $m_N^1 = m_N^2 = m_\Phi = m_{Z'}$, for simplicity, we find

$$\alpha_X < \frac{2\pi}{b_X \ln\left[\frac{M_{pl}}{m_{Z'}}\right]}, \tag{7.3.3}$$

where $b_X = (72 + 64x_H + 41x_H^2)/6$ is the beta function coefficient.

In Figure 7.6 we show the LHC Run-2 bounds on α_X as a function of $m_{Z'}$ for $x_H = -1$, 0, and +1. In the top panel, the solid (dashed) lines from top to bottom denote the upper bounds on α_X for $x_H = -1$, 0, and +1, respectively, obtained from the ATLAS results [74] (the CMS results [75]). For $m_{Z'} \lesssim 4 - 4.5$ TeV, the CMS bounds are slightly more severe than those from the ATLAS results. Combining the ATLAS and CMS results, we obtain the upper bound shown in the bottom panel. The solid lines corresponds to the combined upper bounds for $x_H = -1$, 0, and +1 from top to bottom, respectively. The perturbativity bounds of (7.3.3) for $x_H = -1$, 0, and +1 are shown as the horizontal dashed-dotted lines from top to bottom, respectively.

7.4 Complementarity between the cosmological and the LHC constraints

Now we combine the constraints that we have obtained in the previous two sections. The right-handed neutrino dark matter abundance has led to the lower bound on the $U(1)_X$ gauge coupling for fixed $m_{Z'}$ and x_H, while the upper limit on the production cross section of the Z' boson at the LHC has derived the upper bound on the gauge coupling. Therefore, the two constraints are complementary to each other and, once combined, the model parameter space is more severely constrained.

We show the results for various x_H values in Figure 7.7. The top-left panel shows the results for the minimal $B - L$ model limit ($x_H = 0$) as a function of $m_{Z'}$. The (black) solid line denotes the lower bound on α_X obtained from the cosmological constraints, while the lower dashed line (in red) denotes the upper bound on α_X obtained from the Z' boson search results by the ATLAS [74] and CMS [75] collaborations. Here, the ATLAS and CMS bounds are combined as in the right panel on Figure 7.6. The shaded region is the final result after combining the cosmological and the LHC constraints, leading to the lower mass bound of $m_{Z'} \gtrsim 3.6$ TeV. For a comparison, we have also shown the upper long-dashed line (in red), which is obtained in [45] from the ATLAS [42] and CMS [43] results with the 2015 data. We can see the dramatic improvement from the previous result of $m_{Z'} \gtrsim 2.5$ TeV. The upper bound on α_X from the LEP constraint in (7.5) is depicted as the dotted line, which turns out to be weaker than the LHC bound. We also show the theoretical upper bound on α_X in (7.3.3) as the dashed-dotted line. If we impose this

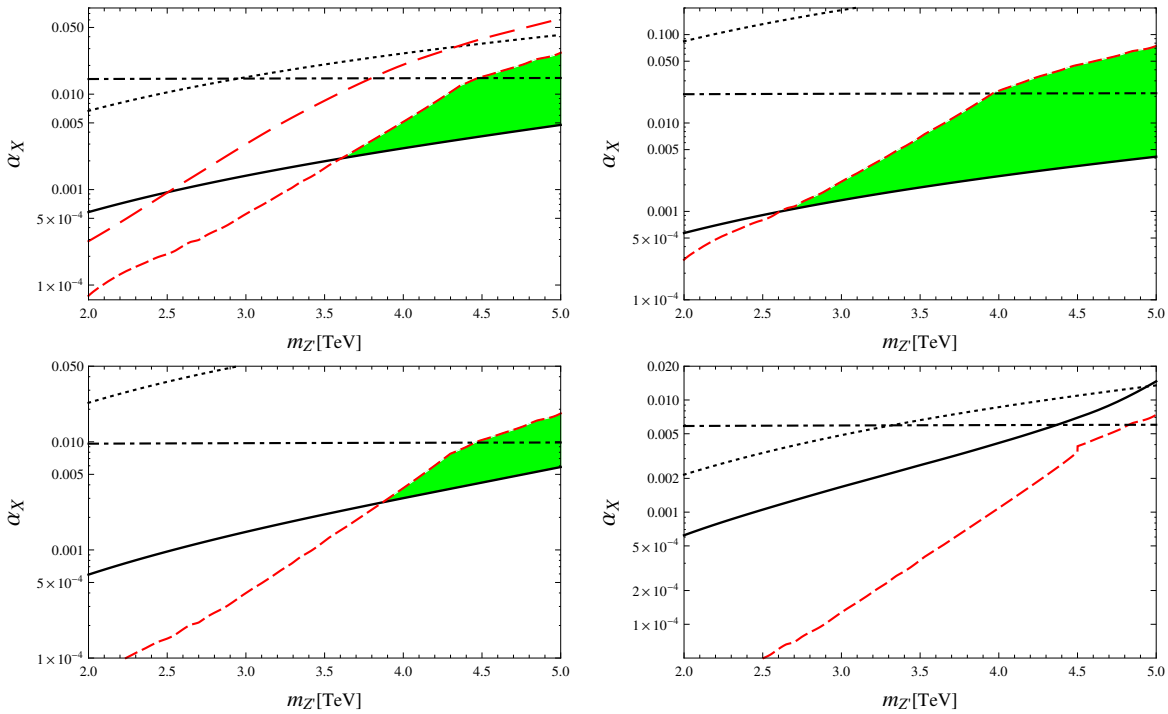

Figure 7.7: Allowed parameter region for the Z' portal right-handed neutrino dark matter scenario. The top-left panel shows the results for the minimal $B-L$ model limit ($x_H = 0$). The (black) solid line denotes the lower bound on α_X obtained from the cosmological bounds, while the lower dashed line (in red) denotes the upper bound on α_X obtained from the Z' boson search results at the LHC. The shaded region is the final result after combining the cosmological and the LHC constraints, leading to the lower mass bound of $m_{Z'} \gg 3.6$ TeV. For a comparison, we have also shown the upper long-dashed line (in red) obtained in [45] by using the LHC results in 2015. The LEP upper bound in [5, 6] is depicted as the dotted line. We also show the perturbativity bound on α_X as the dashed-dotted line. The top-right, bottom-left, and bottom-right panels are the same as the top-left panel, but $x_H = -1$, -2, and $+1$, respectively.

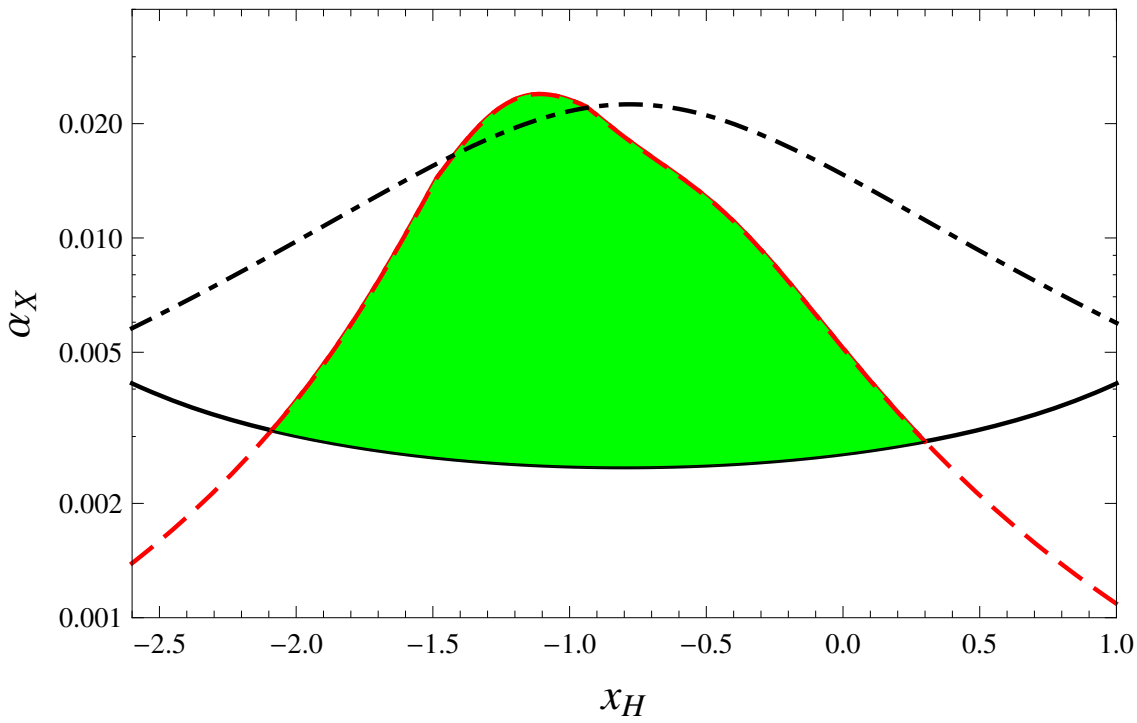

Figure 7.8: Allowed parameter region for the Z' portal right-handed neutrino dark matter scenario for $m_{Z'} = 4$ TeV. The (black) solid line denotes the cosmological lower bound on α_X, while the dashed line (in red) shows the upper bound on α_X obtained from the combined ATLAS and CMS bounds. The shaded region is the final result for the allowed parameter space after combining the cosmological and the LHC constraints, leading to the allowed range of $-2.1 \leq x_H \leq 0.3$. The LEP bound appears above the plot range. The dashed-dotted line denotes the theoretical upper bound on α_X in (7.3.3).

bound, it provides the most severe upper bound for the range of 4.5 TeV $\lesssim m_{Z'} \lesssim$ 5.0 TeV. In Figure 7.7, the top-right, bottom-left, and bottom-right panels are same as the top-left panel, but $x_H = -1,\ -2$, and $+1$, respectively. We find that the largest allowed region is obtained for $x_H = -1$, while no allowed region has been found for a x_H value outside the range of $-2.5 \leq x_H \leq 1$.

Finally, for a fixed $m_{Z'} = 4$ TeV, we show the allowed parameter region in Figure 7.8. The (black) solid line denotes the cosmological lower bound on α_X. As discussed in Chapter 3, the minimum α_X appears at $x_H = -0.8$. The dashed line (in red) shows the upper bound on α_X obtained from the combined ATLAS and CMS constraints. The shaded region is the final result for the allowed parameter space after combining the

cosmological and the LHC constraints, leading to the allowed range of $-2.1 \leq x_H \leq 0.3$. The LEP upper bound appears above the plot range. The dashed-dotted line denotes the theoretical upper bound from the perturbativity of the running $\alpha_X(\mu)$ up to the Planck scale.

The maximum value of α_X to satisfy the LHC bound appears at $x_H \simeq -1$. This means that the cross section of the Z' boson production at the LHC exhibits its minimum at $x_H \simeq -1$. This fact can be roughly understood by using the narrow width approximation. When the decay width of the Z' boson is very narrow, we approximate (7.3.1) as

$$\begin{aligned} \hat{\sigma}(q\bar{q} \to Z' \to l^+l^-) &\simeq \frac{\pi}{1296}\alpha_{X^2}\left[\frac{\pi}{m_{Z'}\Gamma_{Z'}}\delta(M_{ll}^2 - m_{Z'}^2)\right] F_{ql}(x_H) \\ &\propto \frac{F_{ql}(x_H)}{F(x_H)}. \end{aligned} \tag{7.4.1}$$

Using the explicit formulas for $F(x_H)$ and $F_{ql}(x_H)$ given in (7.2.2) and (7.3.2), we can verify that the function $F_{ql}(x_H)/F(x_H)$ exhibits a minimum at $x_H \simeq -1$.

Chapter 8

Conclusions and future plans

8.1 Z'_{B-L} portal dark matter in the minimal $B-L$ extended Standard Model

We have first discussed a simple extension of the SM where the global $B-L$ symmetry in the SM is promoted to the $B-L$ gauge symmetry. In the minimal version of this extension, which is the so-called minimal $B-L$ model, we introduce three right-handed neutrinos with a $B-L$ charge -1 and the $B-L$ (SM singlet) Higgs field with a $B-L$ charge $+2$. The three right-handed neutrinos cancel all the gauge and gravitational anomalies caused by gauging the $B-L$ symmetry. The VEV of the $B-L$ Higgs field breaks the $B-L$ gauge symmetry and generates the $B-L$ gauge boson (Z_{B-L}) mass but also the Majorana masses for the right-handed neutrinos. The SM neutrino mass matrix is then generated after the electroweak symmetry breaking. In order to supplement the minimal $B-L$ model with a dark matter candidate, we have introduced a Z_2 symmetry and one right-handed neutrino of a unique Z_2-odd particle in the model plays the role of the dark matter. In this way, the minimal $B-L$ model with Z_2 symmetry supplements the major missing pieces of the SM, the neutrino mass matrix and a dark matter candidate, while the original particle content of the minimal $B-L$ model is kept intact.

In this model context, we have investigated the "Z'_{B-L} portal" dark matter scenario, where the dark matter particle (Z_2-odd right-handed neutrino) mainly communicates with the SM particles through the Z'_{B-L} boson. We have only three free parameters in our analysis, namely, the gauge coupling (α_{B-L}), the dark matter mass (m_{DM}), and the Z'_{B-L} boson mass ($m_{Z'}$). We have derived the lower bound on α_{B-L} as a function of $m_{Z'}$ by using the cosmological bound on the dark matter relic abundance. On the other hand, the

LHC Run-2 results on the search for a narrow resonance constrain the Z'_{B-L} production cross section at the LHC. We have interpreted the LHC Run-2 results by the ATLAS and the CMS collaborations and obtained the upper bound on α_{B-L} as a function of $m_{Z'}$. Similar (but weaker) upper bounds on α_{B-L} have been obtained from the results by the LEP experiment and the perturbativity condition of the running $B-L$ gauge coupling below the Planck mass. After combining all constraints, we have obtained the allowed parameter space shown in Figure 6.4. We can see that the cosmological bound and the collider constraints are complementary for narrowing down the arrowed parameter space: $m_{Z'} \geq 2.5$ TeV [45].

8.2 Z' portal dark matter in the minimal $U(1)_X$ extended Standard Model

Next we have generalized the minimal $B-L$ model to the minimal non-exotic $U(1)_X$ model, which has the same particle content as the $B-L$ model one while extending the $U(1)_X$ charge assignment. In the $U(1)_X$ model, the $U(1)_X$ charge of a fermion is given by a linear combination of its hypercharge and $B-L$ charge. The anomaly structure is the same as the $B-L$ model, and the three right-handed neutrinos cancel all the gauge and gravitational anomalies. Similarly to the $B-L$ model, the $U(1)_X$ gauge boson (Z') and the three right-handed neutrinos acquire their masses when the $U(1)_X$ gauge symmetry is broken. The seesaw mechanism is implemented in this model as well. In order to supplement the minimal $U(1)_X$ model with a dark matter candidate, we have introduced a Z_2 symmetry and one right-handed neutrino of a unique Z_2-odd particle in the model plays the role of the dark matter. In this way, the Z'_{B-L} portal dark matter scenario in the context of the minimal $B-L$ model is now generalized to the $U(1)_X$ case.

In this generalized model, we have four free parameters in our analysis, namely, the $U(1)_X$ gauge coupling (α_X), the right-handed neutrino dark matter mass (m_{DM}), the Z' boson mass ($m_{Z'}$), and the $U(1)_X$ charge of the SM Higgs doublet (x_H). We have first investigated the allowed parameter space to satisfy the cosmological constraint on the dark matter relic density. It turns out that the dark matter annihilation process must be enhanced to achieve the observed relic density, and therefore $m_{\mathrm{DM}} \simeq m_{Z'}/2$ is always required. As a result, our four free parameters are effectively reduced into three. As in

the Z'_{B-L} portal dark matter scenario, once x_H is fixed, we can derive the lower bound on α_X as a function of $m_{Z'}$ by using the cosmological constraint. We have also investigated the LHC Run-2 constraints on the Z' boson production cross section. The LHC Run-2 results by the ATLAS and the CMS collaborations on the search for a narrow resonance have been interpreted to the constraints on our Z' boson case, and the upper bound on α_X as a function of $m_{Z'}$ has been derived for a fixed x_H. We have found a complementarity between the cosmological bound and the collider constraints for narrowing down the arrowed parameter space. In the $U(1)_X$ model, we have found the lower mass bound as $m_{Z'} \geq 2.7$ TeV. Similar (but weaker) constraints on the model parameters have also been obtained from the LEP constraints and the perturbativity condition of $1/\alpha_X(M_{pl}) > 0$. Future LHC experiments will fully cover the current allowed region, and the Z' boson of the minimal $U(1)_X$ extended SM might be discovered in the near future.

8.3 Future plans

I have a plan to work on the minimal $U(1)_X$ model with alternative $U(1)_X$ charge assignment. The $U(1)_X$ charge assignment for the right-handed neutrinos is not unique, and an alternative charge assignment such as -4 for 2 RHNs while $+5$ for one RHN is known as another way to make the model anomaly free. This charge assignment is interesting because the three RHNs are categorized into $2 + 1$. Using the difference of charges, the RHN with $+5$ charge can be automatically stable. I plan to extend the $U(1)_X$ model I have worked out to this alternative case and investigate the complementarity between the dark matter physics and the LHC physics. Since the RHNs $U(1)$ charges are big, we expect an allowed parameter region is quite different from the one I figured out before. Another interesting feature of the model is that because of the large RHN charge, the Z' boson mainly decays into paris of RHNs and this characteristic Z' boson decay has an impact on Z' boson search as well as the RHN search at the future LHC experiments.

I plan to investigate baryogenesis via leptogenesis scenario in the context of the $U(1)_X$ model that I have been working on. The parameter space of the model for successful leptogenesis is expected to be very limited. I plan to examine if the parameter space overlaps with the allowed region that I have identified from the dark matter physics and the LHC physics.

Appendix A

Rephasing of quarks

The mass terms of quarks are given by

$$\mathcal{L}_{\text{mass}} = -M_u^{ij}\overline{u_L^i}u_R^j - M_d^{ij}\overline{d_L^i}d_R^j + H.c., \tag{A.0.1}$$

where M_u and M_d are 3×3 complex matrices. Using unitary matrices $U_{u/d}$ and $V_{u/d}$, we diagonalize M_u and M_d,

$$\begin{aligned} U_u^\dagger M_u V_u &= D_u = \text{diag}(m_u, m_c, m_t), \\ U_d^\dagger M_d V_d &= D_d = \text{diag}(m_d, m_s, m_b). \end{aligned} \tag{A.0.2}$$

The eigenvalue m_q ($q = u, c, t, d, s,$ and b) are the mass of quark q. Then the mass eigenstates are given by

$$\begin{aligned} u'_L &= U_u^\dagger u_L, \qquad u'_R = V_u^\dagger u_R, \\ d'_L &= U_d^\dagger d_L, \qquad d'_R = V_d^\dagger d_L. \end{aligned} \tag{A.0.3}$$

Under the unitary transformation, the neutral current and the electromagnetic current are invariant. However, the charged current is changed because of the difference between an unitary transformation for up-type and down-type.

$$\begin{aligned} J_\mu^- &= \frac{g_2}{\sqrt{2}}(\overline{u_L}\gamma_\mu d_L) \\ &= \frac{g_2}{\sqrt{2}}(\overline{u'_L}\gamma_\mu U d'_L), \end{aligned} \tag{A.0.4}$$

where $U = U_u^\dagger U_d$. In general, a 3×3 unitary matrix has nine degrees of freedom (three angles and six phases) and can be written by

$$U = P_1 \; U_{\text{KM}} \; P_2, \tag{A.0.5}$$

where P_1 and P_2 are given by

$$\begin{aligned} P_1 &= \mathrm{e}^{i\alpha}\mathrm{e}^{i\beta\lambda_3}\mathrm{e}^{i\gamma\lambda_8}, \\ P_2 &= \mathrm{e}^{i\beta'\lambda_3}\mathrm{e}^{i\gamma'\lambda_8}. \end{aligned} \tag{A.0.6}$$

Here, α, β, β', γ, and γ' are real constants, and λ_3 and λ_8 are the Gell-Mann matrices:

$$\begin{aligned} \lambda_3 &= \begin{pmatrix} 1 & 0 & 0 \\ 0 & -1 & 0 \\ 0 & 0 & 0 \end{pmatrix}, \\ \lambda_8 &= \frac{1}{\sqrt{3}}\begin{pmatrix} 1 & 0 & 0 \\ 0 & 1 & 0 \\ 0 & 0 & -2 \end{pmatrix}. \end{aligned} \tag{A.0.7}$$

We rewrite the charged current as

$$\begin{aligned} J_\mu^- &= \frac{g_2}{\sqrt{2}}(\overline{u'_L}\gamma_\mu P_1 U_{KM} P_2 d'_L) \\ &= \frac{g_2}{\sqrt{2}}(\overline{u''_L}\gamma_\mu U_{KM} d''_L), \end{aligned} \tag{A.0.8}$$

with

$$\begin{aligned} u''_L &= P_1^\dagger u'_L, \\ d''_L &= P_2 d'_L. \end{aligned} \tag{A.0.9}$$

In terms of u''_L and d''_L, the mass terms are rewritten as

$$\begin{aligned} \mathcal{L}_{mass} &= -D_u^{ij}\overline{u'_L}u'_R - D_d^{ij}\overline{d'_L}d'_R + \text{H.c.} \\ &= -D_u^{ij}\overline{u''_L}P_1^\dagger P_1 u''_R - D_d^{ij}\overline{d''_L}P_2 P_2^\dagger d''_R + \text{H.c.} \\ &= -D_u^{ij}\overline{u''_L}u''_R - D_d^{ij}\overline{d''_L}d''_R + \text{H.c.} \end{aligned} \tag{A.0.10}$$

In the last line, we have introduced

$$\begin{aligned} u''_R &= P_1^\dagger u'_R, \\ d''_R &= P_2 d'_R. \end{aligned} \tag{A.0.11}$$

Since the neutral current and the electromagnetic current are invariant under the transformations, unphysical phases in P_1 and P_2 are eliminated. These processes are called "rephasing." After the rephasing, only physical parameters (three mixing angles and one CP phase) are left.

We can generalize the above discussion to a case with N generation quarks. An $N \times N$ unitary matrix has N^2 degrees of freedom (N from diagonal elements and $N(N-1)$ from off diagonal elements). The $2N-1$ degrees of freedom are absorbed by the rephasing of quark fields, as a result, ${}_nC_2 = N(N-1)/2$ mixing angles and $(N-1)(N-2)/2$ CP-violating phases are left as observables. Note that observable CP phases appear for $N \leq 3$ [61].

References

[1] **ATLAS** Collaboration, G. Aad *et al.*, "Observation of a new particle in the search for the Standard Model Higgs boson with the ATLAS detector at the LHC," Phys. Lett. **B716** (2012) 1–29, `arXiv:1207.7214 [hep-ex]`.

[2] **CMS** Collaboration, S. Chatrchyan *et al.*, "Observation of a new boson at a mass of 125 GeV with the CMS experiment at the LHC," Phys. Lett. **B716** (2012) 30–61, `arXiv:1207.7235 [hep-ex]`.

[3] **UA1** Collaboration, G. Arnison *et al.*, "Experimental Observation of Isolated Large Transverse Energy Electrons with Associated Missing Energy at s**(1/2) = 540-GeV," Phys. Lett. **122B** (1983) 103–116. [,611(1983)].

[4] **UA1** Collaboration, G. Arnison *et al.*, "Experimental Observation of Lepton Pairs of Invariant Mass Around 95-GeV/c**2 at the CERN SPS Collider," Phys. Lett. **126B** (1983) 398–410.

[5] **SLD Electroweak Group, SLD Heavy Flavor Group, DELPHI, LEP, ALEPH, OPAL, LEP Electroweak Working Group, L3** Collaboration, "A Combination of preliminary electroweak measurements and constraints on the standard model," `arXiv:hep-ex/0312023 [hep-ex]`.

[6] **DELPHI, OPAL, LEP Electroweak, ALEPH, L3** Collaboration, S. Schael *et al.*, "Electroweak Measurements in Electron-Positron Collisions at W-Boson-Pair Energies at LEP," Phys. Rept. **532** (2013) 119–244, `arXiv:1302.3415 [hep-ex]`.

[7] **ATLAS, CMS** Collaboration, G. Aad *et al.*, "Measurements of the Higgs boson production and decay rates and constraints on its couplings from a combined ATLAS and CMS analysis of the LHC pp collision data at $\sqrt{s} = 7$ and 8 TeV," JHEP **08** (2016) 045, `arXiv:1606.02266 [hep-ex]`.

[8] **Super-Kamiokande** Collaboration, Y. Fukuda *et al.*, "Evidence for oscillation of atmospheric neutrinos," Phys. Rev. Lett. **81** (1998) 1562–1567, `arXiv:hep-ex/9807003 [hep-ex]`.

[9] **SNO** Collaboration, Q. R. Ahmad *et al.*, "Measurement of the rate of $\nu_e + d \to p + p + e^-$ interactions produced by ^8B solar neutrinos at the Sudbury Neutrino Observatory," Phys. Rev. Lett. **87** (2001) 071301, `arXiv:nucl-ex/0106015 [nucl-ex]`.

[10] P. Minkowski, "$\mu \to e\gamma$ at a Rate of One Out of 10^9 Muon Decays?," Phys. Lett. **67B** (1977) 421–428.

[11] T. Yanagida, "HORIZONTAL SYMMETRY AND MASSES OF NEUTRINOS," Conf. Proc. **C7902131** (1979) 95–99.

[12] R. N. Mohapatra and G. Senjanovic, "Neutrino Mass and Spontaneous Parity Violation," Phys. Rev. Lett. **44** (1980) 912.

[13] S. L. Glashow, "The Future of Elementary Particle Physics," NATO Sci. Ser. **B61** (1980) 687.

[14] M. Gell-Mann, P. Ramond, and R. Slansky, "Complex Spinors and Unified Theories," Conf. Proc. **C790927** (1979) 315–321, `arXiv:1306.4669 [hep-th]`.

[15] **WMAP** Collaboration, G. Hinshaw *et al.*, "Nine-Year Wilkinson Microwave Anisotropy Probe (WMAP) Observations: Cosmological Parameter Results," Astrophys. J. Suppl. **208** (2013) 19, `arXiv:1212.5226 [astro-ph.CO]`.

[16] **Planck** Collaboration, P. A. R. Ade *et al.*, "Planck 2013 results. XV. CMB power spectra and likelihood," Astron. Astrophys. **571** (2014) A15, `arXiv:1303.5075 [astro-ph.CO]`.

[17] **Planck** Collaboration, P. A. R. Ade *et al.*, "Planck 2015 results. XIII. Cosmological parameters," Astron. Astrophys. **594** (2016) A13, `arXiv:1502.01589 [astro-ph.CO]`.

[18] B. W. Lee and S. Weinberg, "Cosmological Lower Bound on Heavy Neutrino Masses," Phys. Rev. Lett. **39** (1977) 165–168.

[19] R. N. Mohapatra and R. E. Marshak, "Local B-L Symmetry of Electroweak Interactions, Majorana Neutrinos and Neutron Oscillations," Phys. Rev. Lett. **44** (1980) 1316–1319. [Erratum: Phys. Rev. Lett.44,1643(1980)].

[20] R. E. Marshak and R. N. Mohapatra, "Quark - Lepton Symmetry and B-L as the U(1) Generator of the Electroweak Symmetry Group," Phys. Lett. **91B** (1980) 222–224.

[21] C. Wetterich, "Neutrino Masses and the Scale of B-L Violation," Nucl. Phys. **B187** (1981) 343–375.

[22] A. Masiero, J. F. Nieves, and T. Yanagida, "B^{-}l Violating Proton Decay and Late Cosmological Baryon Production," Phys. Lett. **116B** (1982) 11–15.

[23] W. Buchmuller, C. Greub, and P. Minkowski, "Neutrino masses, neutral vector bosons and the scale of B-L breaking," Phys. Lett. **B267** (1991) 395–399.

[24] N. Okada and O. Seto, "Higgs portal dark matter in the minimal gauged $U(1)_{B-L}$ model," Phys. Rev. **D82** (2010) 023507, `arXiv:1002.2525 [hep-ph]`.

[25] S. F. King, "Large mixing angle MSW and atmospheric neutrinos from single right-handed neutrino dominance and U(1) family symmetry," Nucl. Phys. **B576** (2000) 85–105, `arXiv:hep-ph/9912492 [hep-ph]`.

[26] P. H. Frampton, S. L. Glashow, and T. Yanagida, "Cosmological sign of neutrino CP violation," Phys. Lett. **B548** (2002) 119–121, `arXiv:hep-ph/0208157 [hep-ph]`.

[27] N. Okada and Y. Orikasa, "Dark matter in the classically conformal B-L model," Phys. Rev. **D85** (2012) 115006, `arXiv:1202.1405 [hep-ph]`.

[28] T. Basak and T. Mondal, "Constraining Minimal $U(1)_{B-L}$ model from Dark Matter Observations," Phys. Rev. **D89** (2014) 063527, `arXiv:1308.0023 [hep-ph]`.

[29] H. An, X. Ji, and L.-T. Wang, "Light Dark Matter and Z' Dark Force at Colliders," JHEP **07** (2012) 182, `arXiv:1202.2894 [hep-ph]`.

[30] H. An, R. Huo, and L.-T. Wang, "Searching for Low Mass Dark Portal at the LHC," Phys. Dark Univ. **2** (2013) 50–57, arXiv:1212.2221 [hep-ph].

[31] D. E. Soper, M. Spannowsky, C. J. Wallace, and T. M. P. Tait, "Scattering of Dark Particles with Light Mediators," Phys. Rev. **D90** (2014) no. 11, 115005, arXiv:1407.2623 [hep-ph].

[32] M. Das and S. Mohanty, "Leptophilic dark matter in gauged $L_\mu - L_\tau$ extension of MSSM," Phys. Rev. **D89** (2014) no. 2, 025004, arXiv:1306.4505 [hep-ph].

[33] L. Basso, O. Fischer, and J. J. van der Bij, "Natural Z$'$ model with an inverse seesaw mechanism and leptonic dark matter," Phys. Rev. **D87** (2013) no. 3, 035015, arXiv:1207.3250 [hep-ph].

[34] X. Chu, Y. Mambrini, J. Quevillon, and B. Zaldivar, "Thermal and non-thermal production of dark matter via Z'-portal(s)," JCAP **1401** (2014) 034, arXiv:1306.4677 [hep-ph].

[35] E. Dudas, L. Heurtier, Y. Mambrini, and B. Zaldivar, "Extra U(1), effective operators, anomalies and dark matter," JHEP **11** (2013) 083, arXiv:1307.0005 [hep-ph].

[36] A. Alves, S. Profumo, and F. S. Queiroz, "The dark Z' portal: direct, indirect and collider searches," JHEP **04** (2014) 063, arXiv:1312.5281 [hep-ph].

[37] J. Kopp, L. Michaels, and J. Smirnov, "Loopy Constraints on Leptophilic Dark Matter and Internal Bremsstrahlung," JCAP **1404** (2014) 022, arXiv:1401.6457 [hep-ph].

[38] P. Agrawal, Z. Chacko, and C. B. Verhaaren, "Leptophilic Dark Matter and the Anomalous Magnetic Moment of the Muon," JHEP **08** (2014) 147, arXiv:1402.7369 [hep-ph].

[39] D. Hooper, "Z' mediated dark matter models for the Galactic Center gamma-ray excess," Phys. Rev. **D91** (2015) 035025, arXiv:1411.4079 [hep-ph].

[40] E. Ma and R. Srivastava, "Dirac or inverse seesaw neutrino masses with B-L gauge symmetry and S_3 flavor symmetry," Phys. Lett. **B741** (2015) 217–222, `arXiv:1411.5042 [hep-ph]`.

[41] A. Alves, A. Berlin, S. Profumo, and F. S. Queiroz, "Dark Matter Complementarity and the Z′ Portal," Phys. Rev. **D92** (2015) no. 8, 083004, `arXiv:1501.03490 [hep-ph]`.

[42] **ATLAS** Collaboration, "Search for new phenomena in the dilepton final state using proton-proton collisions at $\sqrt{s} = 13$ TeV with the ATLAS detector," ATLAS-CONF-2015-070 .

[43] **CMS** Collaboration, "Search for a Narrow Resonance Produced in 13 TeV pp Collisions Decaying to Electron Pair or Muon Pair Final States," CMS-PAS-EXO-15-005 .

[44] T. Appelquist, B. A. Dobrescu, and A. R. Hopper, "Nonexotic neutral gauge bosons," Phys. Rev. **D68** (2003) 035012, `arXiv:hep-ph/0212073 [hep-ph]`.

[45] N. Okada and S. Okada, "Z'_{BL} portal dark matter and LHC Run-2 results," Phys. Rev. **D93** (2016) no. 7, 075003, `arXiv:1601.07526 [hep-ph]`.

[46] N. Okada and S. Okada, "Z'-portal right-handed neutrino dark matter in the minimal $\mathrm{U}(1)_X$ extended Standard Model," Phys. Rev. **D95** (2017) no. 3, 035025, `arXiv:1611.02672 [hep-ph]`.

[47] E. Hubble, "A relation between distance and radial velocity among extra-galactic nebulae," Proc. Nat. Acad. Sci. **15** (1929) 168–173.

[48] E. Kolb and M. Turner, The Early Universe, vol. 69. Westview Press, 1994.

[49] F. Hoyle and M. S. Vogeley, "Voids in the 2dF Galaxy Redshift Survey," Astrophys. J. **607** (2004) 751–764, `arXiv:astro-ph/0312533 [astro-ph]`.

[50] **Planck** Collaboration, N. Aghanim *et al.*, "Planck 2015 results. XI. CMB power spectra, likelihoods, and robustness of parameters," Astron. Astrophys. **594** (2016) A11, `arXiv:1507.02704 [astro-ph.CO]`.

[51] **COBE** Collaboration, G. F. Smoot *et al.*, "Structure in the COBE differential microwave radiometer first year maps," Astrophys. J. **396** (1992) L1–L5.

[52] F. Zwicky, "Die Rotverschiebung von extragalaktischen Nebeln," Helv. Phys. Acta **6** (1933) 110–127. [Gen. Rel. Grav.41,207(2009)].

[53] A. G. Doroshkevich, V. N. Lukash, and E. V. Mikheeva, "A solution to the problems of cusps and rotation curves in dark matter halos in the cosmological standard model," Phys. Usp. **55** (2012) 3–17, `arXiv:1209.0388 [astro-ph.CO]`.

[54] Y. Nambu and G. Jona-Lasinio, "Dynamical Model of Elementary Particles Based on an Analogy with Superconductivity. 1.," Phys. Rev. **122** (1961) 345–358.

[55] Y. Nambu and G. Jona-Lasinio, "DYNAMICAL MODEL OF ELEMENTARY PARTICLES BASED ON AN ANALOGY WITH SUPERCONDUCTIVITY. II," Phys. Rev. **124** (1961) 246–254.

[56] J. Goldstone, "Field Theories with Superconductor Solutions," Nuovo Cim. **19** (1961) 154–164.

[57] P. W. Higgs, "Broken symmetries, massless particles and gauge fields," Phys. Lett. **12** (1964) 132–133.

[58] **Particle Data Group** Collaboration, C. Patrignani *et al.*, "Review of Particle Physics," Chin. Phys. **C40** (2016) no. 10, 100001.

[59] D. Pocanic *et al.*, "Precise measurement of the pi+ —¿ pi0 e+ nu branching ratio," Phys. Rev. Lett. **93** (2004) 181803, `arXiv:hep-ex/0312030 [hep-ex]`.

[60] N. Cabibbo, "Unitary Symmetry and Leptonic Decays," Phys. Rev. Lett. **10** (1963) 531–533. [,648(1963)].

[61] M. Kobayashi and T. Maskawa, "CP Violation in the Renormalizable Theory of Weak Interaction," Prog. Theor. Phys. **49** (1973) 652–657.

[62] B. Pontecorvo, "Mesonium and anti-mesonium," Sov. Phys. JETP **6** (1957) 429. [Zh. Eksp. Teor. Fiz.33,549(1957)].

[63] Z. Maki, M. Nakagawa, and S. Sakata, "Remarks on the unified model of elementary particles," Prog. Theor. Phys. **28** (1962) 870–880.

[64] N. Okada, S. Okada, and D. Raut, "Inflection-point inflation in hyper-charge oriented $\mathrm{U}(1)_X$ model," Phys. Rev. **D95** (2017) no. 5, 055030, `arXiv:1702.02938 [hep-ph]`.

[65] M. E. Peskin and D. V. Schroeder, An Introduction To Quantum Field Theory. Westview Press, 1995.

[66] Z. M. Burell and N. Okada, "Supersymmetric minimal B-L model at the TeV scale with right-handed Majorana neutrino dark matter," Phys. Rev. **D85** (2012) 055011, `arXiv:1111.1789 [hep-ph]`.

[67] **ATLAS** Collaboration, G. Aad *et al.*, "Search for high-mass dilepton resonances in pp collisions at $\sqrt{s} = 8$ TeV with the ATLAS detector," Phys. Rev. **D90** (2014) no. 5, 052005, `arXiv:1405.4123 [hep-ex]`.

[68] **CMS** Collaboration, "Search for Resonances in the Dilepton Mass Distribution in pp Collisions at $\sqrt{s} = 8$ TeV," CMS-PAS-EXO-12-061 (2013) .

[69] J. Pumplin, D. R. Stump, J. Huston, H. L. Lai, P. M. Nadolsky, and W. K. Tung, "New generation of parton distributions with uncertainties from global QCD analysis," JHEP **07** (2002) 012, `arXiv:hep-ph/0201195 [hep-ph]`.

[70] V. D. Barger, W.-Y. Keung, and E. Ma, "Doubling of Weak Gauge Bosons in an Extension of the Standard Model," Phys. Rev. Lett. **44** (1980) 1169.

[71] M. Carena, A. Daleo, B. A. Dobrescu, and T. M. P. Tait, "Z' gauge bosons at the Tevatron," Phys. Rev. **D70** (2004) 093009, `arXiv:hep-ph/0408098 [hep-ph]`.

[72] J. Heeck, "Unbroken B-L symmetry," Phys. Lett. **B739** (2014) 256–262, `arXiv:1408.6845 [hep-ph]`.

[73] S. Iso, N. Okada, and Y. Orikasa, "Resonant Leptogenesis in the Minimal B-L Extended Standard Model at TeV," Phys. Rev. **D83** (2011) 093011, `arXiv:1011.4769 [hep-ph]`.

[74] **ATLAS** Collaboration, "Search for new high-mass resonances in the dilepton final state using proton-proton collisions at $\sqrt{s} = 13$ TeV with the ATLAS detector," ATLAS-CONF-2016-045 .

[75] **CMS** Collaboration, "Search for a high-mass resonance decaying into a dilepton final state in 13 fb^{-1} of pp collisions at $\sqrt{s} = 13$ TeV," CMS-PAS-EXO-16-031 .